

Jefferson Laboratory

Physics Division

Annual Report

February 2004

Contents

1.1	HALL A Overview	1
1.2	E01-012	3
1.3	E93-050	8
1.4	E94-104	10
1.5	E95-001	15
1.6	E97-110	19
1.7	E97-111	23
1.8	E98-108	27
1.9	E99-117	30
2.1	Hall B Overview	35
2.2	E93-009	37
2.3	E01-107	40
2.4	g8a	49
2.5	E89-017	55
2.6	E89-036	60
2.7	E89-042	65
2.8	E91-023	70
2.9	E93-006	76
2.10	E93-008	81
2.11	E94-003	85
2.12	E94-017	89

2.13 E6	95
2.14 E94-019	97
2.15 E94-102	99
2.16 E99-006	104
2.17 E00-112	110
3.1 Hall C Overview	114
3.2 E01-004	116
3.3 E93-026	119
3.4 E00-006	124
3.5 E01-006	132

1.1 HALL A Overview

Thirty experiments have been completed since the hall started operations in 1997. Seven of those thirty were completed since the last status report: E99-114, E98-108, E01-001, E00-007, E01-020, E01-012, and E97-110. Experiment E99-114 (Hyde-Wright, Nathan, and Wojtsekhowski) measured the real photon Compton scattering amplitude from the proton over a wide range of s and t using a newly built, large-acceptance, calorimeter. The goal of experiment E98-108 (Baker, Chang, Frullani, Iodice, and Markowitz) was to separate the longitudinal and transverse response functions in the electroproduction of kaons. E98-108 had taken most of its data during 2001 except for some kinematics which required beam energies of 5.7 GeV. Those were completed during this period. Experiment E01-001 (Arrington and Segel) performed a new measurement of G_E/G_M for the proton. The experiment measured ratios of unpolarized cross sections in an attempt to reduce systematic errors which often plague the more traditional Rosenbluth technique of obtaining G_E and G_M . Experiment E00-007 (Gilman, Holt, and Meziani) measured the proton polarization angular distribution in deuteron photo-disintegration. Experiment E01-020 (Boeglin, Jones, Klein, Mitchell, Ulmer, and Voutier) measured the short-distance structure of the deuteron and reaction dynamics in ${}^2H(e, e'p)$. Experiment E01-012 (Chen, Choi, and Liyanage) performed measurements of the neutron (${}^3\text{He}$) spin structure functions in the resonance region. Experiment E97-110 (Chen, Deur, and Garibaldi), a study of the GDH rule and spin structure of ${}^3\text{He}$ and the neutron using nearly-real photons, was completed.

Since the last report, the general purpose Hall A instrumentation has been operated reliably. The Moller and the Compton polarimeters were used by those experiments which made use of polarized beams. The energy measurements systems ARC and “e-p” were also operated. The Ring Imaging Čerenkov (RICH) counter, which is expected to be used during 2004, underwent further beam tests and improvements. Rate measurements for the Deep-Virtual Compton Scattering (DVCS) experiments, which are also expected to take data during 2004, were performed in order to refine the detector system design. The DVCS detector and target system have been nearly completed by early 2004. A beam-line luminosity monitor, to be used by the parity violation experiments scheduled for 2004, was tested with good results. The design and implementation of the detector and support platform for a third magnetic spectrometer for Hall A (so-called “Big Bite”) is making very good progress. This third spectrometer is expected to take data in early 2005.

The major problems encountered by the hall since the last status report have been related to the septum magnets, delivery and operation. The septum magnets are required by several experiments highly-rated by the Physics Advisory Committee (PAC) such as parity violation and spin structure function measurements. To meet the performance requirements

imposed by the experiments and space constraints in the hall pivot area, an aggressive design had to be used. Unfortunately, manufacturing turned out to be more challenging than expected and the delivery schedule of the septum magnets suffered substantial, unexpected and yet nearly continuous slips which made it necessary to schedule other experiments at short notice. Operation of the septum magnets had also a slow start due to technical problems lingering from manufacturing. Most of these problems have been resolved by early 2004. One experiment, E97-110, has already made use of one of the septum magnets.

1.2 E01-012

Hall A experiment 01-012: Measurement of neutron
(^3He) spin structure functions in the resonance region
J. P. Chen, S. Choi, N. Liyanage, spokespersons

The goal of this experiment is to perform a precision extraction of the neutron spin structure function g_1^n and the virtual photon asymmetry A_1^n in the resonance region over a moderate Q^2 range (up to $Q^2 = 4(\text{GeV}/c)^2$) using Hall A polarized ^3He target. The results from this experiment, combined with Deep-Inelastic-Scattering data, will provide a precision test of quark-hadron (Bloom-Gilman) duality predictions for neutron spin structure function g_1^n and the virtual photon asymmetry A_1^n . The Bloom-Gilman duality has been experimentally demonstrated for spin independent structure function F_2 . Duality is observed when the smooth scaling curve at high momentum transfer is an average over the resonance bumps at lower momentum transfer, but at the same value of scaling variable x_{Bj} . Results from E01-012 will enable one of the first precision tests of spin and flavor dependence of quark-hadron duality. The demonstration of duality for spin structure functions will enable the use of resonance data to study the nucleon spin structure in the very high x_{Bj} region.

The Experiment: E01-012 ran in January and February, 2003. We used the polarized beam and the polarized ^3He target to measure the inclusive $^3\vec{\text{H}}\text{e}(e, e')X$ reaction. Both Hall A High Resolution spectrometers (HRS) were used in a symmetric configuration in electron detection mode. Three beam energies, 3 GeV, 4 GeV and 5 GeV were used with spectrometer angles of 25° and 32° . At each kinematic setting, parallel and perpendicular asymmetries were measured with the target spin parallel and perpendicular to the electron beam respectively.

The highest Q^2 setting proposed for this experiment was 5.4 GeV^2 reachable with a beam energy of 5.7 GeV. Highest beam energy available during the running period was 5.0 GeV and hence the highest Q^2 was limited to 4.0 GeV^2 . The Q^2/W phase-space covered by this experiment is given in Figure 1.

The polarized ^3He target performed well during the experiment yielding an average polarization of 37% and requiring only one target cell change. Figure 2 shows the target polarization during the experiment. Beam polarization was measured at each energy using the Moller polarimeter. Figure 3 shows the beam polarization. E01012 was the first experiment to run alongside the G0 experiment at Jefferson Lab. The beam helicity scheme was changed just before this experiment to meet the requirements of G0 and we had to overcome

many difficulties at the beginning of the experiment to properly decode beam helicity.

Current Status: The data analysis is in progress. We have finished the Beam Position calibration, optics calibration, analysis of Vertical Drift Chamber (VDC) efficiency and trigger efficiency, and the calibration of Particle Identification (PID) detectors (Cerenkov and Lead-glass). Figure 4 shows a PID plot indicating the level of pion rejection. Figure 5 shows preliminary results for ^3He elastic asymmetry measured for calibration. The first-pass preliminary physics raw asymmetries were extracted. Currently the analysis of ^3He elastic data and target polarimetry data is in progress. The extraction of asymmetries, calculation of cross sections, radiative corrections and the extraction of the neutron information from the ^3He observables will follow. We are expecting to have preliminary results by the end of this summer.

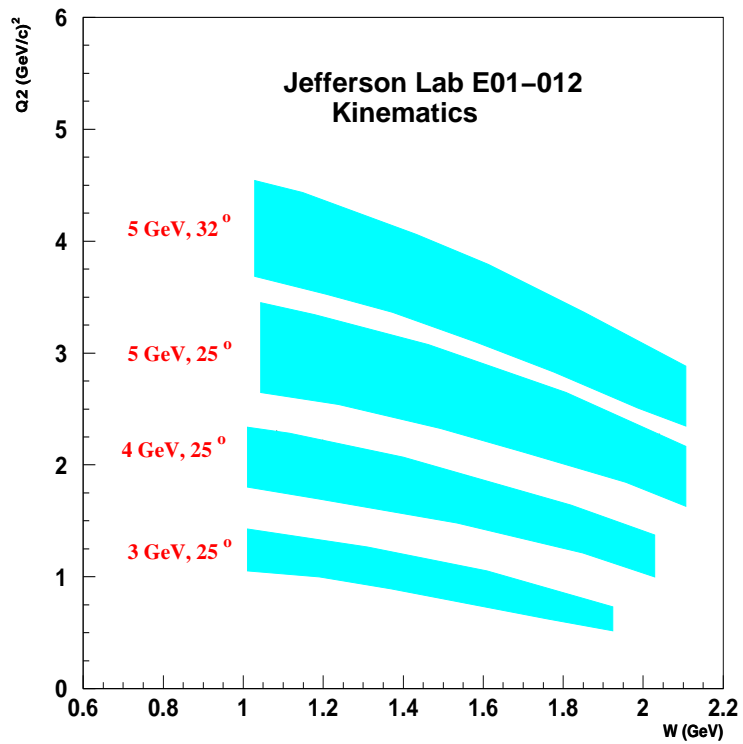


Figure 1: The Q^2 and W coverage for E01-012

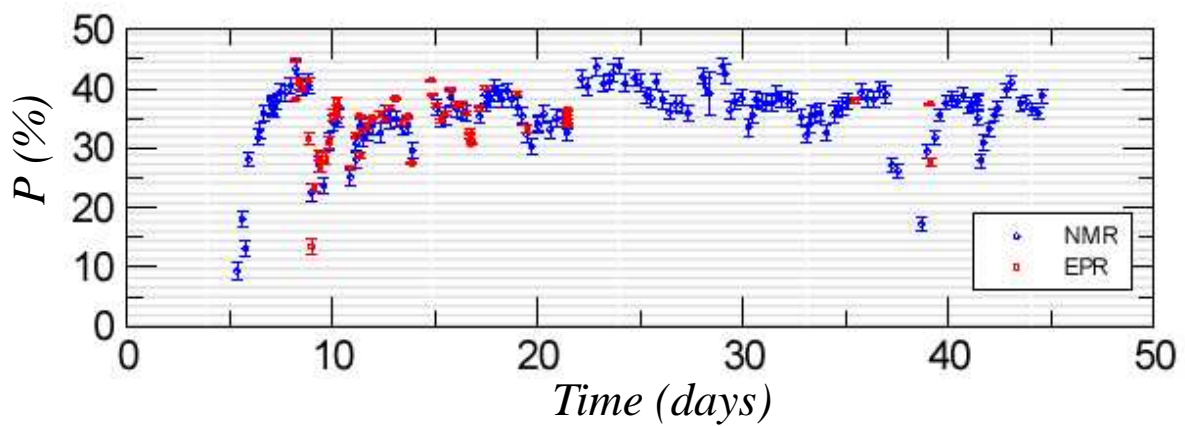


Figure 2: Target polarization during E01-012

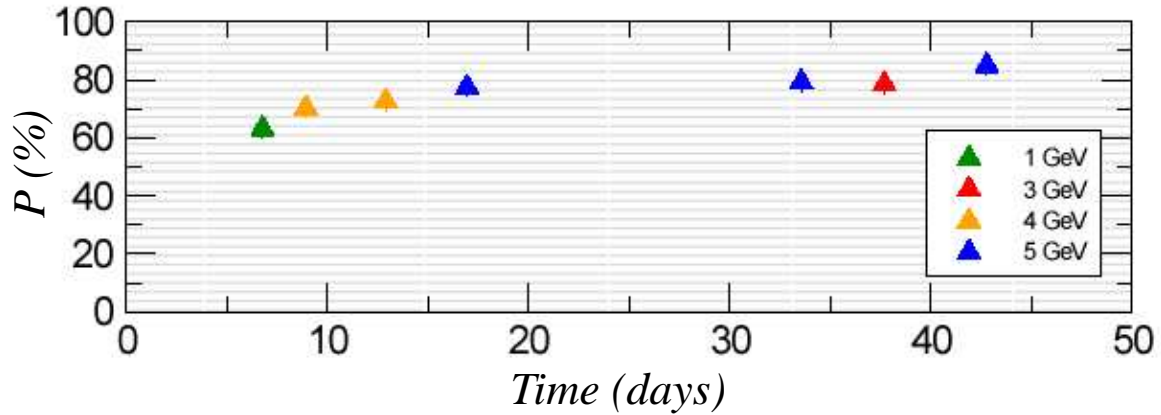


Figure 3: Beam polarization during E01-012

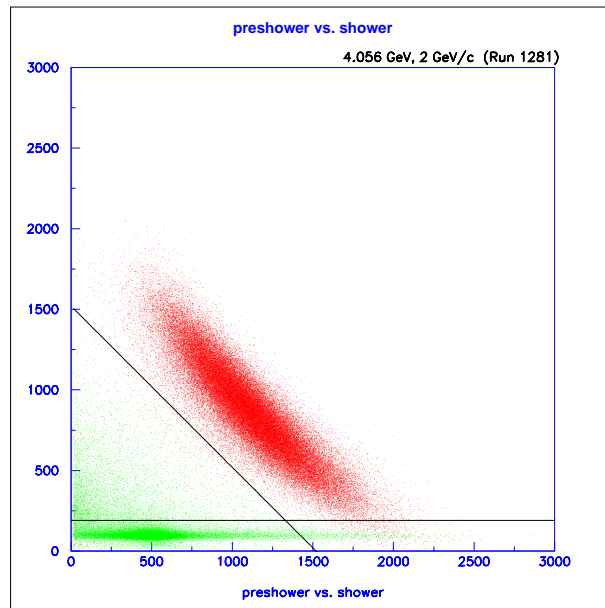


Figure 4: A particle ID plot of energy deposited in the pre-shower detector versus energy deposited in the shower detector for one of the runs. The red dots show the events that passed the Gas-Cerenkov cut for electrons while the green dots show the events rejected by the Gas-Cerenkov. The pre-shower and shower cuts, indicated by black lines on the plot, further enhance the pion rejection. The pion contamination is reduced to 2×10^{-4} level with these combined cuts.

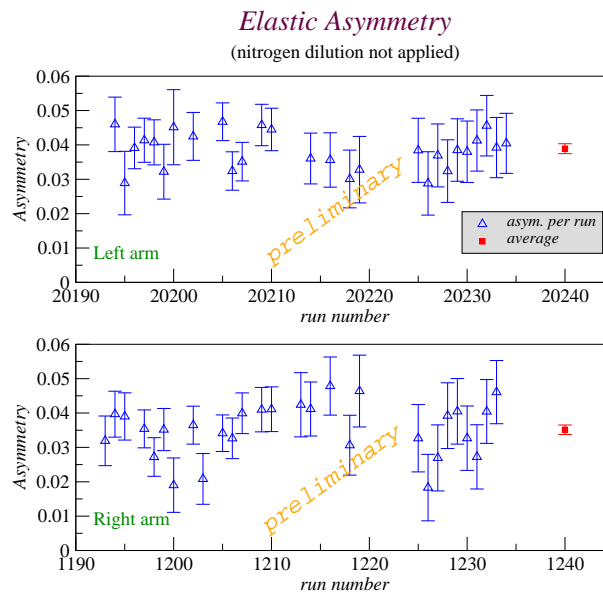


Figure 5: Preliminary results for ^3He elastic asymmetry measured during E01-012. Radiative corrections and nitrogen dilution corrections have not been applied.

1.3 E93-050

NUCLEON STRUCTURE STUDY BY VIRTUAL COMPTON SCATTERING

Spokespersons: P.Bertin, C.Hyde-Wright, G.Fournier
The JLab Hall A Collaboration

1.3.1 Introduction

Experiment E93-050 [1] was performed in 1998 at JLab Hall A. By studying the process $ep \rightarrow ep\gamma$ one has access to the virtual Compton scattering subprocess $\gamma^*p \rightarrow \gamma p$. The physics goals related to this process were:

- to measure the Generalized Polarizabilities [2] of the proton at high Q^2 , around 1 and 2 GeV^2 .
- to study the resonance behaviour in the region of W from 1 to 2 GeV for the first time.

1.3.2 Experiment Status

E93-050 was one of the Hall A Commissioning Experiments. It used the 4 GeV unpolarized electron beam, the 15cm liquid hydrogen target and the two HRS in coincidence. The experimental analysis is completed and several papers have been submitted for publication at the end of 2003.

1.3.3 Results

The results of the experiment are four-fold:

1) The Generalized Polarizabilities of the proton have been determined at $Q^2= 0.9$ and 1.8 GeV^2 from $p(e, e'p)\gamma$ data below pion threshold, using the approach of the Low Energy Expansion [3]. These results have been submitted for publication in PRL [5].

2) The Generalized Polarizabilities of the proton have been determined at $Q^2= 0.9$ and 1.8 GeV^2 from $p(e, e'p)\gamma$ data up to $W=1.2 \text{ GeV}$ using the approach of the Dispersion Relation model [4]. These results have been submitted for publication in PRL [6].

3) The Virtual Compton Scattering process has been measured in the resonance region

up to $W=1.9$ GeV, at $Q^2=1$ GeV² and backward CM angles. Absolute cross sections and the ratio of π^0 production to photon production are the subject of a forthcoming paper [7].

4) We obtained high-precision cross sections for exclusive π^0 electroproduction at $Q^2=1$ GeV² and backward CM angles. These results and the comparison to models are the subject of a paper submitted for publication in PRC [8].

References

- [1] P.Y. Bertin, C. Hyde-Wright, P. Guichon *et al.*, CEBAF Proposal PR93050 (1993).
<http://hallaweb.jlab.org/experiment/E93-050/vcs.html>
- [2] P.A.M. Guichon, G.Q. Liu and A.W. Thomas, Nucl. Phys. A 591 (1995) 606.
- [3] P.A.M. Guichon and M. Vanderhaeghen, Prog. Part. Nucl. Phys. 41 (1998) 125.
- [4] B. Pasquini *et al.*, Eur. Phys. J. A 11 (2001) 185; D. Drechsel, B. Pasquini and M. Vanderhaeghen, Phys. Rept 378 (2003) 99.
- [5] S. Jaminion *et al.*, hep-ph/0312293, submitted to PRL.
- [6] G. Laveissière *et al.*, hep-ph/0312294, submitted to PRL.
- [7] G. Laveissière *et al.*, in preparation.
- [8] G. Laveissière *et al.*, nucl-ex/0308009, submitted to PRC.

1.4 E94-104

The Fundamental $\gamma n \rightarrow \pi^- p$ Process from ^2H , ^4He , and ^{12}C in the 1.2 - 6.0 GeV Region
Spokespersons: H. Gao and R.J. Holt, JLab Hall A collaboration and E94-104 Collaboration

1.4.1 Introduction

The major objective of the experiment is to investigate the transition from nucleon-meson degrees of freedom to quark-gluon degrees of freedom in the description of exclusive processes via studying photopion productions at high energy and large momentum transfer. The experiment is focused on investigations of exclusive processes of $\gamma p \rightarrow \pi^+ n$ from hydrogen, and $\gamma n \rightarrow \pi^- p$ from deuterium and ^4He .

1.4.2 Experiment Status

The experiment was carried out in Hall A in the spring of 2001. Two papers have been published [1, 2] based on the results from this experiment and the Ph.D. thesis student of this experiment, Lingyan Zhu from MIT just defended her Ph.D. thesis successfully in December 2003.

1.4.3 Results

Fig. 1 shows the results of the scaled differential cross section ($s^7 \frac{d\sigma}{dt}$) for the $\gamma p \rightarrow \pi^+ n$ process (upper panel) and the $\gamma n \rightarrow \pi^- p$ process (lower panel) at $\theta_{cm} = 90^\circ$. The new results on $\gamma p \rightarrow \pi^+ n$ with fitted value $n = 9.0 \pm 0.2$ agree with those of Anderson *et al.* [3] and exhibit the scaling behavior predicted by the constituent counting rule with 9 elementary fields. The new results on $\gamma n \rightarrow \pi^- p$ greatly extend the existing measurements and exhibit, for the first time, a global scaling behavior at high energy for this reaction with fitted value $n = 8.6 \pm 0.2$. Data in these two channels show possible oscillations around the scaling behavior in similar ways as suggested by the insets in Fig. 1. Note that this possible oscillatory behavior occurs above the known baryon resonance region. Measurements with much finer binning, planned at JLab [9], are essential for the confirmation of such oscillatory scaling behavior. Another interesting feature of the data is an apparent enhancement in the scaled differential cross section below the scaling region, at a center-of-mass energy ranging approximately from 1.8 GeV to 2.5 GeV. This effect was also observed in neutral pion photoproduction [5, 6]. The observed enhancement around 2.2 GeV might relate to some unknown baryon resonances, the so-called ‘missing resonances’ predicted in this region by the constituent quark model [10].

The observed enhancement might be associated with the strangeness production threshold. These differential cross section results together with charged pion ratio formed from these data were published [1] in 2003 in Physical Review Letters.

Experiment E94-104 provides the first nuclear transparency data [2] for the $\gamma n \rightarrow \pi^- p$ process in ${}^4\text{He}$. The extracted nuclear transparency for the ${}^4\text{He}$ target along with calculations are shown in Fig. 2. The Glauber calculation [11] uses ${}^4\text{He}$ configurations obtained from the variational wave function [12]. The color transparency (CT) effect was included [13] according to the quantum diffusion model [14], and was normalized to the Glauber calculation without CT at the lowest energy point. In Fig. 2 the traditional nuclear physics calculation appears to deviate from the data at the higher energies. The absolute magnitude of the calculations with CT was normalized to the calculation without CT at the lowest energy point. However, it is the momentum transfer squared ($|t|$) dependence of the transparency which is of greater significance. The $|t|$ dependence is not affected by the normalization systematic uncertainties. Thus, these data suggest the onset of deviation from traditional calculations, but future experiments with significantly improved statistical and systematic precision are essential to put these results on a firmer basis.

References

- [1] L. Y. Zhu *et al.*, Phys. Rev. Lett. **91**, 022003 (2003).
- [2] D. Dutta *et al.*, Phys. Rev. C **68**, 021001(R) (2003).
- [3] R. L. Anderson *et al.*, Phys. Rev. D **14**, 679 (1976).
- [4] H.-J. Besch *et al.*, Z. Phys. C **16**, 1 (1982).
- [5] H. Genzel, P. Joos, and W. Pfeil, Photoproduction of Elementary Particles (Springer-Verlag, Berlin, 1973), Group I Volume 8 of Numerical Data and Functional Relationships in Science and Technology, edited by K.-H. Hellwege.
- [6] HEPDATA: REACTION DATA Database, <http://durpdg.dur.ac.uk/hepdata/reac.html>.
- [7] I. I. Strakovsky (private communication); R. A. Arndt *et al.*, nucl-th/0205067, (2002), accepted by Phys. Rev. C; <http://gwdac.phys.gwu.edu/>.
- [8] I. I. Strakovsky (private communication); S. S. Kamalov, *et al.*, Phys. Rev. C **64**, 032201 (2001)(A dynamical model); D. Drechsel, *et al.*, Nucl. Phys. A **645**, 145 (1999)(a unitary isobar model); <http://www.kph.uni-mainz.de/MAID/>.

MAID2001 refers to the Nov. 2001 version of the MAID solution from S. S. Kamalov.

- [9] Jefferson Lab Experiment E02-010, Spokespersons: D. Dutta, H. Gao, R.J. Holt.
- [10] S. Capstick, Phys. Rev. D **46**, 2864 (1992); S. Capstick and W. Roberts, Phys. Rev. D **49**, 4570 (1994).
- [11] R. J. Glauber, in *Lectures in Theoretical Physics*, edited by W. E. Brittin *et al.*, (Interscience, New York, 1959).
- [12] A. Arriaga, V. R. Pandharipande and R. B. Wiringa, Phys. Rev. C **52**, 2362 (1995).
- [13] H. Gao, R. J. Holt and V. R. Pandharipande, Phys. Rev. C **54**, 2779 (1996).
- [14] G. R. Farrar, H. Liu, L.L. Frankfurt, and M.I. Strikman, Phys. Rev. Lett. **61**, 686 (1988).

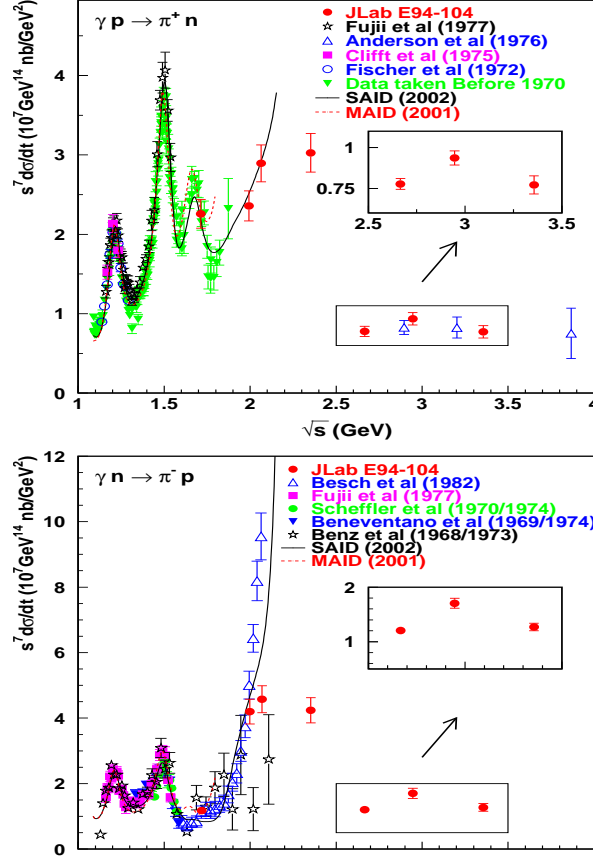


Figure 1: The scaled differential cross section $s^7 \frac{d\sigma}{dt}$ versus center-of-mass energy for the $\gamma p \rightarrow \pi^+ n$ (upper plot) and $\gamma n \rightarrow \pi^- p$ (lower plot) at $\theta_{cm} = 90^\circ$. The data from JLab E94-104 are shown as solid circles. The error bars for the new data and Anderson *et al.*'s data [3], include statistical and systematic uncertainties, except that those in the insets only include point-to-point uncertainties to highlight the possible oscillatory scaling behavior. The open squares in the lower plot were averaged from data at $\theta_{cm} = 85^\circ$ and 95° [4]. Other data sets [5, 6] are shown with only statistical errors. The solid line was obtained from the recent partial-wave analysis of single-pion photoproduction data [7] up to $E_\gamma=2$ GeV, while dash line from the MAID analysis [8] up to $E_\gamma=1.25$ GeV.

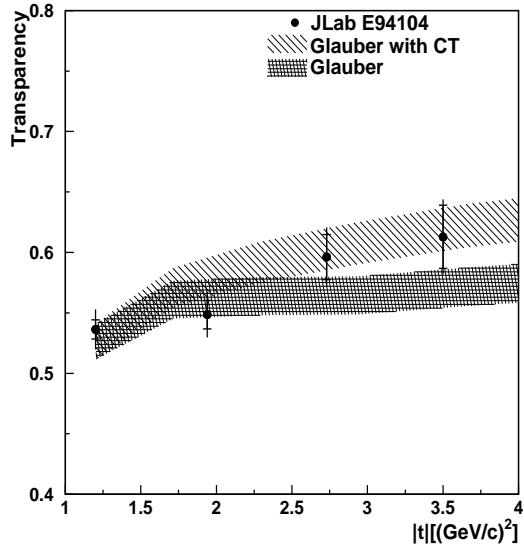
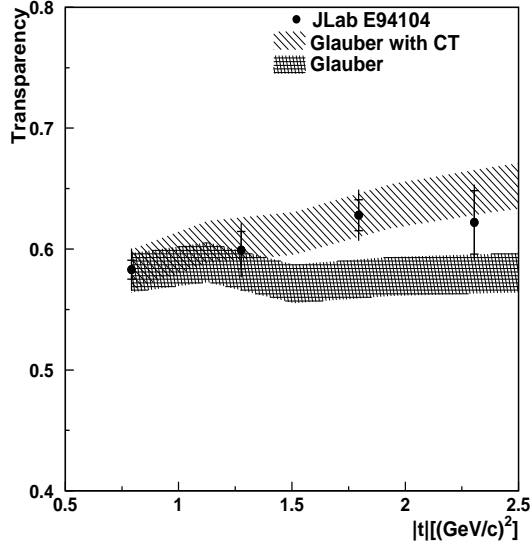


Figure 2: The nuclear transparency of ${}^4\text{He}(\gamma, p \pi^-)$ at $\theta_{cm}^\pi = 70^\circ$ and 90° , as a function of momentum transfer square $|t|$. The inner error bars shown are statistical uncertainties only, while the outer error bars are statistical and point-to-point systematic uncertainties (2.7%) added in quadrature. In addition there is a 4% normalization/scale systematic uncertainty which leads to a total systematic uncertainty of 4.8%.

1.5 E95-001

Precise Measurement of the Transverse Asymmetry
in Quasielastic ${}^3\vec{\text{He}}(\vec{e}, e')$ and the Neutron
Magnetic Form Factor

H. Gao, J.-O. Hansen, Spokespersons and
The Jefferson Lab E95-001 collaboration

1.5.1 Introduction

JLab experiment E95-001 was completed in the spring of 1999. The purpose of this experiment was two-fold. The first goal was to measure the transverse asymmetry $A_{T'}$ on top of the quasielastic peak of ${}^3\vec{\text{He}}(\vec{e}, e')$ and then to extract the neutron magnetic form factor G_M^n from these data. $A_{T'}$ was measured at six kinematic points corresponding to $Q^2 = 0.1$ to 0.6 $(\text{GeV}/c)^2$ in steps of 0.1 $(\text{GeV}/c)^2$. G_M^n has been extracted for $Q^2 = 0.1$ and 0.2 $(\text{GeV}/c)^2$ using Faddeev calculations and results were published in a letter [1]. Most recently, G_M^n for the remaining Q^2 values in the range from 0.3 to 0.6 $(\text{GeV}/c)^2$ have been extracted using a Plane-Wave Impulse Approximation (PWIA) calculation and the results were published [2]. The second goal was to measure the quasielastic asymmetry in the threshold region of ${}^3\vec{\text{He}}(\vec{e}, e')$. Two kinematic points corresponding to $Q^2 = 0.1$ and 0.2 $(\text{GeV}/c)^2$ were covered and the results were published in another letter [3]. This experiment produced two MIT Ph.D. theses.

1.5.2 Experiment

The experiment was carried out in Hall A, using a longitudinally polarized beam incident on a high-pressure polarized ${}^3\text{He}$ gas target based on the technique of spin-exchange optical pumping. Electrons scattered from the target were detected in the two Hall A high resolution spectrometers, HRSe and HRSh. Both spectrometers were configured to detect electrons in single-arm mode. The HRSe was set for kinematics near the top of quasielastic peak while HRSh covered both elastic peak and elastic threshold regions. The elastic measurement allowed for a continuous monitoring of the product of the beam and target polarizations.

1.5.3 Results

To extract G_M^n for the two lowest Q^2 kinematics, the transverse asymmetry data were averaged over a 30 MeV bin around the quasi-elastic peak. A Faddeev calculation with both final

state interactions (FSI) and meson exchange currents (MEC) [4] was employed to generate $A_{T'}$ as a function of G_M^n in the same ω region. By comparing the measured asymmetries with the predictions, the G_M^n values at $Q^2 = 0.1$ and 0.2 $(\text{GeV}/c)^2$ were extracted. To extract G_M^n for Q^2 values between 0.3 and 0.6 $(\text{GeV}/c)^2$, the PWIA calculation [5] was employed. The model uncertainty inherent in the PWIA extraction procedure has been studied [2] and the total uncertainty of our PWIA results was estimated to be about 4–6%. The extracted values of G_M^n are shown in Fig. 1 along with results from previous measurements and several theoretical calculations.

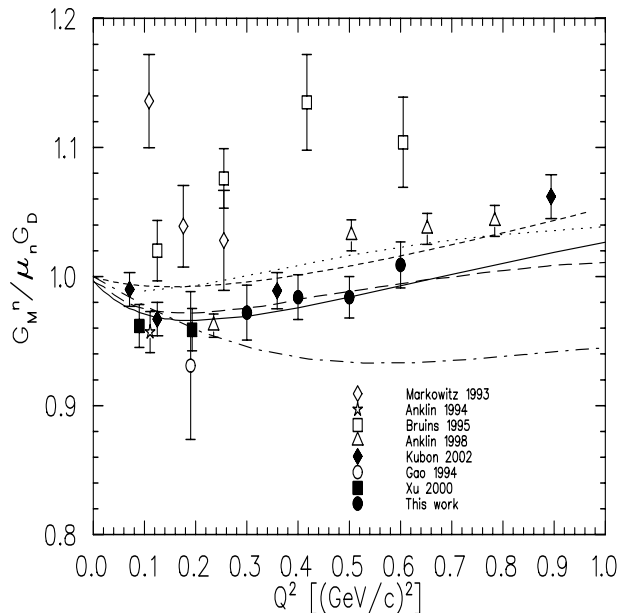


Figure 1: The neutron magnetic form factor G_M^n in units of the standard dipole form factor $(1 + Q^2/0.71)^{-2}$, at Q^2 values of 0.1 and 0.2 extracted based on Faddeev calculations, and 0.3 to 0.6 $(\text{GeV}/c)^2$ extracted using PWIA calculations. The error bars shown do not include the model dependent uncertainties, which are typically 3–4%. Also shown are measurements published since 1990 and a few selected theoretical models. The Q^2 data points of Anklin 94 [6] and Gao 94 [7] have been shifted slightly for clarity. The solid curve is the Höhler nucleon form factor parameterization [8], the long-dashed curve is a recent calculation based on a fit of the proton data using dispersion theory arguments [9], and the dotted curve is a recent analysis based on the vector meson dominance model [10]. The dashed curve is a Skyrme/soliton model calculation [11], and the dash-dotted curve is a relativistic quark model calculation [12].

Results for the physics asymmetry at both kinematics in the threshold region are shown in Fig. 2. All theoretical calculations were performed using AV18 [13] as the NN interaction potential and the Höhler nucleon form factor parametrization [8]. PWIA calculations [14, 15]

are shown as dot-dashed lines. Non-relativistic Faddeev calculations with FSI only [16] are shown as dashed lines. Non-relativistic Faddeev calculations which include both FSI and MEC [16] are shown as dotted lines without the inclusion of the Δ isobar current, and solid lines with the inclusion of the Δ isobar current. The MEC's (π and ρ exchanges) were chosen according to a prescription given by Riska [17], which guarantees to a large extent the consistency of the MECs to the NN force used. The good agreement between the full calculation and the data at $Q^2 = 0.1$ (GeV/c)² suggests the validity of the current way of treating FSI and MEC in the full calculation. The small discrepancy at $Q^2 = 0.2$ (GeV/c)² may be due to the fact that some Q^2 -dependent effects, such as the relativistic effect, are not included in the current non-relativistic Faddeev calculation.

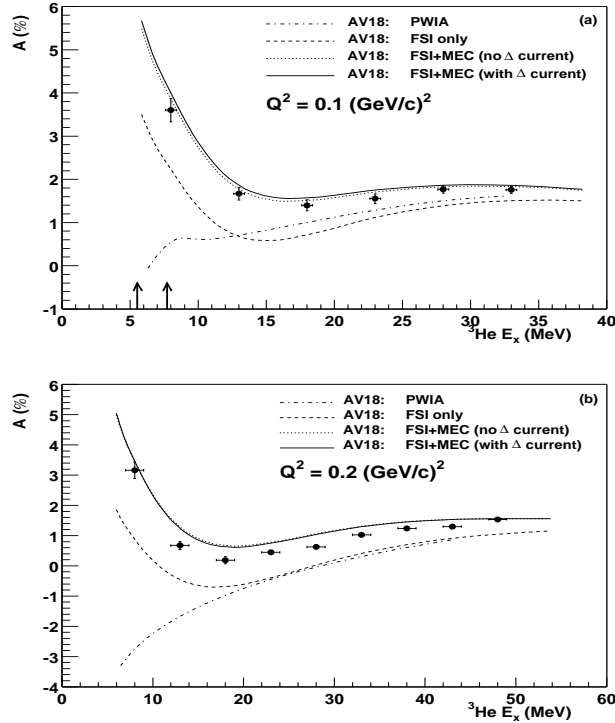


Figure 2: The physics asymmetry together with theoretical calculations for (a) $Q^2 = 0.1$ (GeV/c)² and (b) $Q^2 = 0.2$ (GeV/c)². The theoretical calculations are all performed using AV 18 potential, but with different reaction mechanisms. The arrows point to the two-body and three-body breakup thresholds.

References

- [1] W. Xu *et al.*, Phys. Rev. Lett. **85**, 2900 (2000).
- [2] W. Xu *et al.*, Phys. Rev. C **67**, 012201(R) (2003).
- [3] F. Xiong *et al.*, Phys. Rev. Lett. **87**, 242501 (2001).
- [4] V.V. Kotlyer, H. Kamada, W. Glöckle, J. Golak, Few-Body Syst. **28**, 35 (2000).
- [5] A. Kievsky, E. Pace, G. Salmè, M. Viviani, Phys. Rev. C **56**, 64 (1997).
- [6] H. Anklin *et al.*, Phys. Lett. **B336**, 313 (1994).
- [7] H. Gao *et al.*, Phys. Rev. C **50**, R546 (1994); H. Gao, Nucl. Phys. **A631**, 170c (1998).
- [8] G. Höhler *et al.*, Nucl. Phys. **B114**, 505 (1976).
- [9] P. Mergell, U.-G. Meißner, D. Drechsel, Nucl. Phys. **A596**, 367 (1996).
- [10] E.L. Lomon, Phys. Rev. C **64**, 035204 (2001); Phys. Rev. C **66**, 045501 (2002).
- [11] G. Holzwarth, Z. Phys. **A356**, 339 (1996); hep-ph/0201138.
- [12] F. Schlumpf, Phys. Rev. D **44**, 229 (1993).
- [13] R.B. Wiringa *et al.*, Phys. Rev. C **51**, 38 (1995).
- [14] C. Ciofi degli Atti *et al.*, Phys. Rev. C **51**, 1108 (1995).
- [15] A. Kievsky *et al.*, Phys. Rev. C **56**, 64 (1997).
- [16] J. Golak *et al.*, Phys. Rev. C **63**, 034006 (2001).
- [17] D.O. Riska, Phys. Scr. **31**, 107 (1985).

1.6 E97-110

The GDH Sum Rule, the Spin Structure of ^3He
and the Neutron using Nearly Real Photons
Spokespersons: J.-P. Chen, A. Deur, F. Garibaldi.
The Hall A and E97-110 Collaborations.

1.6.1 Introduction

The goal of the experiment is to measure the generalized Gerasimov-Drell-Hearn integral (GDH) at low Q^2 on the neutron and ^3He .

The GDH sum rule at $Q^2 = 0$ The GDH sum rule has been first derived at $Q^2=0$ [1]. For spin 1/2 targets it reads

$$\int_{\nu_0}^{\infty} (\sigma^{1/2} - \sigma^{3/2}) \frac{d\nu}{\nu} = -2\pi^2 \alpha \frac{\kappa^2}{M^2},$$

where $\sigma^{1/2}$ ($\sigma^{3/2}$) is the polarized photoproduction cross section when the photon helicity is anti-aligned (aligned) with the target spin. ν_0 is the pion photoproduction threshold, ν the photon energy, κ the anomalous magnetic moment of the target and M its mass.

The generalized GDH sum rule The GDH *integral* can be extended to finite Q^2 by considering electroproduction cross sections instead of photoproduction ones. Recently Ji and Osborn derived a generalized GDH *sum rule* and showed that the Bjorken and the GDH sum rules are limiting cases of the generalized GDH sum rule [2]. It is written

$$4 \int_{\nu_0}^{\infty} G_{1(2)} \frac{d\nu}{\nu} = \overline{S_{1(2)}},$$

where $G_{1(2)}$ are the spin structure functions of the nucleon and $\overline{S_{1(2)}}$ are the forward Compton amplitudes with the elastic contribution subtracted.

The forward Compton amplitudes are presently calculable using chiral perturbation theory at low Q^2 and Operator Product Expansion at larger Q^2 [2], [3], [4]. Eventually lattice QCD calculations will provide calculations at any Q^2 . Data at intermediate Q^2 have already been taken in Hall A (exp. E94-010) [5], . The main goal of this experiment is to provide benchmark data on the neutron at low Q^2 to compare to χ PT calculations. It is also important to check the GDH sum rule at the real photon point. We will do so by extrapolation from nearly real photon data. This will be the first verification of the original GDH sum rule on the neutron. We can also form the GDH sum rule on the ^3He nucleus. Studying this quantity brings information about the ^3He nuclear structure.

The experiment The experiment ran in April-May and July-August 2003. It was the first experiment to use a septum magnet. The left septum was not available. We used the polarized beam and the polarized ^3He target to measure the inclusive $^3\text{He}(\vec{e}, e')X$ reaction. To form the extended GDH integral, both the asymmetry and cross section need to be extracted. The nucleus excitation spectrum was covered from quasi-elastic to the resonances and beyond. The kinematics coverage is given in Fig. 1.

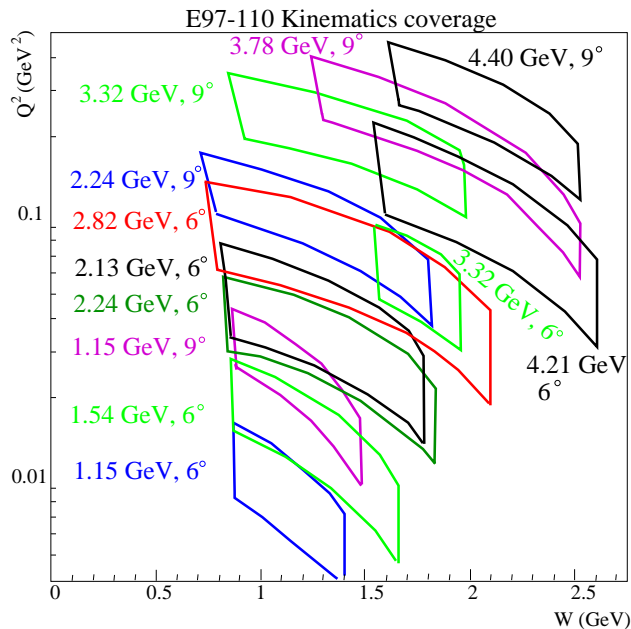


Figure 1: *Kinematics coverage of the experiment. W stands for the invariant mass of the recoiling hadronic system.*

The first part of the experiment occurred in April-May 2003. During the commissioning

the septum magnet was found to be mis-wired. This caused in particular a significant loss in acceptance. However the large rates at forward angles and low beam energies were compensating for it and the data did not suffer loss in statistics. The online analysis of the elastic data showed that the asymmetries are less sensitive to complications of having been taken with a mis-wired septum. During the first run we took the large rate kinematics that were requiring the newly designed target cell (“ice-cream cone cell”). This cell, by minimizing the rescattering background and radiative tails, allowed us to reach large enough W for a meaningful integration.

The septum was fixed in June and successfully commissioned. The experiment was mostly completed in July-August 2003. Online analysis showed a good data quality and good understanding of the background. The online elastic cross sections agree reasonably with the expectation.

1.6.2 Experiment Status

The spectrometer optics analysis for run 2 is close to completion. The analysis under way comprises the detectors, the left arm/BCM data and the backgrounds. Transfer functions for the Septum/HRS are now available. The next steps are to carry out the optics and detector analyses for run 1, then proceed on to the analysis of the data for run 2. This analysis comprises target analysis (polarization, density), elastic analysis, acceptance study using carbon data, background study and simulation, extraction of the cross sections and asymmetries, radiative corrections and finally extraction of the physics quantities of interest: The extended GDH integral, the spin structure functions g_1 and g_2 and their moments. After the completion of the run 2 analysis, the run 1 will be analyzed. Such a choice is driven by the fact that the run 1 data will be more delicate to analyze and the run 2 analysis will provide valuable experience.

1.6.3 Expected Results

The Q^2 -position of the expected results with their uncertainty is given in Fig. 2.

References

- [1] S. Gerasimov. *Yad. Fiz.* 2 598 (1965). S. D. Drell and A. C. Hearn. *Phys. Rev. Lett.* **16** 908 (1966)

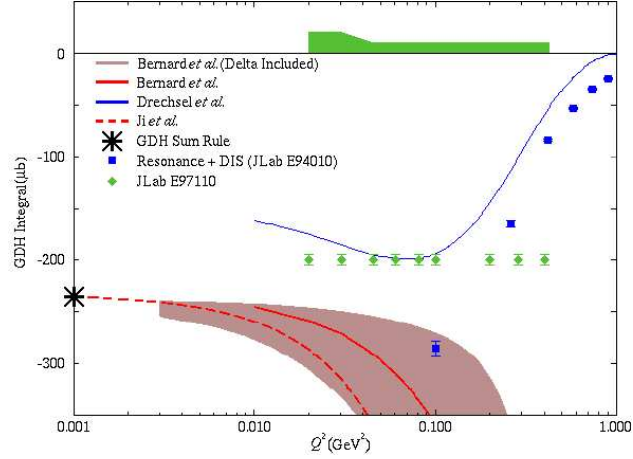


Figure 2: Q^2 -position of the expected results with their uncertainty

- [2] X. Ji and J. Osborn. J. Phys G27 127 (2001)
- [3] V. Bernard, N. Kaiser, U-G. Meissner. Phys.Rev. D48 3062-3069 (1993); V. Bernard, T. R. Hemmert, U-G. Meissner. Phys.Lett. B545 105-111 (2002)
- [4] X. Ji, C-W Kao, J.Osborne. Phys.Rev. D61 074003 (2000)
- [5] M. Amarian *et al.*, Phys. Rev. Lett. **89**, 242301 (2002); M. Amarian *et al.*, Phys. Rev. Lett. **92**, 022301 (2004)

1.7 E97-111

Systematic Probe of Short-Range Correlations via the Reaction ${}^4\text{He}(e, e'p)$
J. Mitchell, B. Reitz, and J.A. Templon, Spokespersons,
and the Hall A Collaboration.

1.7.1 Introduction

Experiment E97-111 measured the unseparated cross section for the $(e, e'p)$ reaction on ${}^4\text{He}$ at recoil momenta up to 530 MeV/c. In the plane-wave impulse approximation, many calculations predict a sharp minimum in the cross section for recoil momenta around 450 MeV/c and show that its location is sensitive to the short-range part of the internucleon potential. However, reaction dynamic effects such as final-state interactions (FSI) and meson-exchange currents (MEC) can obscure such a minimum. To distinguish and study these effects, data were taken at several different kinematic points. Many ideas have been formulated about how to suppress contamination from these reaction dynamic processes in experiments. They can be partly avoided or at least minimized utilizing parallel kinematics, where the recoiled proton is detected along the q -axis. Therefore both \vec{q} and \vec{p}_s must line up to the final ejected-proton momentum and contaminating or multistep processes are suppressed. These qualitative arguments for utilizing parallel kinematics are also supported by calculations [Bi95, Sa97].

The beam energies available at JLab allow a substantial variation in the four momentum transfer Q^2 for a given ϵ_m, p_m region. Those variations are helpful in two respects: to help discriminate between one- and two-body currents contributing to the cross section and to suppress the contaminant two-body currents. The one-body direct knockout process of interest only depends on Q^2 through the electron-proton cross section σ_{ep} , while MEC and IC contributions are expected to have a very different Q^2 behavior. Higher values of Q^2 will help to suppress MEC and IC contributions due to the additional $1/Q^2$ dependences of the meson propagators $N\pi$ and $N\rho$, and of the $NN\pi$ ($NN\rho$) form factors.

Close to quasi-elastic kinematics, the momentum transfer essentially determines the momentum of the outgoing proton. FSI are a strong function of the proton energy. From proton scattering experiments it is known that they are lowest at proton momenta of about 700 MeV/c. Above this momentum, absorption effects begin to increase, but the elastic rescattering continues to decrease. However, for the case of the two-body breakup the latter effect is more important; therefore higher momentum transfer appears to be favorable in terms of suppressing FSI.

1.7.2 Experiment Status

The E97-111 experiment ran in the fall of 2000 using the standard equipment available in Hall A. The main emphasis was on measuring the ${}^4\text{He}(e,e'p){}^3\text{H}$ cross section at recoil momenta up to 530 MeV/c in parallel kinematics at two different beam energies 2.389 GeV and 3.170 GeV/c. Additional data were taken in two quasi-perpendicular kinematics, with ω fixed to 525 and 487 MeV and Q^2 values of 1.78 and 1.82 (GeV/c)². The exclusiveness of the two-body breakup channel is guaranteed by means of cuts on the missing energy ϵ_m . The ${}^4\text{He}(e,e'p){}^3\text{H}$ reaction will only occur at $\epsilon_m = 19.81\text{MeV}/c$. The continuum is well separated, with a threshold for the three-body breakup of 26.1 MeV and 28.3 MeV for the four-body breakup.

1.7.3 Preliminary Results

Preliminary results for the reduced cross sections in the PY2 kinematics are shown in Fig. 1. The error bars show the statistical error only. The cross section is divided by the elementary e-p off-shell cross section σ_{CC1} , using the description of [Fo83] and the recoil factor η , to remove the basic kinematical dependence on the polarization of the virtual photon. The reduced cross section falls monotonically within this momenta range. Two sets of theoretical predictions are shown. The first set from J.M. Laget [Lapc] consists of a PWIA calculation (dashed), a calculation including FSI (dotted), and the full calculation (solid), including FSI as well as MEC and IC. For the FSI at lower energies the phase shift description of [La94] was used, which describes elastic NN scattering. At higher energies the high energy parameterization of the NN scattering amplitude of [La03] was used, its imaginary part representing the absorptive part of the NN interaction.

The second group of calculations is from H. Morita and C. Ciofi degli Atti [Mopc]. The first curve (long dashes) is a Glauber type calculation (labeled G), and the dashed-dotted curve (labeled G+FFT) additionally includes finite formation time (FFT) effects [Mo02]. Although data were taken in parallel kinematics and at high momentum transfers, the reduced cross section still falls monotonically in the investigated region, with no sign of a minimum or a change in the slope. This feature appears in all but the PWIA calculations. Neither of the full calculations preserves the minimum in the spectral function at this kinematical setting. Laget's calculations indicate that this is mainly due to FSI, whereas the inclusion of MEC and IC has only a small effect on the predicted cross section. These calculations also show that below 280 MeV/c the PWIA cross section is larger than the one of the full calculation; above that value the PWIA cross section is smaller. This indicates that the FSI tends to shift cross section from low p_m (where the spectral function is high) to the

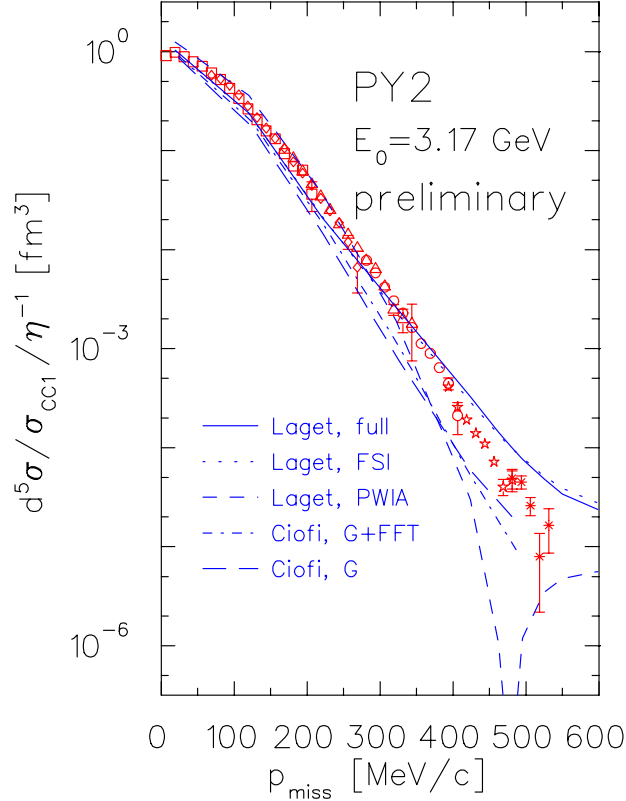


Figure 1: Preliminary results for the reduced cross sections at a beam energy of 3170 MeV. The error bars only show the statistical uncertainty. The dashed line (short dashes) shows the theoretical prediction by Laget in PWIA, the solid line depicts the full calculation, the dotted line only includes FSI. The dashed curve (long dashes) is a Glauber calculation by Ciofi and Morita, the dash-dotted curve additionally includes finite formation time effects.

dip region (where the PWIA cross section is tiny). The FFT effects, which are believed to restore the minimum at very high momentum transfers, are in these kinematics not of great importance. At lower recoil momenta the full calculations of both groups give a reasonable description of the data. Starting at around 350 MeV/c they start to differ from the data and among themselves. Whereas the Laget calculation overpredicts the cross section, the Ciofi calculation underpredicts it at high missing momenta.

All production data of E97-111 have been replayed, as well as the runs for optics calibration, for the calibration of angular offsets, for target boiling studies, and for the ${}^3\text{He}(e, e)$ elastic reaction. To finalize the results further studies of detector efficiencies are ongoing. The elastic data need further analysis to obtain the absolute normalization. Finally, a careful

study of acceptance cuts and other systematic uncertainties is on it's way.

References

- [Bi95] A. Bianconi and M. Radici, Phys. Lett. B **363**, 24 (1995).
- [Sa97] L.L. Frankfurt, M.M. Sargsian, and M.I. Strikman, Phys. Rev. C **56**, 1124 (1997).
- [Fo83] T. deForest, Jr., Nucl. Phys. **A392**, 232 (1983).
- [Lapc] J.M. Laget, private communication.
- [La94] J.M. Laget, Nucl. Phys. **A579**, 333 (1994).
- [La03] J.M. Laget, nucl-th/0303052 (2003).
- [Mopc] C. Ciofi degli Atti and H. Morita, private communication.
- [Mo02] H. Morita, M.A. Braun, C. Ciofi degli Atti, and D. Treleani, Nucl. Phys. **A699**, 328c (2002).

1.8 E98-108

Electroproduction of Kaons upto $Q^2=3 \text{ GeV}/c^2$ SPOKESPERSONS and COLLABORATION INFORMATION

O. K. Baker, C. C. Chang, S. Frullani, M. Iodice, P. Markowitz, for the Kaon and Hall A Collaborations

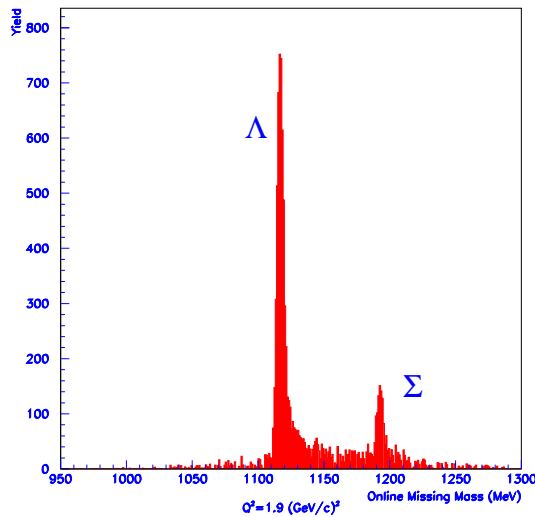


Figure 1: The online missing mass yield taken in March 2002 at $Q^2 = 1.9 \text{ (GeV}/c)^2$, $W = 1.95 \text{ GeV}$ and $t = t_{min}$.

1.8.1 Introduction

The E98-108 collaboration collected data initially in January, March and April 2001 and finished running in March 2002. [Shown above in Fig. 1.8 is the online missing mass spectra from the March 2002 kinematics.] At a total of 30 kinematics points, the experiment measured the $H(e, e'K^+)Y$ cross section. Kinematics used momentum transfers of 1.90 and 2.35 $(\text{GeV}/c)^2$ and invariant masses between 1.8 and 2.2 GeV to measure the cross section as a function of ε (the photon longitudinal polarization), as well as measurements left and right of the direction of \vec{q} . Preliminary σ_L , σ_T , and σ_{LT} cross sections have been extracted from the data. The transverse cross section σ_T , and longitudinal-transverse interference cross section σ_{LT} are used to constrain the reaction mechanism. The behavior of the longitudinal cross

section σ_L is mapped as a function of the Mandelstam variable t at fixed Q^2 . The kaon form factor is expected to be sensitive to σ_L , albeit in a model dependent way. The data will allow the kaon electroproduction reaction mechanism to be determined and eventually allow the kaon form factor to be modelled as well.

The experiment required building two new aerogel Čerenkov radiation detectors with indices of refraction of 1.015 and 1.055. The first detector, due to the low index of refraction, required special handling of the delicate aerogel radiator. The first detector fired only on pions or lighter particles, but not on kaons or protons. The second aerogel was built primarily by the MIT group and fired on either kaons or protons but not pions. The use of two aerogels in anticoincidence is a novel PID idea. The response of the two new aerogels as a function of momenta has been studied in detail for protons, kaons and pions.

1.8.2 Experiment Status

The doctoral student analyzing the data (Marius Coman of Florida International University) is presently focussing on the systematic analysis (acceptance, normalizations, efficiencies and calibrations). For example, target “boiling” corrections are typically 4–6%, while VDC efficiency corrections (both for the detector firing all four planes and for reconstructing one unique track) typically total 20%. The wire chamber efficiency, electronic and computer deadtimes, and cut efficiencies have been determined. Radiative corrections have been done using the MCEEP simulation code; a comparison to the SIMC simulation code is underway.

1.8.3 Preliminary Results

Preliminary separated longitudinal and transverse response function results as a result of the invariant 4-momentum transfer t are shown in Fig. 1.8.3. The upper panel shows the Hall A data at $Q^2=2.35$ (GeV/c)² while the lower curve shows the transverse response function. The error bars will decrease by a factor of 2–3 when the analysis is final.

The response functions were previously measured at lower Q^2 in Hall C by experiment E93-018. Plotted in Fig. 1.8.3 is the ratio of the longitudinal to the transverse response function from E93-018 and a point at the higher Q^2 of this experiment.

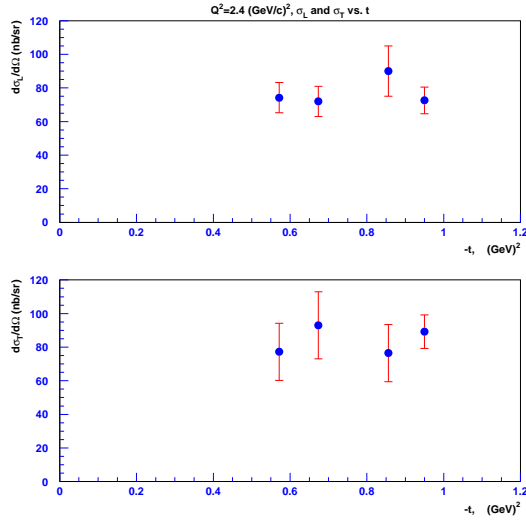


Figure 2: The longitudinal (upper) and transverse (lower) response function at $Q^2= 2.35$ GeV/c^2 for $H(e,e'K^+)$ as a function of the invariant 4-momentum, t .

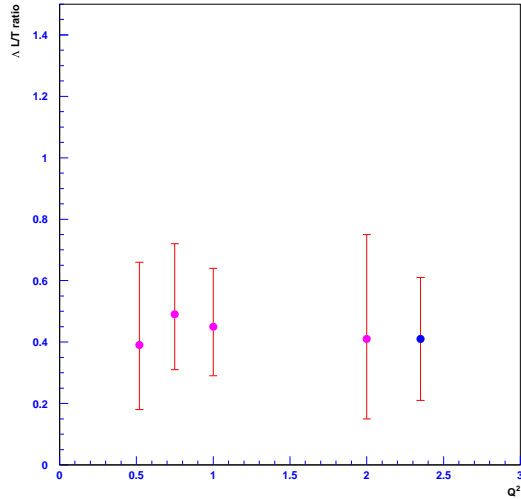


Figure 3: Shown are ratios of the longitudinal to transverse responses as a function of Q^2 from the previous E93-018 and from this experiment.

1.9 E99-117

Precision Measurement of the Neutron Asymmetry A_1^n
at Large x_{Bj} using CEBAF at 5.7 GeV

Jian-Ping Chen, Zein-Eddine Meziani, Paul Souder,
and the Jefferson Lab Hall A Collaboration

1.9.1 Introduction

The nucleon structure is an important topic in hadronic physics, The spin structure of the nucleon can provide crucial information on how quarks and gluons are bound together inside the nucleon, and how they interact with each other via strong interactions. In the 1980's, experiments on the proton spin showed a surprising result in that only about 10% of the proton spin came from the quarks, in contrast to the predictions based on the relativistic constituent quark model (RCQM), where valence quarks account for 75% of the nucleon spin. Since then, extensive experimental and theoretical effort has been spent on this topic. Current understanding of the nucleon spin is that the total spin is distributed among valence quarks, $q\bar{q}$ sea quarks, their orbital angular momenta (OAM), and gluons' spin and angular momentum. Only about (20 – 30)% of the nucleon spin is carried by the quarks.

To further study the nucleon spin, it is necessary to understand the contribution from the quark OAM and the total angular momentum of the gluons. However, the nucleon is in general difficult to model because of the presence of a large amount of $q\bar{q}$ sea and gluons. Moreover, the theory of the strong interaction – Quantum Chromo-dynamics (QCD) – is highly non-perturbative, which makes calculations of the nucleon structure functions intractable.

The only kinematic region where one could avoid the two issues mentioned above is the nucleon valence quark region, also described as the high x region with $x = \frac{Q^2}{2M\nu}$ the Bjorken scaling variable. Here M is the nucleon mass, Q^2 is the four momentum transfer squared and ν is the energy transfer from the incident electron to the target. In this region the nucleon can be viewed as being made of only three valence quarks. Hence RCQM can be used to predict the polarized structure of the nucleon. In this model [1], the virtual photon asymmetry A_1 is expected to approach unity for both the proton and the neutron. In addition, the polarized parton distribution functions (PDF) are predicted to be $\Delta u/u \rightarrow 1$ and $\Delta d/d \rightarrow -1/3$ as $x \rightarrow 1$. Also, it has been shown that perturbative QCD (pQCD) can be applied in this region, which also predicts that $A_1^{p,n} \rightarrow 1$ as $x \rightarrow 1$ [2]. However, based on the assumption that the quark OAM is negligible, leading twist pQCD gives the prediction that both $\Delta u/u \rightarrow 1$ and $\Delta d/d \rightarrow 1$ as $x \rightarrow 1$, in contrast to the RCQM predictions. The

prediction that both u and d quarks should have their spin aligned parallel to the nucleon spin is also called hadron helicity conservation (HHC). Experimentally, existing data on the neutron for $x > 0.4$ have large uncertainties and cannot distinguish between different predictions. Moreover, the precision is even not good enough to exclude the possibility of $A_1^n \leq 0$.

1.9.2 Experiment Status

The goal of E99-117 was to provide the first precision data of A_1^n in the large x region. The experiment ran from June 1 to August 31 of 2001. The 5.7-GeV longitudinally polarized electron beam was used together with the polarized ^3He target in Hall A. The beam polarization was measured by the Moller polarimeter and was continuously monitored by the Compton polarimeter during the experiment, giving an average value of $(79.7 \pm 2.4)\%$. The target polarization was measured by both NMR and EPR polarimetry. Results from the two methods agreed very well, giving an average in-beam polarization of $(40.0 \pm 1.5)\%$. The two High Resolution Spectrometers (HRS) were used to detect the scattered electrons. They were configured at the same scattering angles and momentum settings to double the statistics. Data for inclusive deep inelastic scattering $^3\vec{\text{He}}(\vec{e}, e')$ were collected at three kinematics at $x = 0.33, 0.47, \text{ and } 0.61$, and $Q^2 = 2.71, 3.52, \text{ and } 4.83 \text{ (GeV}/c)^2$, respectively. The invariant mass square W^2 was above 4 GeV^2 for all three points. Both longitudinal and transverse electron asymmetries A_{\parallel} and A_{\perp} were measured, from which A_1 and g_1/F_1 can be extracted using

$$A_1 = \frac{1}{D(1 + \eta\xi)} A_{\parallel} - \frac{\eta}{d(1 + \eta\xi)} A_{\perp} \quad \text{and} \quad \frac{g_1}{F_1} = \frac{1}{D'} [A_{\parallel} + A_{\perp} \tan(\theta/2)]$$

where D, η, ξ, d and D' are variables related to the kinematics and the ratio $R \equiv \sigma_L/\sigma_T$. Similarly, the asymmetry A_2 and ratio g_2/F_1 were extracted from data. Next, the extracted ^3He asymmetries were corrected for the radiative effects. Then the neutron asymmetries A_1^n and A_2^n and structure function ratios g_1^n/F_1^n and g_2^n/F_1^n were extracted from the ^3He results using a model which takes into account a variety of nuclear effects, including that from the presence of non-nucleonic degrees of freedom.

In addition to the DIS measurements, longitudinal asymmetry of $\vec{e} - ^3\vec{\text{He}}$ elastic scattering was measured to check the product of the beam and target polarizations. The elastic cross section was also extracted from data as a check of the systematics. Both the elastic asymmetry and cross section agree with the simulation within their uncertainties. False asymmetries, checked with an unpolarized carbon target, were found to be negligible compared to the statistical uncertainties of the measured ^3He asymmetries.

1.9.3 Results

The data analysis was completed in late 2002. Details of the analysis can be found in Ref. [3]. Compared to previous world data in the region of $x > 0.4$, the precision of A_1^n , g_1^n/F_1^n and g_1^n were improved by about an order of magnitude. The new results at $x = 0.33$ are in good agreement with previous world data. The A_1^n results from all three x points showed, for the first time, a clear trend that A_1^n turns positive at large x , as predicted by RCQM and pQCD. The new A_1^n data also agree with predictions using the LSS2001 parameterizations and a global fit to world data based on the statistical model, but do not agree with the BBS and LSS(BBS) parameterizations, which have HHC imposed. This indicates that there might be a problem in the assumption that the quark has zero OAM.

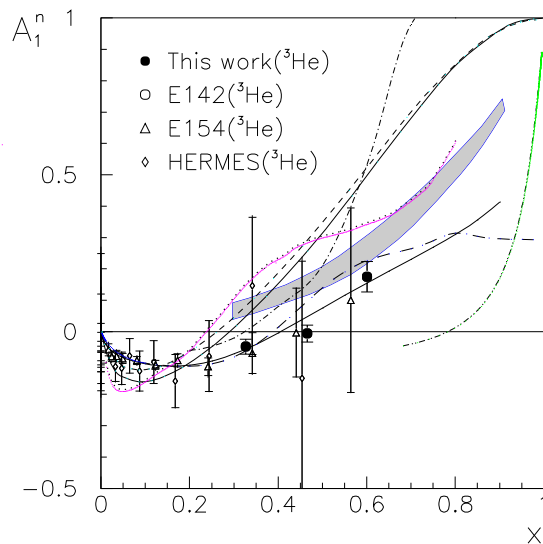


Figure 1: Our A_1^n results compared with theoretical predictions and previous world data obtained from polarized ^3He targets. Curves: predictions of A_1^n from SU(6) symmetry (zero), constituent quark model (shaded band) and statistical model (long-dashed); predictions of g_1^n/F_1^n from pQCD HHC based BBS parameterization (higher solid) and LSS(BBS) parameterization (dashed), and LSS 2001 NLO polarized parton densities (lower solid). See Ref. [4] for references and the models used by the remaining curves.

Combined with previous world proton data and a fit to ratio $R^{du} = (d + \bar{d})/(u + \bar{u})$, polarized quark distribution functions (PDF) were extracted from the new g_1^n/F_1^n results based on the quark-parton model. The results are shown in Fig. 2. The new $\Delta q/q$ results agree well with the predictions from the RCQM [1], the LSS 2001 NLO parameterization,

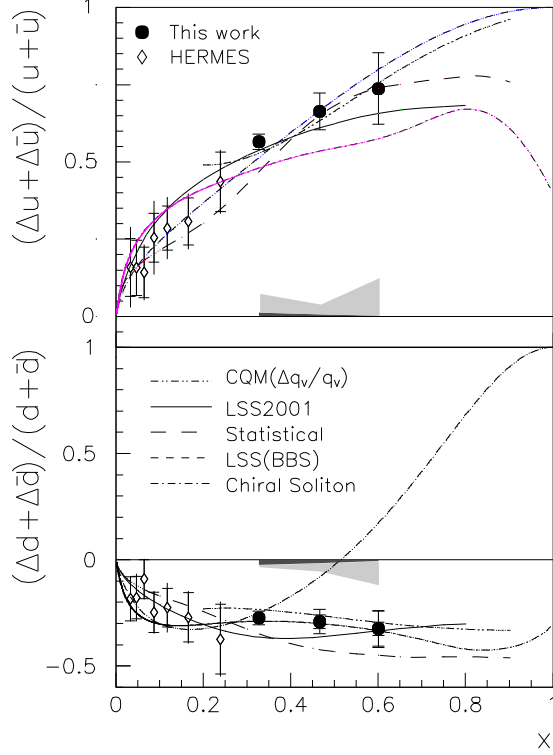


Figure 2: Results for $(\Delta u + \Delta \bar{u})/(u + \bar{u})$ and $(\Delta d + \Delta \bar{d})/(d + \bar{d})$ in the quark-parton model, along with HERMES data. The error bars show the total uncertainties. See Ref. [4] for the meaning of shaded bands.

and the statistical model calculation. But results for the d quark do not agree with the predictions from the LSS(BBS) parameterization based on the HHC.

The fact that the new results do not agree with predictions based on HHC may indicate that quark OAM still contributes significantly to the nucleon spin in the kinematic region explored by this experiment. This observation probably indicates that quark OAM must be taken into account properly when calculating the nucleon structure functions. It is also possible that the Q^2 and x values of this experiment are not high enough to reach the perturbative regime of QCD. An extension of the A_1^n measurement to higher x and Q^2 values is therefore a necessary next step of the nucleon spin structure study.

The above results on A_1^n and $\Delta q/q$ were published in Phys. Rev. Lett. [4]. A longer archive paper is currently being written. In addition to the results published in PRL, the long paper will give all other final results, including the asymmetries and the structure functions

A_1 , A_2 , g_1/F_1 , g_2/F_1 , g_1 and g_2 for ${}^3\text{He}$ and for the neutron, and the asymmetries of inclusive pion photo-productions.

References

- [1] N. Isgur, *Phys. Rev. D* **59**, 034013 (1999).
- [2] G.R. Farrar and D.R. Jackson, *Phys. Rev. Lett.* **35**, 1416 (1975).
- [3] X. Zheng, *Ph. D. thesis*, M.I.T., Cambridge, Massachusetts (2002).
- [4] X. Zheng *et al.*, *Phys. Rev. Lett.*, **92**, 012004 (2004).

2.1 Hall B Overview

Hall B's mission is to carry out experiments that require the detection of multi-particle final states, or experiments that can only be performed at low luminosity. Final states with several particles are typical in reactions involving the production of excited mesons and baryons, or in nuclear break-up reactions. The luminosity may have to be limited to keep accidental coincidences low, e.g. for a tagged bremsstrahlung photon beam or for experiments requiring the coincident detection of particles that are only loosely correlated. Solid-state polarized targets can only be operated at low luminosity. High detection efficiency for multi-particle events and a useful event rate at limited luminosity both require a detection system with a large acceptance.

To carry out this program, Hall B is equipped with a large acceptance magnetic detector, the CEBAF Large Acceptance Spectrometer (CLAS). CLAS is a magnetic toroidal multi-gap spectrometer. Its magnetic field is generated by six super-conducting coils arranged around the beam line to produce a field which is oriented primarily in the ϕ -direction. The particle detection system consists of drift chambers to determine the track of charged particles, gas Cerenkov counters for electron identification, scintillation counters for triggering and measuring the time-of-flight, and electromagnetic calorimeters to detect showering particles (electrons and photons) as well as neutrons. The gaps are individually instrumented to form six independent magnetic spectrometers. This facilitates pattern recognition and track reconstruction at high luminosity.

For electron scattering experiments, a small normal-conducting toroid ("mini-torus") surrounding the target keeps (low momentum) charged electromagnetic background from reaching the innermost drift chamber.

For tagged photon experiments, a radiator is inserted in front of the bremsstrahlung tagging spectrometer which occupies an enlarged tunnel section at the entrance of the hall. The primary electron beam is deflected vertically into a low-power beam dump. Equipment to monitor the tagged photon beam is located behind CLAS in the downstream tunnel section.

A Møller polarimeter to measure the polarization of the incident electron beam is located in the upstream beam tunnel. For electron scattering experiments, the primary electron beam - after passing through the target - is stopped in a Faraday cup to measure the beam current.

A two-stage trigger system is used to initiate data conversion and readout. The Level

I trigger makes use of the fast information from the time-of-flight counters, the Cerenkov counters, and the electromagnetic calorimeters. Level 2 adds track finding using the hit pattern in the drift chambers.

The data acquisition system collects the digitized information on the events, and transfers it to the counting house for temporary storage on disk. Periodically, the data get transferred to the Computer Center's tape silo for later off-line analysis. An event rate of up to 4,000 events/sec corresponding to a steady data rate of approximately 20 Mbytes/sec has been reached.

Physics research with CLAS began in December 1997. Since then, data were collected on a total of 56 PAC-approved experiments. Due to the use of an open trigger, different experiments can often share the same beam conditions, and be executed simultaneously.

In 2003 the E1 run group consisting of 15 approved experiments, completed its data taking with over 120 days of beam time. The physics covered ranges from measurements of the $N - \Delta$ and $N - N^*$ resonance transition form factors, the search for so-called missing quark model states, strangeness production, to deep inelastic processes. We also began the program to study quark propagation and color coherence effects in nuclei (EG2 run group), and carried out beam tests in preparation of the PrimEx and DVCS experiments which are planned for 2004 and 2005, respectively.

Two long accelerator down times in the spring and fall of 2003 were used for major maintenance and repair work on the drift chamber system. Several thousand preamplifiers were replaced as they showed signs of corrosion. During the summer of 2003 the drift chamber system showed increased current instabilities that were traced to increased humidity in the drift chamber gas volumes. A de-humidification system was implemented to better control the humidity level in the gas.

Publications during the year 2003 covered physics from spin structure functions, N^* studies and a possible new resonance seen in 2-pion production, hyperon production, to the exotic $\Theta^+(1540)$ baryon seen both in exclusive strangeness production on deuterium and hydrogen targets.

2.2 E93-009

The EG1 Run Group in Hall B
Gail Dodge, Analysis Coordinator

2.2.1 Introduction

The goal of the EG1 collaboration is to map out the spin structure functions and exclusive and semi-inclusive double and single spin asymmetries of the nucleon. Our data cover a wide kinematic range, in and above the resonance region ($Q^2 = 0.05 \dots 5.0 \text{ GeV}^2$ and $W \leq 3.2 \text{ GeV}$). The run group consists of four approved and one conditionally approved experiments:

- E91-015 “Helicity Structure of Pion Photoproduction;” D. Sober, spokesperson
- E91-023 “Measurement of Polarized Structure Functions in Inelastic Electron Proton Scattering;” V. Burkert, D. Crabb, R. Minehart, spokespersons
- E93-009 “The Polarized Structure Function G_{1n} and the Q^2 Dependence of the Gerasimov-Drell-Hearn Sum Rule for the Neutron;” S. Kuhn, M. Taiuti, G. Dodge, spokespersons
- E93-036 “Measurement of Single Pion Electroproduction from the Proton with Polarized Beam and Polarized Target;” R. Minehart, M. Anghinolfi, H. Weller, spokespersons
- E94-003 “Study of the $\Delta(1232)$ Using Double Polarization Asymmetries,” conditionally approved; V. Burkert, R. Minehart, P. Stoler, spokespersons.

With the inclusive data we are able to determine the spin structure function $g_1(x, Q^2)$ and its first moment, $\Gamma_1(Q^2) = \int_0^1 g_1(x, Q^2) dx$, which is constrained at the real photon point by the Gerasimov-Drell-Hearn Sum Rule and at large Q^2 by the results of deep inelastic scattering (DIS) experiments (see Figure 1). The onset of scaling in the ratio g_1/F_1 , the possibility of observing duality in g_1 and the SU(3) symmetry-breaking behavior of the asymmetry $A_1(x)$ at large x (see Figure 2) are additional topics of current interest. We are also studying the single and double polarization asymmetries of exclusive pion, rho and omega production, which are sensitive to details of the nucleon resonance structure. Furthermore, we can investigate Generalized Parton Distributions (GPDs) with exclusive processes like photon or pion production with deeply virtual photons. Finally we are studying semi-inclusive deep inelastic pion production to access the transverse momentum distribution of partons and flavor-dependent polarized quark distributions.

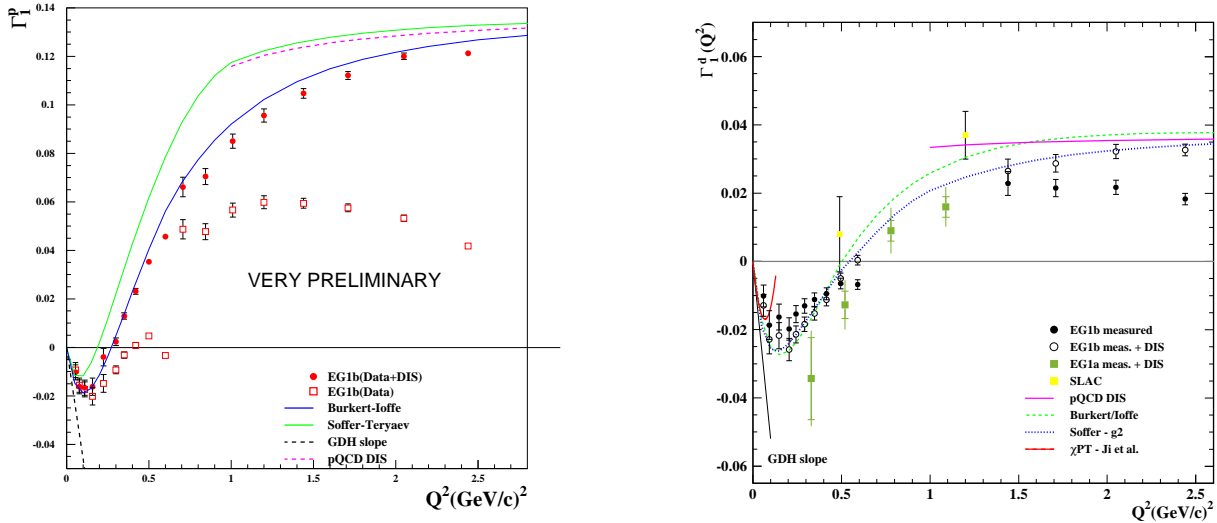


Figure 1: Preliminary results for $\Gamma_1^p(Q^2)$ (left) and $\Gamma_1^d(Q^2)$ (right) using the 1.6, 5.6 and 5.7 GeV EG1b data. The open squares (left) and closed circles (right) represent the measured part of the integral. The unmeasured part of the DIS region is included using a model and shown as the closed circles (left) and open circles (right). (Several model predictions are drawn as well.)

2.2.2 Experiment Status

All data (over 25 billion triggers) for EG1 were taken in two runs, in 1998 (EG1a) and 2000–2001 (EG1b). Polarized electrons with energies of 1.6-1.7 GeV, 2.3-2.6 GeV, 4.2 GeV and 5.6-5.7 GeV were scattered from dynamically polarized cryogenic ammonia targets ($^{15}\text{NH}_3$ and $^{15}\text{ND}_3$). We took data with both polarities of the CLAS toroidal magnetic field to maximize our coverage of the kinematic phase space. In 2003 we published three papers on the results of the 1998 data [Yu03, Bi03, Fa03] (one paper was already published in 2002 [De02]). We continued the calibration and data processing (cooking) of the 2000–2001 data, finishing these tasks for the 1.6, 1.7, 5.6 and 5.7 GeV data. Preliminary results on the inclusive spin structure functions have been presented at many conferences and two students, Vipuli Dharmawardane and Yelena Prok, will complete their PhDs based on the analysis of these data in spring 2004. Analysis of the exclusive and semi-inclusive channels, including an investigation of deeply virtual Compton scattering using the 5.6-5.7 GeV data, is ongoing.

Three new students have joined the EG1 collaboration and will concentrate on the analysis of the 2.3-2.6 and 4.2 GeV data. These data are still being calibrated.

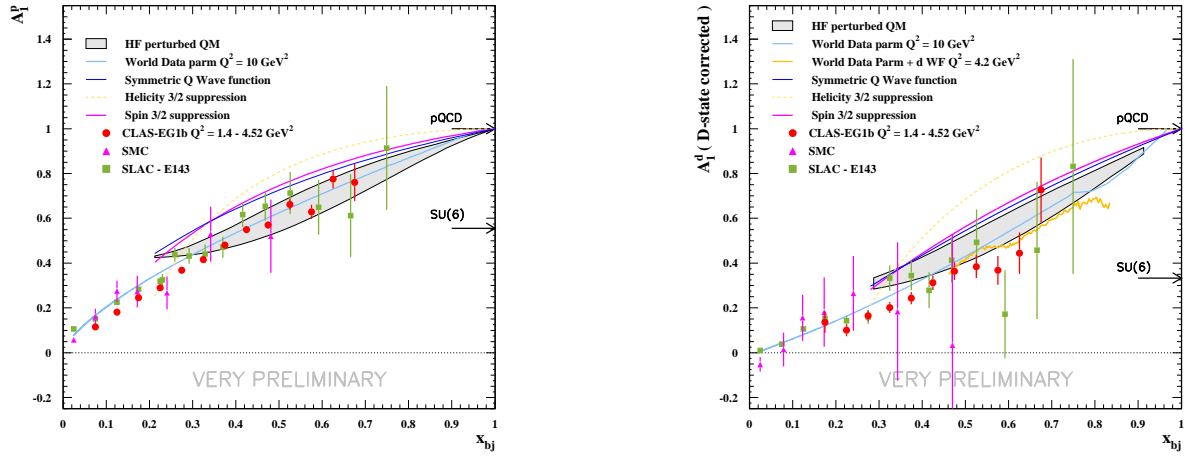


Figure 2: Preliminary results for $A_1^p(x)$ (left) and $A_1^d(x)$ (right) from EG1b data are shown as the closed circles. Various quark model predictions are included.

References

- [Yu03] J. Yun, *et al.*, Phys. Rev. C **67**, 055204 (2003).
- [Bi03] A.S. Biselli, *et al.*, Phys. Rev. C **68**, 035202 (2003).
- [Fa03] R. Fatemi, *et al.*, Phys. Rev. Lett. **91**, 222002 (2003).
- [De02] R. De Vita, *et al.*, Phys. Rev. Lett. **88**, 082001 (2002).

2.3 E01-107

CLAS

Gary Adams, Carlos Salgado, and Dennis P. Weygand

Abstract

The g6c data run was initiated at the CEBAF Large Acceptance Spectrometer (CLAS) on August 17, 2001, and ended abruptly on September 11. The experiment was proposed as a search for exotic mesons, and currently has evidence for *both* exotic mesons and exotic baryons. One thesis based on these data was successfully defended in 2003, and a second will be completed in 2004. The first publication from these data was published on January 24, 2004, and several more papers are in preparation.

2.3.1 Pentaquarks

Analysis of data taken during the g6c data run has recently been published in Physical Review Letters [1]. While this experiment was first proposed as a search for exotic mesons, ironically the first published result was the observation of an exotic baryon, the $\Theta^+(1540)$. We currently have the world's most significant signal for the $\Theta^+(1540)$, which was first seen at Spring8 [2]. In our data, the Θ^+ signal was seen in the reaction $\gamma p \rightarrow K^+ K^- \pi^+ n$, where the neutron is reconstructed from missing four-momentum.

While the signal was seen in the raw mass spectra, a single cut greatly reduced the background, resulting in the signal shown in Fig. 1 inset. That single cut was selecting events with a forward π^+ , which suggested that the Θ^+ observed was actually coming from the decay of a higher mass N^* or Δ resonance. When cutting on the Θ^+ events, and plotting the resulting nK^+K^- effective mass, an apparent narrow state is seen around of mass of 2400 MeV/c². This spectrum is shown in Fig. 2.

Recently, the NA49 has reported apparently corroborating evidence for this state in the reaction $pp \rightarrow pK_s K^- X$ [3]. When plotting the pK_S effective mass, no clear evidence for the Θ^+ is seen; however, when selecting events with the $pK_S K^-$ effective mass near 2400 MeV/c², a peak near the Θ^+ mass becomes apparent. The relevant data from their report is included below (Fig. 3). While Jefferson Laboratory may not have priority on the discovery of the Θ^+ , if the $N^*/\Delta(2400)$ result persists, we can claim priority here.

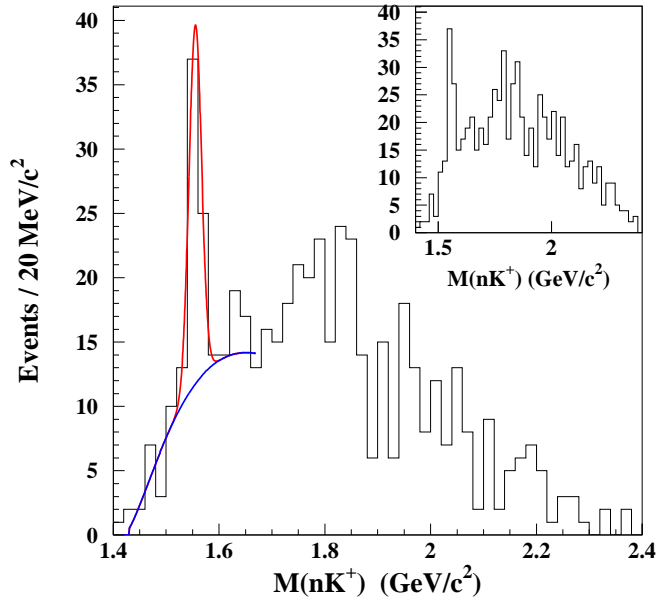


Figure 1: The nK^+ invariant mass spectrum in the reaction $\gamma p \rightarrow \pi^+ K^- K^+(n)$ with the cut $\cos\theta_{\pi^+}^* > 0.8$ and $\cos\theta_{K^+}^* < 0.6$. $\theta_{\pi^+}^*$ and $\theta_{K^+}^*$ are the angles between the π^+ and K^+ mesons and photon beam in the center-of-mass system. The background function we used in the fit was obtained from the simulation. The inset shows the nK^+ invariant mass spectrum with only the $\cos\theta_{\pi^+}^* > 0.8$ cut.

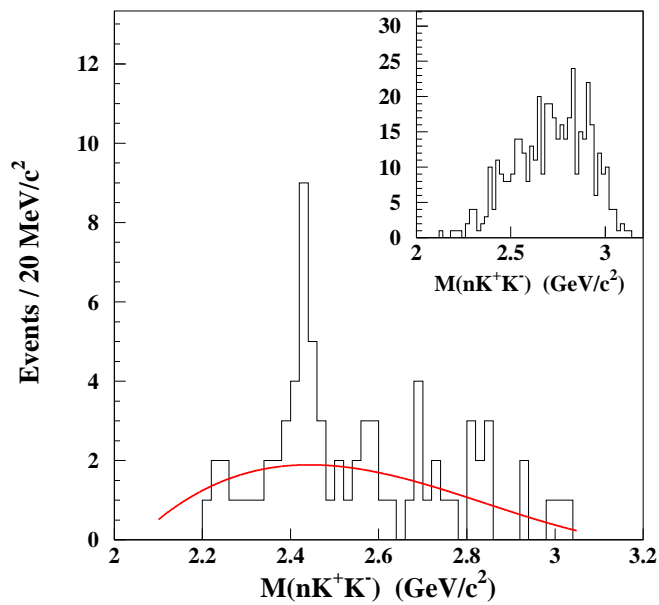


Figure 2: The nK^+K^- invariant mass spectrum calculated from the missing mass off the π^+ in the reaction $\gamma p \rightarrow \pi^+K^-K^+(n)$ with the cuts $\cos\theta_{\pi^+}^* > 0.8$ and $\cos\theta_{K^+}^* < 0.6$. $\theta_{\pi^+}^*$ and $\theta_{K^+}^*$ are the angles between the π^+ or K^+ mesons and photon beam in the center-of-mass system. These events have $M(K^+n)$ between 1.54 and 1.58 GeV/c^2 . The shape of the background curve was obtained from a phase-space simulation. The inset shows the nK^+K^- invariant mass spectrum for all other events in Fig. 1.

2.3.2 Exotic Mesons

The g6c experiment was originally proposed as a search for photo-produced exotic mesons, i.e. mesons which are not composed of a $q\bar{q}$ pair. The most direct evidence for exotic mesons (like exotic baryons) is to identify states with quantum numbers which are excluded for $q\bar{q}$. Two such combinations are $J^{PC} = 1^{-+}$ and $J^{PC} = 2^{+-}$. E852 performed at Brookhaven National Laboratory's Alternating Gradient Synchrotron has already observed two $J^{PC} = 1^{-+}$ states, the $\pi_1(1400)$ [4] and the $\pi_1(1600)$ [5, 6].

We have concluded the partial wave analysis of the reaction $\gamma p \rightarrow \pi^+\pi^-\pi^0p$. In this channel, the three charged particles are reconstructed in CLAS, and the π^0 is measured from missing four-momentum. Since the recoil proton must be observed in CLAS, low

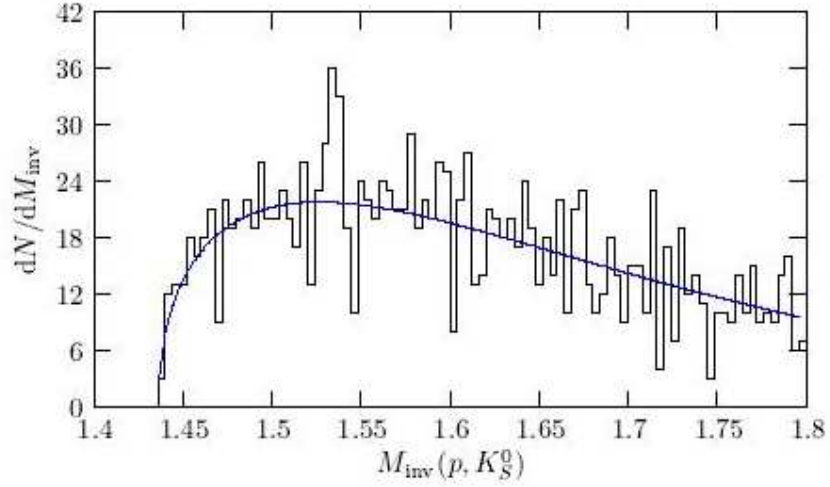


Figure 4: Invariant mass distribution of pK_S^0 pairs, if the $M_{\text{inv}}(pK_S^0k^-)$ invariant mass is in the range $2.4 \pm 0.1 \text{ GeV}/c^2$

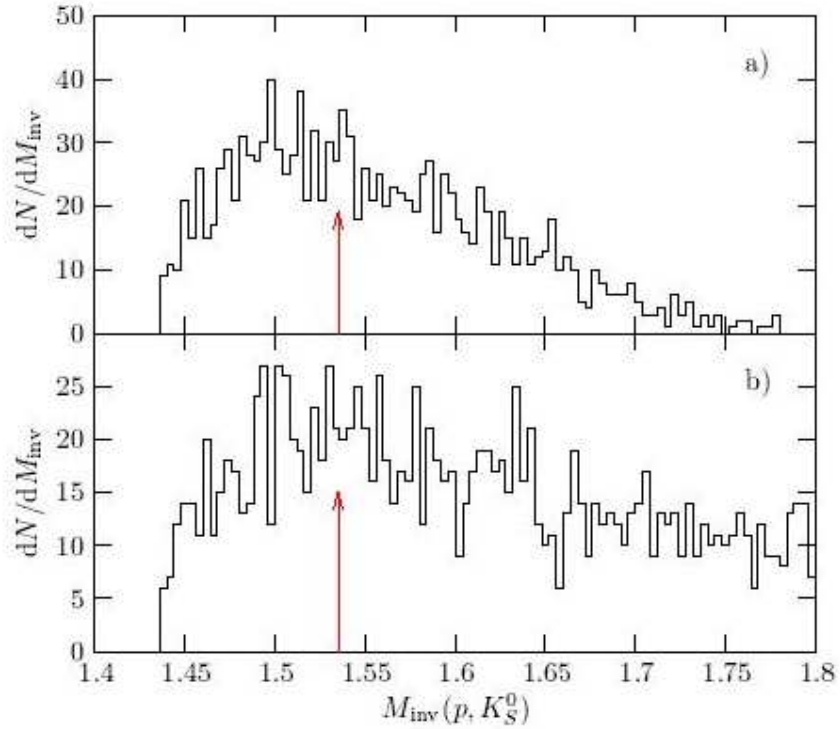


Figure 5: Invariant mass distribution of pK_S^0 pairs, if the $M_{\text{inv}}(pK_S^0k^-)$ invariant mass is in the ranges a.) $2.1\text{--}2.3 \text{ GeV}/c^2$ or b.) $2.5\text{--}2.7 \text{ GeV}/c^2$

Figure3: Excerpt from the NA49 report on the observation of the $\theta^+(1540)$.

momentum protons are lost, corresponding to very low momentum-transfer meson events. As a consequence, there is considerable background from baryon resonances, for example, $\gamma p \rightarrow \rho N^*$. Since no suitable cuts were found to eliminate these events from the partial wave analysis (PWA), they were incorporated in a coherent way. To our knowledge, this is the first time such an analysis has been conducted.

The results of this analysis have been very exciting. In the $J^{PC} = 1^{-+}$ exotic isovector wave, clear evidence for the $\pi_1(1600)$ is observed (see Fig. 4) with a mass and width consistent with the previous observation of E852. In addition, a $J^{PC} = 2^{+-}$ exotic isoscalar wave is observed (Fig. 5). This is the first observation of an isoscalar exotic, as well as the first observation of an exotic state with quantum numbers other than $J^{PC} = 1^{-+}$.

We are also currently analyzing the reaction $\gamma p \rightarrow \pi^+\pi^+\pi^-n$. Condo *et al.* [7] have reported possible evidence for an exotic $J^{PC} = 1^{-+}$ state at a mass of 1740 MeV/c² decaying to $\pi^+\pi^+\pi^-$; however the analysis was not a full partial wave analysis, but rather relied on angular distributions. While our analysis of this channel is not yet final, we now believe we understand the nature of this state. The results of the partial wave analysis are shown in Figs. 6 and 7. The $J^{PC} = 2^{++}$ partial wave clearly identifies the well-established $a_2(1320)$, while the high mass bump near 1700 MeV/c² appears to be the well-established $\pi_2(1670)$. Currently, there is scant evidence for the $\pi_1(1600)$ in this channel. This observation, taken with the clear evidence of the $\pi_1(1600)$ in the neutral exchange data described above, indicates an isoscalar exchange mechanism for this state.

2.3.3 Summary

While originally proposed as a exotic meson search, the g6c experiment has shown clear signals for *both* exotic mesons and exotic baryons, and has revitalized the field of hadron spectroscopy. The last PAC (PAC25) had seven pentaquark proposals and one exotic meson proposal, while the previous PAC had two letters-of-intent for exotic meson searches. Groundbreaking work on photoproduced exotic spectroscopy has been begun here, and will be followed by new experiments both at CLAS and ultimately the GlueX facility.

References

- [1] V. Kubarovsky, L. Guo, D.P. Weygand *et al.*, *Phys. Rev. Lett.* **92**, 032001 (2004);
- [2] T. Nakano *et al.*, *Phys. Rev. Lett.* **91**, 012002 (2003); arXiv:hep-exp/0301020.

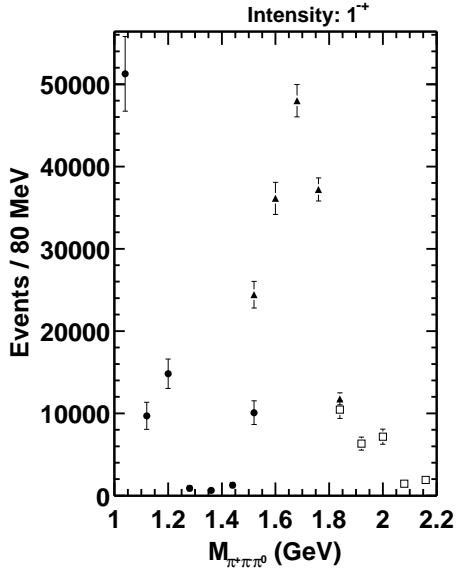


Figure 4: $J^{PC} = 1^{-+}$ partial wave from the exclusive reaction $\gamma p \rightarrow p\pi^+\pi^-\pi^0$.

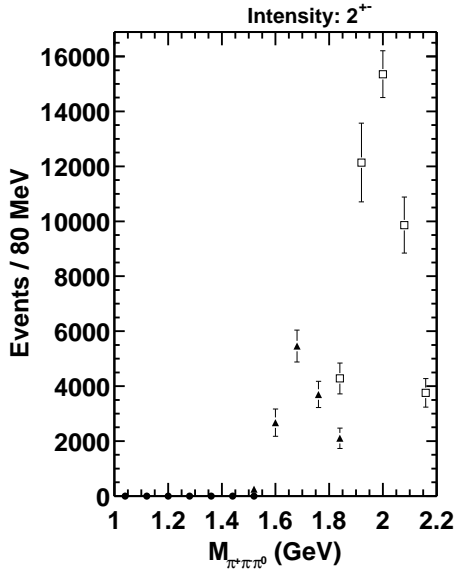


Figure 5: $J^{PC} = 2^{+-}$ partial wave from the exclusive reaction $\gamma p \rightarrow p\pi^+\pi^-\pi^0$.

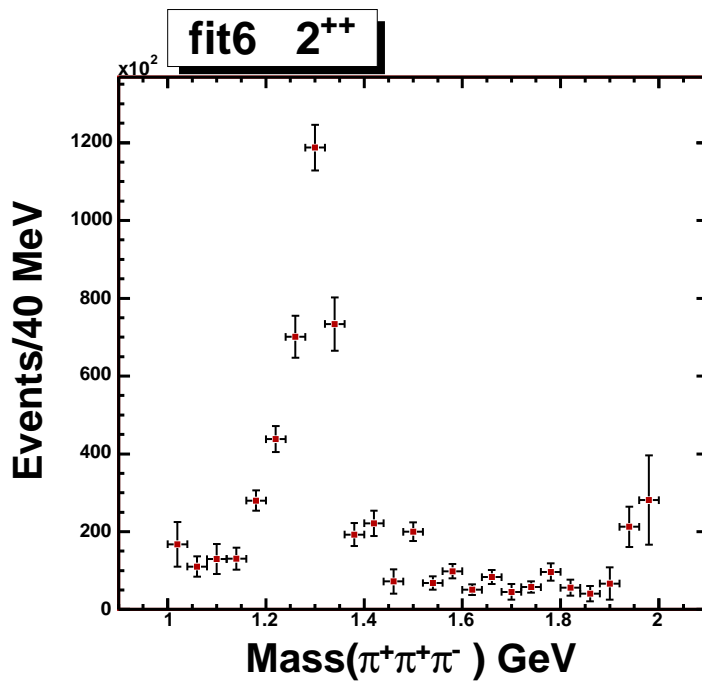


Figure 6: $J^{PC} = 2^{++}$ (a_2) partial wave from the exclusive reaction $\gamma p \rightarrow n\pi^+\pi^+\pi^-$.

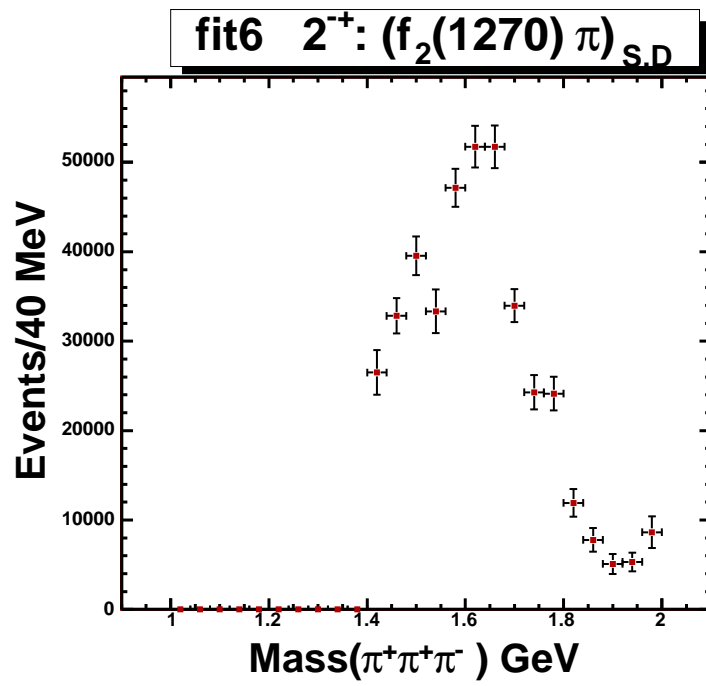


Figure 7: $J^{PC} = 2^{-+}$ (π_2) partial wave from the exclusive reaction $\gamma p \rightarrow n\pi^+\pi^+\pi^-$.

- [3] NA49 collaboration, D. Barna and F. Sikler, <http://na49info.cern.ch/cgi-bin/wwwd-util/NA49/FILE?ftp/NA49/Notes/Physics/thetaplus-bp.pdf>.
- [4] D. R. Thompson *et al.*, *Phys. Rev. Lett.* **79**:1630-1633,1997.
- [5] G. S. Adams *et al.*, *Phys. Rev. Lett.* **81**:5760-5763,1998.
- [6] E. I. Ivanov *et al.*, *Phys. Rev. Lett.* **86**:3877-3980,2001.
- [7] G. T. Condo *et al.*, *Phys. Rev. D***43**:2787-2791,1991.

2.4 g8a

CLAS-g8a: Photoproduction of Hyperons and Vector Mesons Using a Beam of Linearly Polarized Photons

We report on the status of the g8a analysis. The g8a run comprises the following experiments: E94-109 [1], E98-109 [2], E99-013 [3], and CAA 2001-02 [4].

The commissioning of the coherent Bremsstrahlung facility in Hall B and first data taking period for CLAS-g8 took place in the summer of 2001 [5]. We collected nearly 1.8 billion triggers, where at least one charged particle was detected in the CLAS for photon energies between 1.75 to 2.25 GeV, i.e. within the coherent peak. Between fall 2002 and spring 2003 the data were reconstructed on the JLab computer farm (or ‘cooked’ in CLAS parlance). Various tests and improvements on particle identification were performed to ensure the quality of the reconstructed data. The ‘cooked’ data were analyzed with respect to the following reactions:

$$\vec{\gamma}p \rightarrow p\rho^0 \rightarrow p\pi^+\pi^- \quad (1)$$

$$\vec{\gamma}p \rightarrow p\Phi \rightarrow pK^+K^- \quad (2)$$

$$\vec{\gamma}p \rightarrow p\omega \rightarrow p\pi^+\pi^-\pi^0 \quad (3)$$

$$\vec{\gamma}p \rightarrow K^+\Lambda \rightarrow K^+p\pi^- \quad (4)$$

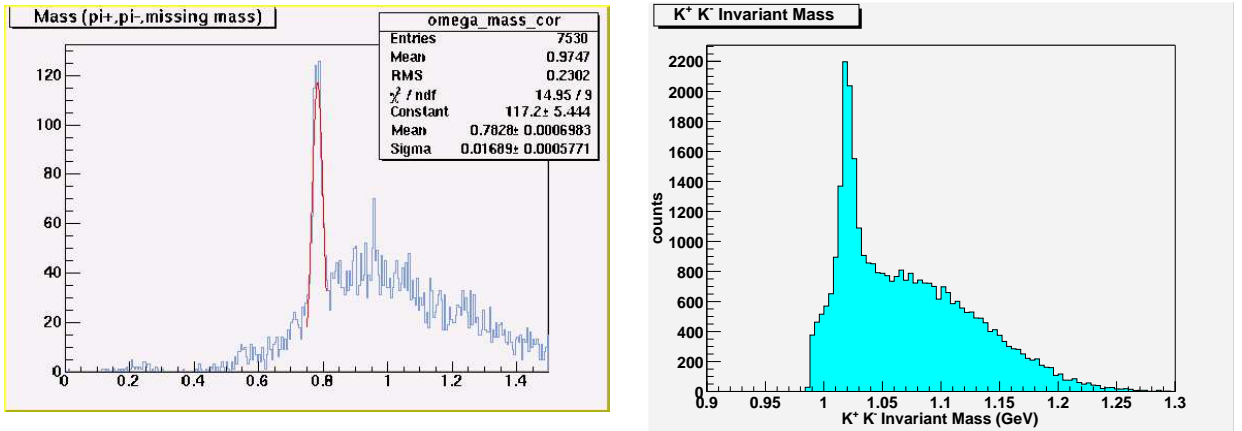


Figure 1: Invariant mass spectra $M(\pi^+\pi^-\pi^0)$ (left) and $M(K^+K^-)$ (right) for selected events showing prominent peaks of the produced ω meson (left) and Φ meson (right).

To extract the corresponding final-state particles of interest, we require identification of two positively charged particles ($p\pi^+$ or K^+p) in the data sample and we determine the

remaining particle by means of the missing mass technique. For the case of ω production all three charged particles must be detected. The invariant mass spectra as shown in Fig. 1 exhibit clear signals of the produced resonant states for the $p\omega$ and Φ channels. Separation of these resonant states from background is performed by means of sideband subtraction and/or fitting procedures.

The polarization of vector mesons can be described by combinations of density matrix elements [7], which are commonly presented in either the helicity frame or Gottfried-Jackson frame. Both coordinate frames refer to the decay plane of the vector meson, but are defined by different orientations of the quantization axis. After imposing background subtraction, we plot in the *left* panel of Fig. 2 the $\cos\theta_{hel}$ distribution of the Φ -meson over a wide range in t , the 4-momentum transfer squared. We see that this $\cos\theta_{hel}$ distribution assumes a $\sin^2\theta_{hel}$ -like behavior, which is characteristic of either Pomeron or positive-parity exchange in the t -channel. The data plotted as a function of Φ_{hel} have been normalized by the weighted CLAS acceptance. And as evidenced in the *right* panel of Fig. 2, we see a modulation of the Φ -meson production, which is typical for vector meson production using planar polarized photons.

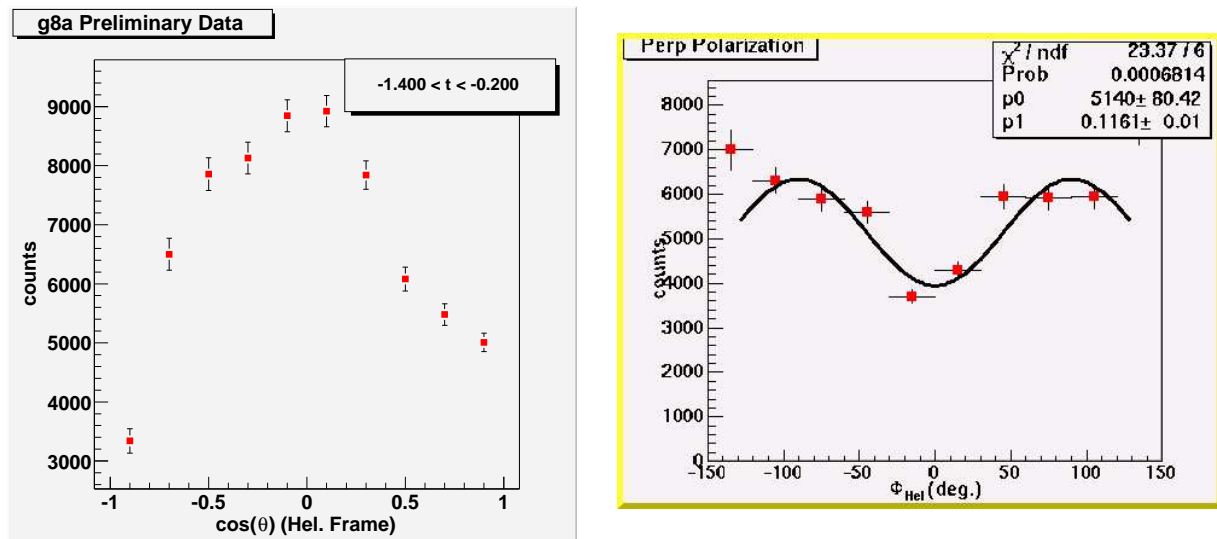


Figure 2: Decay distributions of $\Phi \rightarrow K^+K^-$ in the helicity frame for one of the data set of photon orientations. The data are plotted vs. $\cos\theta_{hel}$ on the left and vs. ϕ_{hel} on the right.

Photon beam asymmetries have been extracted for two reactions (1) and (4), forming the core of Ph.D. theses of our students (Christopher Gordon and Joseph Melone) at the University of Glasgow. Their respective analyses are fairly mature and we expect them both to graduate by summer, 2004. Preliminary results were first reported in Ref. [6].

Exclusive $\vec{\gamma}p \rightarrow p\pi^+\pi^-$ reactions are obtained by detecting all three outgoing particles in CLAS. The main problem of identifying a clean ρ^0 signal ($\rho^0 \rightarrow \pi^+\pi^-$ ($\simeq 100\%$)) are kinematical reflections of πN^* and $\pi\Delta^{(*)}$, where $N^*, \Delta \rightarrow \pi N$. The Dalitz plots in Fig. 3 show the problem of isolating the ρ^0 more clearly: The high intensity signal in both plots for $M^2(\pi^+\pi^-)$ around 0.6 GeV^2 corresponds to ρ^0 ; The horizontal bands passing through the vertical ρ^0 band correspond to the overlapping baryon resonances. Several cuts were performed to enhance the ρ^0 signal. The preliminary results presented below refer to $|t| < 0.45 \text{ GeV}^2$, since the identification deteriorates at larger momentum transfer.

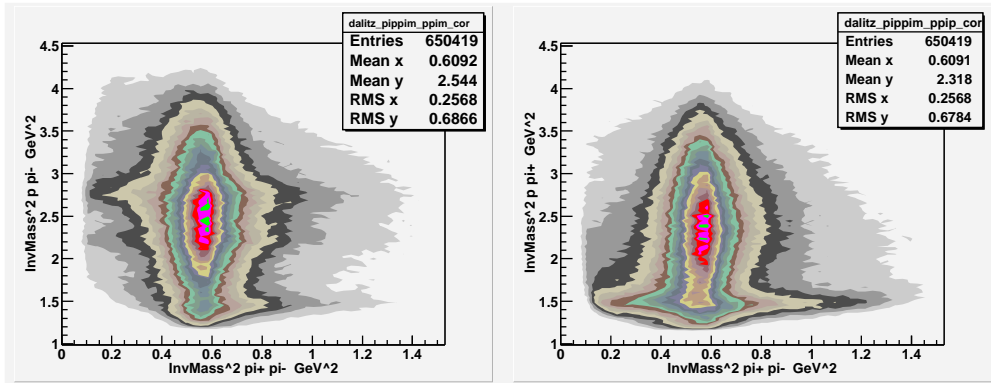


Figure 3: Dalitz plots showing the invariant mass squared $M^2(\pi^+\pi^-)$ against $M^2(p\pi^-)$ (*left*) and against $M^2(p\pi^+)$ (*right*). The ρ^0 signal appears as vertical (red) band centered around 0.6 GeV^2 , and overlapping baryon resonances appear as horizontal bands.

The photon beam asymmetry, Σ , can be extracted by measuring the yields, Y_{\parallel} and Y_{\perp} , of the ρ^0 to emerge in the plane of the photon polarization and perpendicular to it (eq. 5). An alternative definition of Σ can be obtained by integrating the complete angular distribution, $W(\cos\theta_{hel}, \phi_{hel}, \Phi)$, with respect to the polar and azimuthal angles, θ_{hel} and ϕ_{hel} , of the π^+ decay product in the helicity frame [7]. Integration over the decay angles yields eq. 6, where Φ is the angle between the photon polarization vector and the production plane and P_{γ} the degree of linear polarization. The large solid angle coverage of CLAS affords us an excellent means for making this measurement.

$$\Sigma = \frac{1}{P_{\gamma}} \frac{Y_{\parallel} - Y_{\perp}}{Y_{\parallel} + Y_{\perp}} \quad (5)$$

$$W(\Phi) = 1 - \Sigma P_{\gamma} \cos 2\Phi \quad (6)$$

A selection of perpendicularly linearly polarized photon data taken with the coherent edge at 2.0 GeV has been sampled to measure Φ . This measurement – in conjunction with an

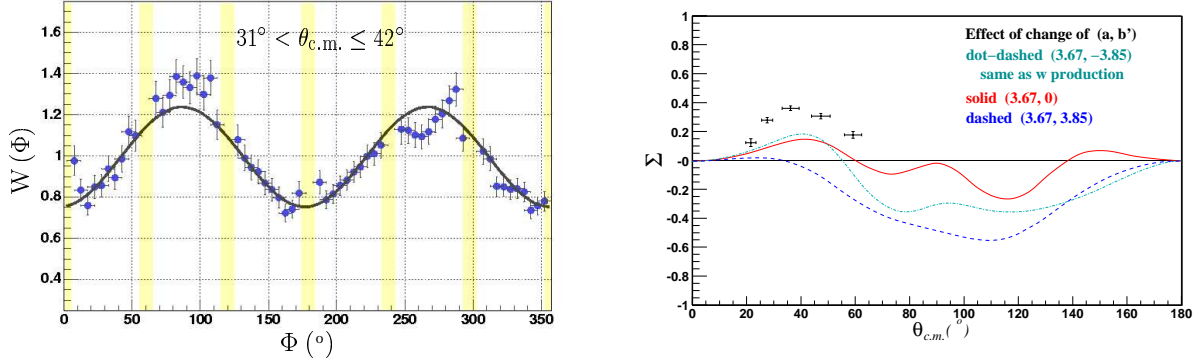


Figure 4: *Left*: Azimuthal distribution of ρ^0 for one bin in the production angle θ_{cm} ; the vertical shaded areas denote angular ranges where no data were collected due to limited detector acceptance. *Right*: Preliminary photon beam asymmetry of ρ^0 compared with model calculations from Qiang Zhao [8].

estimate of the degree of linear polarization – allows us to extract the photon asymmetry Σ by making use of eq. 6. We apply the same event selection criteria, with identical kinematic cuts, to the unpolarized data obtained from our amorphous radiator runs and extract the Φ behavior from this data set as well. To eliminate systematics and regions of non-fiducial acceptance, we divide the Φ distribution from the polarized data by the corresponding scaled unpolarized distribution. The results of this method are shown in Fig. 4 (*left*) for one bin in polar angle ($31^\circ < \theta_{c.m.} \leq 42^\circ$). In Fig. 4 (*right*) we plot the photon beam asymmetry parameter as a function of c.m. polar angle with a model calculation of Qiang Zhao [8] superimposed.

In the effort to extract the photon beam asymmetry for the reaction $\vec{\gamma}p \rightarrow K^+\Lambda$, we have analyzed the hyperon decay of $\Lambda \rightarrow p\pi^-$. The main problem of unambiguously determining this reaction comes from π^+ s bleeding into the K^+ signal. Demanding the kinematical constraint of detecting a negative pion in coincidence with the proton greatly reduces this contamination. Each set of the polarized data is normalized by the corresponding amorphous data set. This procedure reduces acceptance systematics resulting from the non-fiducial regions of CLAS.

In Fig. 5 (*left*) we plot the normalized azimuthal distribution for $K^+\Lambda$ production for one bin in $\theta_{cm}(K^+)$ for the data set with horizontally (*perp*) polarized photons. Since the differential cross section of $\gamma p \rightarrow K^+\Lambda$ for $E_\gamma \sim 2.0$ GeV peaks in forward direction, the preponderance of the data fall within the forward region of the CLAS detectors. The plot on the *right* panel in Fig. 5 shows the preliminary extracted photon beam asymmetry for three

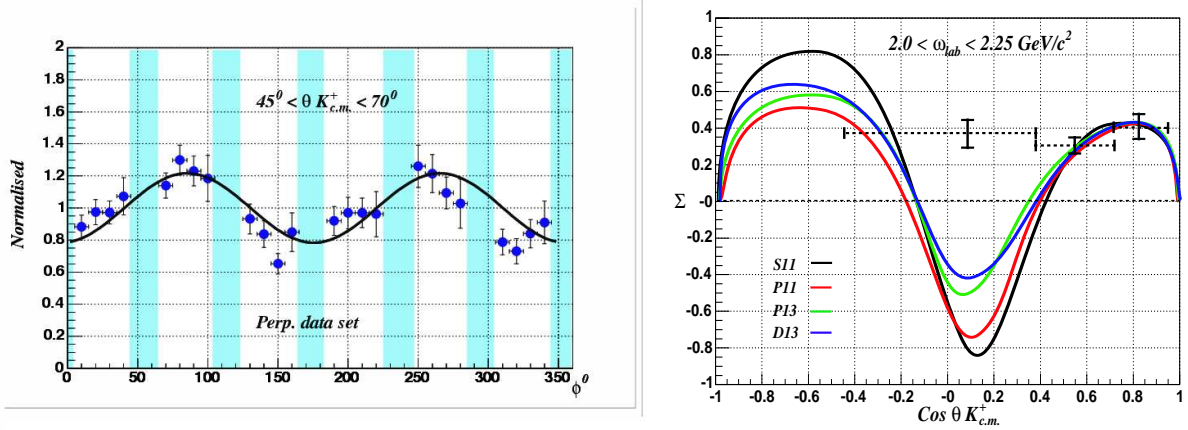


Figure 5: *Left*: Production rate of $K^+\Lambda$ as function of the azimuthal $\phi_{lab}(K^+)$ for horizontal (*perp*) photon polarization. The vertical shaded areas denote angular ranges where no data could be collected due to limited detector acceptance. *Right*: Preliminary photon beam asymmetry of $\vec{\gamma}p \rightarrow K^+\Lambda$ compared with model calculations [9] including a set of possible “missing” resonances (see text for description).

bins in $\theta_{cm}(K^+)$, where we superimpose quark model calculations by Stijn Janssen [9, 10]. These predictions relate to the presence or absence of various resonances. Several resonant states have been identified as possibly contributing to the differential cross section of the $K^+\Lambda$ channel. The different color-coded curves plotted in Fig. 5 refer to adding the contribution of a given resonance – either established or “missing” – to the calculation. This calculation incorporates Born terms and a core set of baryon resonances (see Ref. [10] for more details). The color scheme refers to the following resonances; $S_{11}(1650)$ (*black*), $P_{11}(1710)$ (*red*), and $P_{13}(1720)$ (*green*). The blue line refers to the “missing resonance” $D_{13}(1895)$.

References

- [1] “Photoproduction of ρ Mesons from the Proton with Linearly Polarized Photons,” cospokespersons: P.L. Cole, J.P. Connelly, and K. Livingston, Jefferson Lab E94-109.
- [2] “Photoproduction of ϕ Mesons with Linearly Polarized Photons,” cospokespersons: D.J. Tedeschi, P.L. Cole, and J.A. Mueller, Jefferson Lab E98-109.
- [3] “Photoproduction of ω Mesons off Protons with Linearly Polarized Photons,” cospokespersons: F.J. Klein and P.L. Cole, Jefferson Lab E99-013.

- [4] “Photoproduction of Associated Strangeness using a Linearly Polarized Beam of Photons,” cospokespersons: J. Kellie, F.J. Klein, and J.C. Sanabria, CLAS Approved Analysis 2001-02.
- [5] P.L. Cole *et al.*, “The Commissioning of the Hall-B Beamline of Jefferson Lab for Coherently Producing a Beam of Linearly-Polarized Photons,” Conf. Proc., EMI2001 – Osaka, Japan, Dec. 2001. World Scientific, 2002.
- [6] C. Gordon, J. Melone *et al.*, “Vector Meson and Associated Strangeness Production Using a Linearly Polarized Photon Beam at Jefferson Lab,” Conf. Proc., 2nd Intl. Conf. on Nucl. and Part. Physics with CEBAF – Dubrovnik, Croatia, May 2003. To be published in World Scientific.
- [7] K. Schilling, P. Seyboth, and G. Wolf, Nucl. Phys. **B15**, 397 (1970); D. Schildknecht and B. Schrempp-Otto, Nuovo Cim. **5A**, 185 (1971).
- [8] Q. Zhao, The University of Surrey, Qiang.Zhao@surrey.ac.uk, *private communication*.
- [9] S. Janssen, J. Ryckebusch, D. Debruyne, and T. Van Cauteren, Phys. Rev. **C65**, 015201 (2001).
- [10] S. Janssen, D.G. Ireland, and J. Ryckebusch, Phys. Lett. B **562**, 51 (2003).

2.5 E89-017

Electroexcitation of the $\Delta(1232)$ in Nuclei

J. D. Kellie[†], D. Branford[‡], D. Protopopescu^{†,1},

D. G. Ireland[†], J. Donnelly[†], K. Livingston[†]

[†]*Glasgow University, Glasgow G12 8QQ, United Kingdom*

[‡]*Edinburgh University, Edinburgh EH9 3JZ, United Kingdom*

(for the CLAS collaboration)

2.5.1 Introduction

Electroproduction of the $\Delta(1232)$ from the nucleon is well understood and as a low energy resonance it dominates the low energy cross-sections of the electron-induced reactions in nuclei, reasonably well separated from broader higher resonances. It is then not surprising that $\Delta(1232)$ is the favorite choice in studies of nuclear-medium effects on resonances. Extensive theoretical literature was devoted to characterizing the electromagnetic excitation of the $\Delta(1232)$ and experimental studies of this resonance carried out within the last two decades were numerous.

In studies carried out using inclusive reactions the $\Delta(1232)$ is identified by calculating the invariant mass W of the hadronic system

$$W^2 = (\omega + M)^2 - \mathbf{q}^2 = M^2 + 2\omega M - Q^2 \quad (1)$$

with the usual notations and M the mass of the nucleon. In one of the most noted articles on this subject Sealock [Se89] used a wide collection of data to perform a systematic study of the $\Delta(1232)$ resonance. It appeared that the $\Delta(1232)$ peak position and width varied with the Q^2 of the virtual photon and with the A of the target nuclei. However, these conclusions are open to question for two reasons. Firstly, because they were based on inclusive data and the $\Delta(1232)$ separation from competing processes - non-resonant pion production (Born terms), two-nucleon knockout, higher resonances - was unavoidably model-dependent. Secondly, data originated from several independent experiments, and then the relative accuracy of the calibrations of the various small-acceptance configurations could have had a major impact.

The present experiment is based on proposal E89-017 [SP89] and aims to use semi-exclusive data, to verify these results. Using semi-exclusive channels gives better control of the background contributions. As opposed to equation (1), in a semi-exclusive measurement the four-vector of the resonance can be reconstructed from the four-vectors of the detected

¹email: protopop@jlab.org

decay products:

$$M_{\Delta}^2 = (P_{\Delta})^2 = (P_p + P_{\pi})^2 \quad (2)$$

where π^- is detected directly and π^0 at its turn through its decay into two photons.

If Sealock's findings could be reproduced in this context, the consequences would be significant, since it would mean that the properties of nuclear constituents are sensitive to the form of excitation and prove that this sensitivity can be assessed directly in electron scattering experiments.

2.5.2 Experiment and Analysis Status

Currently we analyze ^3He data recorded during the e2a (1.162 GeV) and e2b (0.984 GeV) runs, the latter one containing roughly 4 times more statistics. Data were acquired with the CLAS "single electron trigger" configuration. Further improvements in the electron identification were performed off line: vertex cuts were used to eliminate events originating in the windows and temperature shield of the liquid target cell [Pr04], electron momentum corrections were applied to compensate for drift chamber misalignments and uncertainties in the magnetic field mapping. Software fiducial cuts are used to exclude regions of non-uniform detector response. Detector acceptance and tracking efficiencies are estimated using GSIM².

Following the procedures outlined above analyses of the 1.162 GeV e2a data with ^3He and ^{12}C targets were reported in [WI03, SM03], where none of the Q^2 dependence of the $\Delta(1232)$ was reproduced. More refined analysis is currently underway. Simulations were used to correct the proton energy losses in the target material [Pr04]. Radiative effects and bin migration in W, Q^2 coordinates were studied [Pr04]. Fermi motion effects were tested with various phase-space generators and proved to be of little importance in acceptance calculations [Pr04]. Final state particles originating from the Δ decay are identified by missing energy and momentum cuts combined with a restriction on the angle between the momenta of the virtual photon and the ejected Δ . Acceptance-corrected data are binned in Q^2 (0.10 – 0.55 GeV²/c²) and the resonance peak and background are fitted with a double Gaussian to determine the Delta peak position and width. The $\Delta(1232)$ mass is constructed in three alternative ways and the results compared with each other.

²The CLAS GEANT Monte-CARLO Simulation software

2.5.3 Preliminary Results

Preliminary results from the undergoing study of the $(e, e'p\pi^-)$ channel are presented in Figure 1. Although the $(e, e'p\pi^0)$ channel is expected to be 'cleaner', the e2a statistics for this channel are too low to permit any pronouncements now. We are working on the e2b data which is currently at the kinematic corrections and fiducial cuts stage [Do04].

While two-nucleon knockout contributions are minimized by kinematic cuts, contributions from Born terms and higher resonances are to be estimated using MAID-2000 [DT92] theoretical calculations that are currently underway.

If nucleon Fermi motion would be taken into account in the definition of W , equation (1) would have to be rewritten as

$$W_{corr} = \left[W^2(1 + \xi) + Q^2\xi/2M - \xi M^2/2M \right]^{1/2} \quad (3)$$

where $\xi \approx 0.05$ for Fermi momenta of the nucleon of approximately 150 MeV ($p_f^2 = k_F^2/2$, with $k_F = 272$ MeV for proton and $k_F = 216$ MeV for neutron). The quantity W_{corr} calculated as in (3) is also present on Figure 1.

In conclusion, our findings appear to not match the results from [Se89]. However, more confidence is to be attained once the analysis of the e2b batch of data is finalized. Furthermore, studies of the angular distributions of the decay products in the Δ 's center of mass as well as investigation of the momentum-dependent potentials in ${}^3\text{He}$ will complement the present study and give further insight into the structure and dynamics of the $\Delta(1232)$ formation and decay.

References

- [Se89] R. Sealock *et al.*, Phys. Rev. Lett. **62** (1989) 1350
- [SP89] R. Sealock *et al.*, CLAS proposal PR-89-017 (1989)
- [SM03] S. McLauchlan, Ph.D. Thesis, unpublished
- [WI03] W. Ingram, Ph.D. Thesis, unpublished
- [Pr04] D. Protopopescu, Analysis website
URL: http://nuclear.gla.ac.uk/protopop/work/e2a_delta/

[Do04] J. Donnelly, Analysis website
URL: <http://nuclear.gla.ac.uk/joseph/>

[DT92] D. Drechsel and L. Tiator, J. Phys. G, **18** (1992) 449

PRELIMINARY

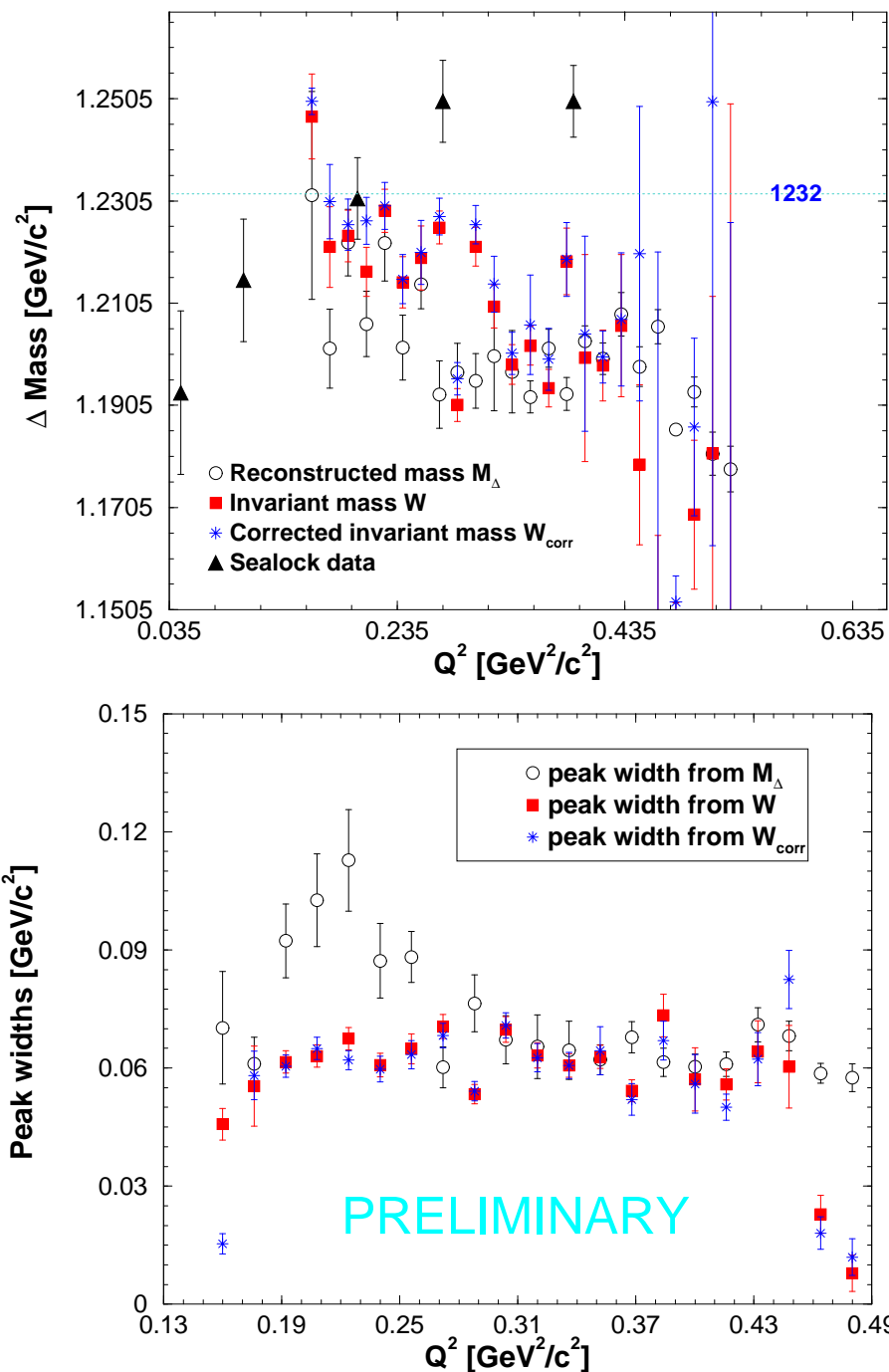


Figure 1: Dependence of $\Delta(1232)$ peak position (upper plot) and width (lower plot) versus Q^2 extracted from ${}^3\text{He}(e, e'p\pi^-)$ e2a data at $E_{beam} = 1.162$ GeV. The three quantities M_Δ , W and W_{corr} are defined by equations (2), (1) and (3) respectively. Sealock data from [Se89] is shown in black triangles on the upper graph. Errors shown are statistical.

2.6 E89-036

Study of Short-Range Properties of Nuclear Matter in Electron-Nucleus and Photon-Nucleus Interaction with Backward Particles using the CLAS Detector

K. Egiyan

2.6.1 Introduction

Due to the strong interaction and short distances between the nucleons in nuclei, there is a significant probability for nucleon wave functions to overlap, resulting in short range nucleon-nucleon correlations (SRC) in nuclei [Fr81,88]. Investigation of SRC is important for at least two reasons. First, because of the short range nature of these correlations, they should contribute significantly to the high-momentum component of the nuclear wave function. Second, scattering from nucleons in SRC will provide unique data on the modification of deeply bound nucleons, which is extremely important for a complete understanding of nucleon structure in general.

2.6.2 Experiment Status

This proposal has been included in E2 run experiment. Measurements and data calibration of the E2 run are finished. Currently, data analysis is in progress. Some data already are published [Eg03].

2.6.3 Results - or Expected Results

1. Study of SRC in the $A(e, e')$ reaction at $x_B > 1$ High-energy inclusive electron scattering from nuclei, $A(e, e')$, is one of the simplest ways to investigate SRC. In particular, it is probably the best way to measure the probabilities of SRC in nuclei. The main problem in these studies is selecting the electron-SRC scattering events from the orders-of-magnitude larger background of inelastic and/or quasi-elastic interaction of electrons with the uncorrelated low-momentum nucleons.

Inclusive $A(e, e')$ scattering at large x_B (i.e., on the low missing energy side of the

quasi-elastic peak) samples quasi-elastic scattering from nucleons with large Fermi momentum with negligible contamination from inelastic processes. In the mean field approximation when the electron scatters on a single nucleon with a residual (A-1) spectator, the nucleon minimum missing momentum p_m contributing to the reaction can be found by measuring the kinematical variables Q^2 and x_B of the scattered electron [Sa01],[Eg03]. Particularly, in $d(e, e')$ scattering the $Q^2 > 1.4$ (GeV/c)², $x_B > 1.5$ cuts correspond to the $p_m > 0.3$ GeV/c cut. Therefore, by the certain Q^2, x_B restriction we can effectively suppress the quasielastic interaction of electrons with low-momentum (uncorrelated) nucleons. On the other hand, at $p_m > 0.3$ GeV/c, nucleon momentum distributions in light and heavy nuclei are similar [Ci96], [Pi92]. This implies that they (momentum distributions) originate predominantly from interactions between nearby nucleons, *i.e.* they are due to short range correlations (SRC). Based on these two observations one can expect that in the high-momentum region (at $p_m > 0.3$ GeV/c) the ratio of weighted (e, e') cross sections ¹ for heavy and light nuclei should scale, *i.e.* they should be independent of electron scattering variables (Q^2 and x_B), with the magnitude of the scaling factor being proportional to the relative probability of SRC in the two nuclei [Fr93].

The ratios $r(A, {}^3\text{He})$ of the cross sections for heavy nuclei and ${}^3\text{He}$ are measured at $0.7 < Q^2 < 2.6$ (GeV/c)² and $0.8 < x_B < 3.0$, for ${}^4\text{He}$, ${}^{12}\text{C}$ and ${}^{56}\text{Fe}$. In Fig.1 they are shown for ${}^{56}\text{Fe}$. It has been obtained that for all nuclei used: (i) at $Q^2 < 1.4$ the ratios increase with x_B in the entire $1 < x_B < 3$ range (see Fig.1a), while (ii) at $Q^2 > 1.4$ (GeV/c)² ratios scaled in two x_B regions: $1.5 < x_B < 2$ and $2.3 < x_B < 3$ (see Fig.1b).

This is an indication that in the scaling regions, indeed: (i) the shapes of high momentum distributions are the same for all nuclei, and only differ by a scale factor, and (ii) SRC dominate the nuclear wave function at large Fermi momenta.

The values of observed scaling factors can be related to the relative probabilities of 2- and 3-nucleon SRC in nuclei with $A \geq 3$.

Our data allows us: (i) To extract the per-nucleon probabilities of 2-nucleon SRC in nuclei ${}^4\text{He}$, ${}^{12}\text{C}$, and ${}^{56}\text{Fe}$, using the calculated and other measured [Fr93] (${}^3\text{He}/\text{Deuterium}$) ratio. (ii) To obtain directly, for the first time, the per-nucleon probabilities of 3-nucleon SRC in the same nuclei relative to the ${}^3\text{He}$.

These data are shown in Table I and in Fig.2.

One can see that: (i) both probabilities have weak A-dependences at $A \geq 12$ and relatively stronger A-dependences at $A < 12$; (ii) per-nucleon probabilities of 3-nucleon SRC are systematically lower than the same of 2-nucleon SRC, in agreement with SRC model predictions [Fr81,88],[Fr93].

¹By the weighted ratio of the cross sections we mean the ratios of the cross sections weighted by A .

	$a_2(A,D)$	$a_3(A, {}^3\text{He})$	$\frac{a_3(A, {}^3\text{He})}{a_2(A,D)}$
${}^3\text{He}$	1.96 ± 0.1	–	–
${}^4\text{He}$	$3.85 \pm 0.21 \pm 0.03$	1.83 ± 0.21	$0.47 \pm 0.08 \pm 0.04$
${}^{12}\text{C}$	$4.93 \pm 0.27 \pm 0.28$	3.68 ± 0.23	$0.75 \pm 0.06 \pm 0.04$
${}^{56}\text{Fe}$	$5.90 \pm 0.32 \pm 0.34$	5.10 ± 0.27	$0.86 \pm 0.06 \pm 0.05$

Table 1: $2(a_2)$ - and preliminary $3(a_3)$ -nucleon SRC relative probabilities.

2. Study of Momentum Distributions in Light Nuclei (Deuterium, ${}^3\text{He}$) at High Momenta.

Our next step in the studying of short range properties of nuclei is to investigate the momentum distributions of nucleons in reaction $A(e, e' p)A-1$ in momentum range (300 - 600 MeV/c) where SRC contribution is dominant in nuclei wave function. A main and very hard problem here is to separate SRC contribution from the FSI contribution. The latter dominates in measured cross sections at momenta > 300 MeV/c. Very preliminary analysis demonstrates that this can be done at least for the deuterium target. Therefore we will start with Deuterium.

References

- [Eg03] K.Sh. Egiyan *et al.*, Phys.Rev. C **68**, 014313 (2003).
- [Fr81,88] L.L. Frankfurt, M.I. Strikman, Phys. Rep. **76**, 215(1981); **160**, 235(1988).
- [Sa01] M.M. Sargsian, International Journal of Modern Physics E, **10**, 405(2001)
- [Ci96] C. Ciofi degli Atti, Phys.Rev. C **53**, 1689, (1996).
- [Pi92] S.C. Pieper, R.B. Wiringa, and V.R. Pandharipande, PRC46, 1741(1992)
- [Fr93] L.L. Frankfurt *et al.*, Phys. Rev. C **48**, 2451 (1993).

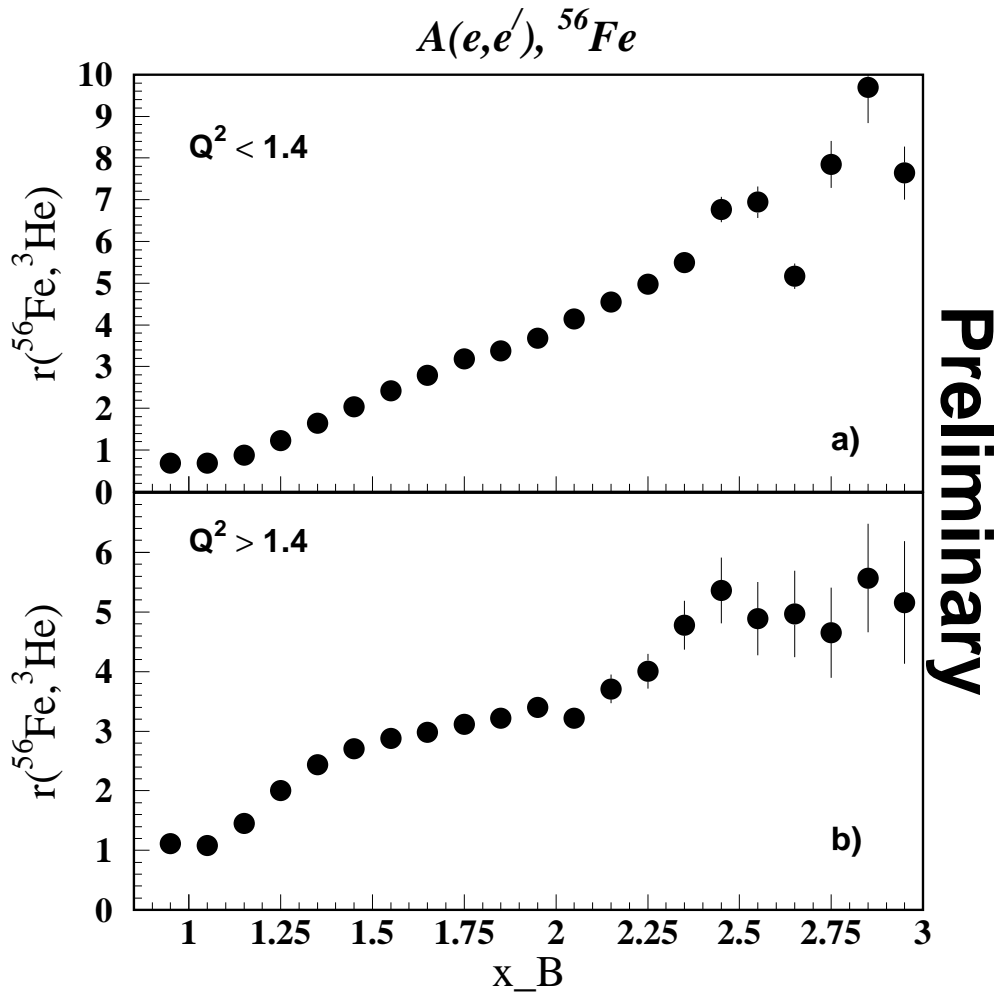


Figure 1: The ratios of $A(e, e')$ cross sections for ${}^{56}\text{Fe}$ and ${}^3\text{He}$ nuclei. At $x_B > 1$: a) - does not include, b) - includes the high ($p_m > 0.3$ GeV/c) Fermi momenta. Note that one of the explanations of the onset of the second scaling at $x_B > 2.3$ (not at $x_B > 2$) is the electron scattering off moving 2-nucleon SRC.

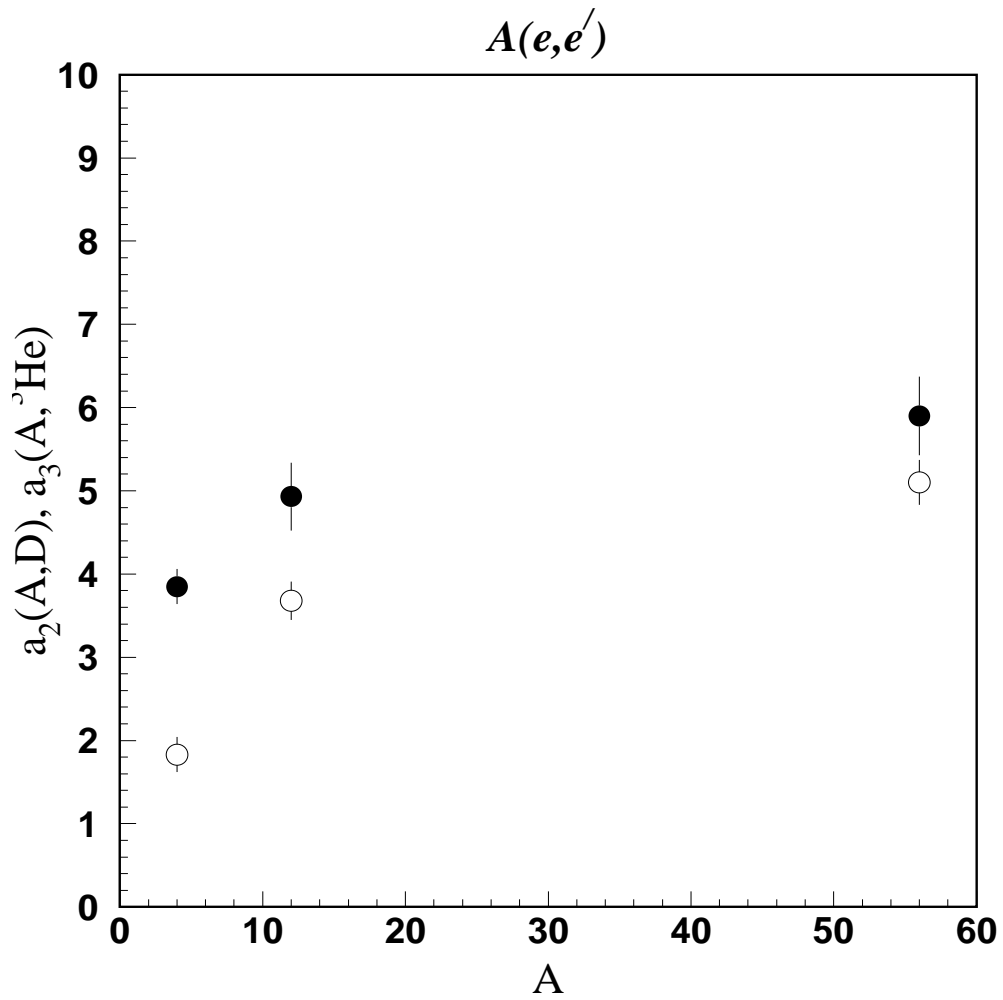


Figure 2: • - $a_2(A, D)$ - the per-nucleon probabilities of 2-nucleon SRC in nuclei relative to deuterium; ○ - (preliminary) $a_3(A, {}^3\text{He})$ - the same probabilities of 3-nucleon SRC in nuclei relative to the ${}^3\text{He}$.

2.7 E89-042

Measurement of the Electron Asymmetry in $p(\vec{e}, e'p)\pi^0$ and $p(\vec{e}, e'\pi^+)n$
in the Mass Region of the $\Delta(1232)$ for $Q^2 < 2(\text{GeV}/c)^2$

V. Burkert and R. Minehart (Spokespersons)
K. Joo and L.C. Smith
and the CLAS Collaboration

2.7.1 Introduction

The goal of the experiment is to measure the electron spin asymmetry and the so-called 5th response function for the charged and neutral pion channels in the resonance region, especially for the $\Delta(1232)$. This provides new and unique information on the interference between resonant and non-resonant amplitudes in pion production. The excitation of the nucleon through electromagnetic interactions is an essential tool in the study of hadronic structure. However, the excited states of the nucleon rapidly decay through emission of pions. Thus the excitation mechanism involves both hadron structure and reaction dynamics, intermixing quark and meson degrees of freedom. To analyze these resonant and non-resonant components, a variety of theoretical approaches have been developed, e.g. chiral perturbation theory, dispersion relations, effective Lagrangian and dynamical models and most recently, lattice QCD. These predictions are subject to considerable model dependence from the treatment of higher order πN rescattering in the initial and final state. By utilizing polarized electron beams to measure single spin polarization observables, one can directly measure the imaginary part of interfering amplitudes. In this way, non-resonant contributions are greatly amplified by the imaginary part of the dominant $\Delta(1232)$ $M_{1+}^{3/2}$ resonant multipole. Measurements of both $p\pi^0$ and $n\pi^+$ channels are essential to test the consistency of the models, since $n\pi^+$ channel is dominated by the Born t -channel pion pole and contact terms, which are absent in the $p\pi^0$ channel.

2.7.2 Experiment Status

Data have been taken mostly at 1.5 GeV and 2.5 GeV during the E1c and E1d run periods in spring 1999 and 2000, and at 1.0 GeV and 2.0 GeV during the E1e run period in 2003. Electron polarization was in the range from 0.6 to 0.7. This report deals only with the data from the E1c run period. The analyses of the π^0 data set have been completed and

published in Physical Review C [1]. The analyses of the π^+ data set have been completed, and a detailed analysis report and a draft of a Physical Review paper was submitted to the Structure of Nucleon Working Group for its review [2]. The results from these analyses have been presented in many invited and contributed talks at conferences around the world.

2.7.3 Results - or Expected Results

For polarized beam and unpolarized target, differential cross section $d^2\sigma^h$ depends on the transverse ϵ and longitudinal ϵ_L polarization of the virtual photon through five structure functions: σ_T , σ_L , and their interference terms σ_{TT} , σ_{LT} , and $\sigma_{LT'}$:

$$\frac{d^2\sigma^h}{d\Omega_\pi^*} = \frac{p_\pi^*}{k_\gamma^*}(\sigma_0 + h\sqrt{2\epsilon_L(1-\epsilon)}\sigma_{LT'}\sin\theta_\pi^*\sin\phi_\pi^*) \quad (1)$$

$$\begin{aligned} \sigma_0 &= \sigma_T + \epsilon_L\sigma_L + \epsilon\sigma_{TT}\sin^2\theta_\pi^*\cos 2\phi_\pi^* \\ &+ \sqrt{2\epsilon_L(1+\epsilon)}\sigma_{LT}\sin\theta_\pi^*\cos\phi_\pi^*, \end{aligned} \quad (2)$$

where $(p_\pi^*, \theta_\pi^*, \phi_\pi^*)$ are the π^0 c.m. momentum, polar and azimuthal angles, $\epsilon_L = (Q^2/|k^*|^2)\epsilon$ and k_γ^* and $|k^*|$ are the virtual photon c.m. momentum and real photon c.m. equivalent energy. h is the electron beam helicity ($h = \pm 1$). The electron beam asymmetry $A_{LT'}$ is directly proportional to the polarized longitudinal-transverse structure function $\sigma_{LT'}$:

$$A_{LT'} = \frac{d^2\sigma^+ - d^2\sigma^-}{d^2\sigma^+ + d^2\sigma^-} \quad (3)$$

$$= \frac{\sqrt{2\epsilon_L(1-\epsilon)}\sigma_{LT'}\sin\theta_\pi^*\sin\phi_\pi^*}{\sigma_0}, \quad (4)$$

where $d^2\sigma^\pm$ is the differential cross section for positive and negative electron beam helicities.

Experimentally, $A_{LT'}$ is determined by scaling the measured asymmetry A_m by the magnitude of the electron beam polarization P_e :

$$A_{LT'} = \frac{A_m}{P_e} \quad (5)$$

$$A_m = \frac{N_{\pi^+} - N_{\pi^-}}{N_{\pi^+} + N_{\pi^-}}, \quad (6)$$

where N_π^\pm is the number of π^0 events for each electron beam helicity state. Acceptance and normalization factors cancel in A_m , making this observable largely free from systematic errors. Radiative corrections were applied using the program recently developed by Akusevich

et al. for exclusive pion electro-production [3]. Corrections were also applied to compensate for cross section variations over the width of a bin. $A_{LT'}$ is determined for individual bins of $(Q^2, W, \cos\theta_\pi^*, \phi_\pi^*)$ as shown in Figure 1 obtained from CLAS data, then multiplied by unpolarized cross section σ_0 which also can be obtained from CLAS data. $\sigma_{LT'}$ will be extracted by fitting the ϕ_π^* distributions with the form in Equation 4.

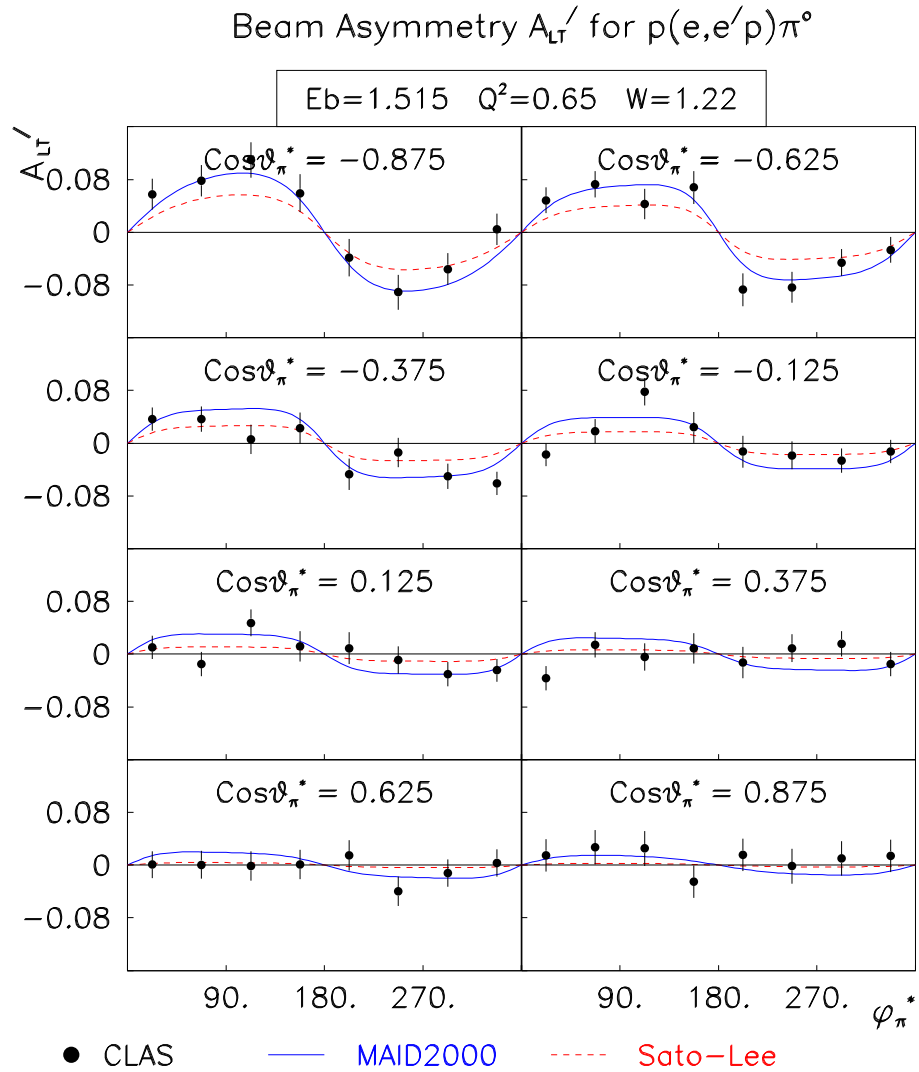


Figure 1: $A_{LT'}$ versus ϕ_π^* for different $\cos\theta_\pi^*$ bins measured at $Q^2= 0.40 \text{ GeV}^2$. Various curves show model predictions. Errors are statistical only.

Figure 2 shows our measurement of σ_{LT} for the $\pi^0 p$ channel (top) [4], $\sigma_{LT'}$ for the $\pi^0 p$ channel (middle) [1] and $\sigma_{LT'}$ for the $\pi^+ n$ channel (bottom) [2]. Also shown are recent model calculations using Sato and Lee (SL) dynamical model [5], the Dubna-Mainz-Taipei

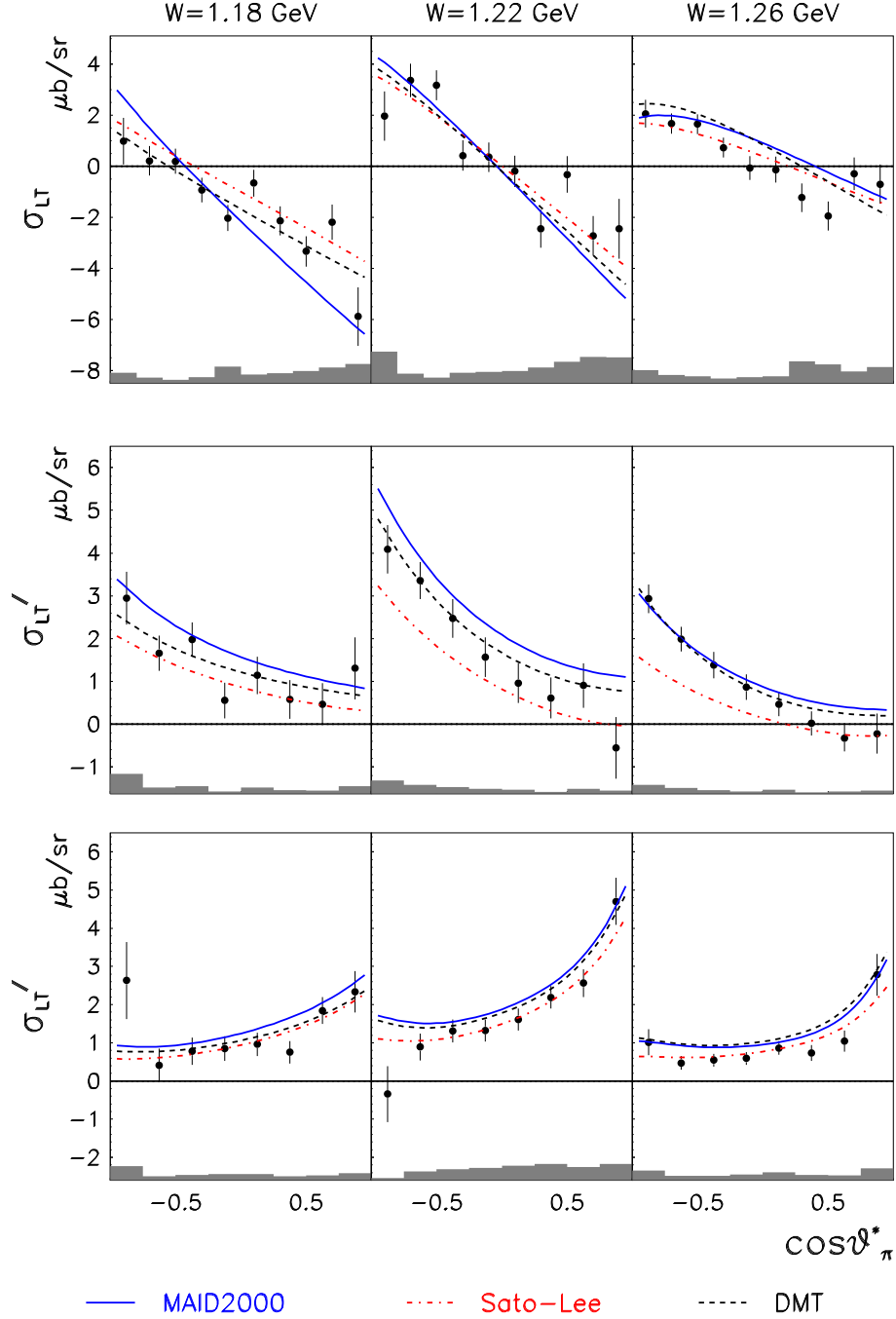


Figure 2: L-T interference structure functions versus $\cos\theta_\pi^*$ extracted at $Q^2=0.40\text{ GeV}^2$ for different W bins. Shaded bars show systematic errors. Various curves show model predictions. σ_{LT} from $\pi^0 p$ channel (top), $\sigma_{LT'}$ from $\pi^0 p$ channel (middle), and $\sigma_{LT'}$ from $\pi^+ n$ channel (bottom)

(DMT) model [6], and the Mainz unitary isobar model (MAID2000) [7]. These models combine resonant amplitudes with background arising from Born diagrams and t-channel vector meson exchange. All models predict nearly the same unpolarized structure function σ_{LT} for the $\pi^0 p$ channel at the $\Delta(1232)$ mass (top panel for $W = 1.22$ GeV), but they differ in their handling of non-resonant contributions (middle panel for $W = 1.22$ GeV). The measured angular distributions for the $\pi^+ n$ channel (bottom panel) show a strong forward peaking for W bins around the $\Delta(1232)$ mass, in contrast to the $\pi^0 p$ channel (middle panel), where backward peaking is seen. While the calculations describe the peaking behavior qualitatively, the largest model variation occurs in the overall magnitude of σ_{LT} , although this is substantially smaller for the $\pi^+ n$ channel. This may result from the strong t -channel pion pole term which is absent in the $\pi^0 p$ channel.

References

- [1] K. Joo *et al*, Phys. Rev. C **68**, 032201 (2003).
- [2] K. Joo *et al*, to be submitted to Phys. Rev. C
- [3] A. Afanasev, I. Akushevich, V.D. Burkert, K. Joo, Phys. Rev. D **66** 074004 (2002)
- [4] K. Joo *et al*, Phys. Rev. Lett., **88**, 122001 (2002).
- [5] T. Sato and T.-S.H. Lee, Phys. Rev. C **63**, 055201 (2001).
- [6] S.S. Kamalov and Shin Nan Yang, Phys. Rev. Lett. **83**, 4494 (1999).; S.S. Kamalov, S.N. Yang, D. Drechsel, O. Hanstein, L. Tiator, nucl-th/0006068.
- [7] D. Drechsel, O. Hanstein, S.S. Kamalov, L. Tiator, Nucl. Phys. **A645**, 145 (1999). Cross sections were calculated from $p\pi^0$ multipoles (up to L=5) downloaded from the MAID web page: <http://www.kph.uni-mainz.de/T/maid/maid.html>.

2.8 E91-023

Measurement of Polarized structure Functions in Inelastic Electron Scattering using CLAS

Volker Burkert, Donald Crabb and Ralph Minehart (Spokespersons)
and the CLAS Collaboration

2.8.1 Introduction

Experiment 91-023 is a major part of the “EG1” run group in Hall B. Polarized electrons are scattered from longitudinally polarized NH_3 targets in the CEBAF Large Acceptance Spectrometer (CLAS) to study inclusive polarization observables. The beam-target spin asymmetries are sensitive to interference between small and large amplitudes, and are expected to help in disentangling the contributions of overlapping resonances as well as to measure amplitudes not otherwise accessible. A focal point of the experiment is the determination of the resonant contribution to the integral of $\int g_1^p(x, Q^2) dx$ which is constrained by the Gerasimov-Drell-Hearn (GDH) sum rule [1] at $Q^2 = 0$ and by the quark axial charges at high Q^2 .

2.8.2 Experiment Status

During the first run of EG1 in the fall of 1998, about 35% of the approved data set for 91-023 was taken with beam energies of 2.5 GeV and 4.2 GeV with a 50%–70% polarized $^{15}\text{NH}_3$ target. By taking data with different values of the CLAS torus field (magnitude and polarity) we were able to accumulate data over a large range of Q^2 (from $Q^2 = 0.1$ to $Q^2 = 2.7$) and W (up to a maximum of $W \approx 2.5$ GeV). The analyses of the inclusive data set was the basis for the Ph.D. theses of Renee Fatemi (U.Va.) and Alex Skabelin (MIT), completed in 2001. Results from these analyses were disseminated widely in invited and contributed talks (NSTAR2000, GDH2000, DNP2000, SPIN2000), and published[2] recently.

The second EG1 run was carried out from Sept. 2000 to March, 2001, completing the data set on NH_3 with beam energies of 1.6, 2.5, 4.2 and 5.7 GeV. The analysis of inclusive electron scattering from these data is the basis of the Ph.D. research of Yelena Prok (U.Va.), who plans to complete her work by June, 2004. Results of this analysis have also been widely disseminated in invited and contributed talks (APS2002&3, Baryons2002, DNP03, GDH2002, SPIN2002&3, PANIC02, CIPANP03).

2.8.3 Results

Yelena Prok's analysis of inclusive electron scattering uses count rate asymmetries, for which the CLAS acceptance and detector efficiencies cancel out. Subtraction of the contribution of the nitrogen, helium and windows is however necessary, and this is done using measurements taken with a carbon target and an empty target. The inclusive scattering cross-section depends on the four-momentum of the exchanged virtual photon (ν, \vec{q}) . The structure functions are usually expressed in terms of the invariant four-momentum transfer $Q^2 = \vec{q}^2 - \nu^2$ and the invariant hadronic mass $W^2 = Q^2 - 2M_p\nu$. For comparison to deep inelastic scattering (DIS) it is convenient to use Q^2 and another invariant, the Bjorken scaling variable $x = Q^2/2M_p\nu$.

The measured inclusive asymmetries can be expressed in terms of two fundamental asymmetries, $A_1(Q^2, W)$ and $A_2(Q^2, W)$ for polarized ep scattering:

$$A_1 + \eta A_2 = \frac{1}{D} \frac{N_+ - N_-}{P_e P_t (N_+ + N_-) f_{dil}}$$

where N_+ (N_-) is the number of events accumulated in one (W, Q^2) bin with the target polarization anti-parallel (parallel) to the beam helicity, normalized by the charge accumulated in the Faraday Cup for each orientation. The dilution factor f_{dil} is the fraction of events from NH_3 due to the atomic protons. The factor D , which is the virtual photon depolarization parameter, includes a dependence on R , the ratio of the longitudinal and transverse cross sections. The factor R is obtained from parametrizations of the world data. Corrections are also made for radiative effects. With the much larger data sample of the EG1b run, the statistical errors have been reduced substantially, and the measured region in W has been extended up to 3.0 GeV. Results for $A_1 + \eta A_2$ at a beam energy of 1.6 GeV are shown in Fig. 1.

Using a parametrization of world data on the scattering of polarized electrons from polarized protons to estimate A_2 , which typically makes a small contribution to the asymmetry, a value for A_1 can be obtained. Using A_1 , along with the unpolarized structure function $F_1(x, Q^2)$ obtained from world data, the spin structure function $g_1^p(x, Q^2)$ can be deduced from A_1 . Preliminary measurements of g_1^p at beam energies of 1.6 GeV and 5.7 GeV are shown in Fig. 2.

It had previously been noted by the SLAC E155 collaboration[3] that for Q^2 in the DIS region the ratio of $g_1(Q^2, x)/F_1(Q^2, x)$ was nearly constant. The ratios obtained in EG1 are shown in Fig. 3 along with ratios obtained in the SLAC experiments. The ratios are seen to approach the DIS values Q^2 between 1 and 2 GeV².

An alternative analysis method is to measure absolute cross sections. The difference in

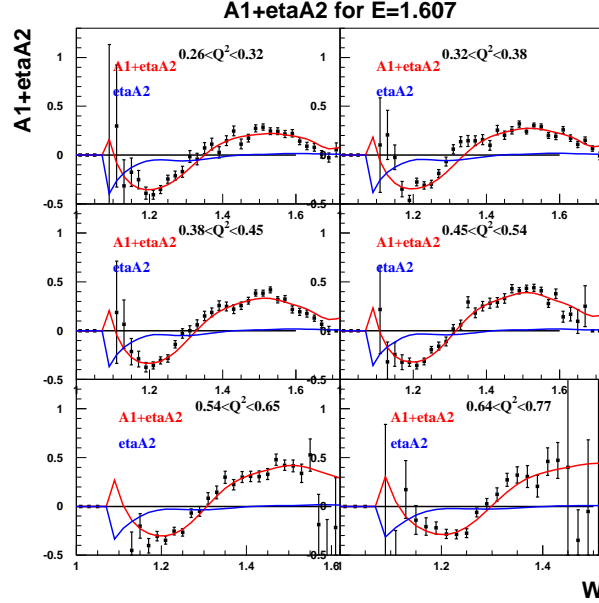


Figure 1: $A_1 + \eta A_2$ vs. W in several Q^2 bins for beam energy of 1.6 GeV.

cross section for opposite beam polarizations is due almost entirely to the atomic protons in the target, so that no dilution factor for N^{15} is needed. The proton spin structure functions can be extracted from the cross section difference and the already well-measured unpolarized cross section. This method requires absolute knowledge of the CLAS acceptance and efficiency. To simplify this determination we use a smaller subset of the data from regions of relatively uniform acceptance and efficiency. For the EG1a data, the results from this approach carried out by A. Skabelin agreed well with those from the asymmetry method used by R. Fatemi. We are also applying this alternative analysis to the EG1b data.

It is hoped that the full EG1 data set may be large enough to determine A_1 and A_2 directly from the data with a Rosenbluth type of kinematical separation. In addition to its obvious experimental desirability this separation would reduce the role of model uncertainties in the extraction of the proton spin structure functions.

References

- [1] S. Gerasimov, *Sov. J. Nucl. Phys.* **2**, 430 (1966); S.D. Drell and A.C. Hearn, *Phys. Rev. Lett.* **16**, 908 (1966).
- [2] R. Fatemi *et al.* (The CLAS Collaboration), *Phys. Rev. Lett.* **91**, 222002 (2003).

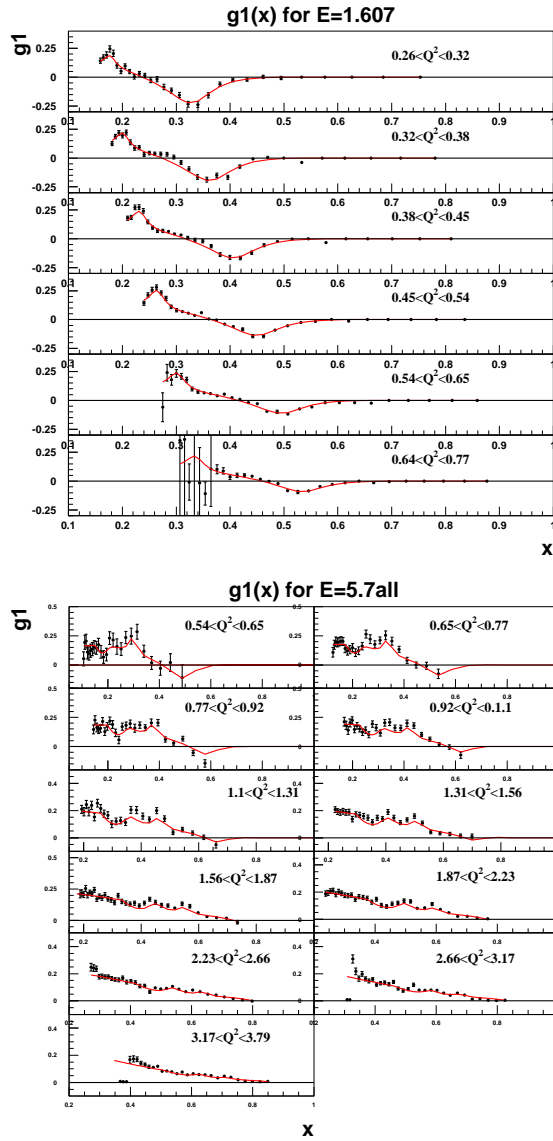


Figure 2: $g_1(x, Q^2)$ vs. x for several values of Q^2 using beam energies of 1.6 GeV and 5.7 GeV.

[3] P.L. Anthony *et al.* (E155 Collaboration), *Phys. Lett. B* **493**, 19 (2000).

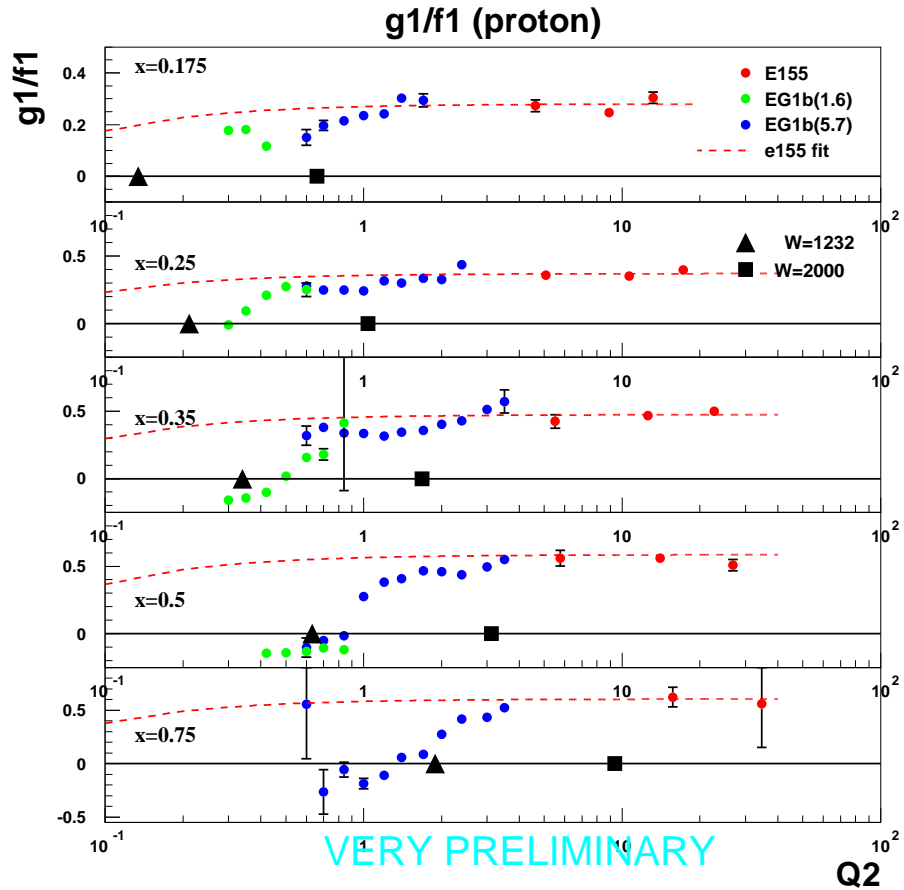


Figure 3: EG1b measurements of $g_1(Q^2, x)/F_1(Q^2, x)$ vs. Q^2 for five bins in x (blue and green points). The red points are from SLAC experiment E155. The dashed line is the E155 fit. The location of the $\Delta(1232)$ and $W = 2$ GeV are marked with a solid triangle and a solid square, respectively.

2.9 E93-006

TWO PION DECAY OF ELECTROPRODUCED LIGHT QUARK BARYON RESONANCES

M. Ripani, V. Burkert, V. Moiseev and the CLAS collaboration

2.9.1 Introduction

The excitation of baryon resonances is genuinely a non-perturbative phenomenon. Measurements of the transition amplitudes from the nucleon to its excited states are sensitive to the spatial and spin structure of the transition. Many of the nucleon excited states in the mass region around and above 1.7 GeV tend to decouple from the single-pion and eta channels, while πN scattering experiments have shown that many of them decay predominantly in multipion channels, such as $\Delta\pi$ or $N\rho$, leading to $N\pi\pi$ final states[1]. A measurement of the transition form factors of these states is very important for testing symmetry properties of the quark model. Moreover, SU(6) symmetric quark models[2, 3] predict more states than have been found in experiments. The present experiment was devoted to a precise measurement of the cross sections for reaction $ep \rightarrow e'p\pi^+\pi^-$, to extract information on poorly known baryon states and to investigate the existence of new, unobserved states.

2.9.2 Experiment Status

Data taking on hydrogen has been successfully completed during 2000 and for a large fraction of the data the detector reconstruction required for the physics analysis has been performed. Physics analysis has been performed for a subset of the data taken at beam energies of 2.567 and 4.247 GeV, with the goal of extracting cross sections for a few momentum transfers and in a broad range of CMS energy W , where we expect to see significant contributions from excited baryons production. The data that were analysed covered the W range 1.4-1.9 GeV for invariant momentum transfer $Q^2=0.5-0.8$ (GeV/c)² and $Q^2=0.8-1.1$ (GeV/c)², and the W range 1.4-2.1 GeV for the highest Q^2 bin, $Q^2=1.1-1.5$ (GeV/c)². Data were corrected for acceptance, reconstruction efficiency, radiative effects, and empty target counts [4]. Results of the isobar analysis were published in [5] and a more extensive presentation and discussion of data and analysis is given in [4].

2.9.3 Results

In Figure 1 (left panel) we report the total cross sections measured with CLAS at three

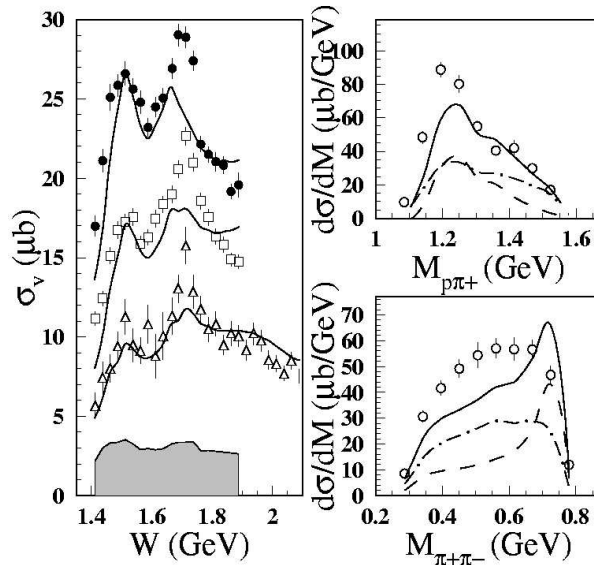


Figure 1: Left: Total cross section for $\gamma_v p \rightarrow p\pi^+\pi^-$ as a function of W . Data from CLAS are shown at $Q^2=0.5-0.8$ (GeV/c) 2 (full points), $Q^2=0.8-1.1$ (GeV/c) 2 (open squares), and $Q^2=1.1-1.5$ (GeV/c) 2 (open triangles). Error bars are statistical only, while the bottom band shows the systematic uncertainties for the lowest Q^2 bin. Right: $\frac{d\sigma_v}{dM_{p\pi^+}}$ (top) and $\frac{d\sigma_v}{dM_{\pi^+\pi^-}}$ (bottom) from CLAS at $Q^2=0.8-1.1$ (GeV/c) 2 and $W=1.7-1.725$ GeV (statistical error bars only). The curves represent our step (A) reference calculation: the dashed line includes all resonances, the dot-dashed line includes only the non-resonant part, and the solid line is the full calculation.

different Q^2 intervals and for W in the resonance region. Starting from a phenomenological model[6], we first produced a reference curve to be compared with the data (step (A) in text and figures), based on existing information on the resonance parameters[7, 8]. Results for step (A) are reported in Fig. 1. A strong discrepancy is evident at W around 1.7 GeV. Moreover, at this energy the reference curve exhibits a lack of $\Delta\pi$ strength in the $p\pi^+$ invariant mass (Fig. 1, right top), and a strong peak in the $\pi^+\pi^-$ invariant mass (Fig. 1, right bottom), connected to sizeable ρ meson production. The latter was traced back to the 70-91% branching ratio of the $P_{13}(1720)$ into this channel[1, 8, 9].

In a second step, we tried different fits of the data, in particular widely varying the photo- and hadronic couplings of the $D_{13}(1700)$ (fit F1), the $P_{13}(1720)$ (fit F2), and the $P_{11}(1710)$ (fit F3). The best fit ($\chi^2/\nu = 3.4$) was obtained in (F2) (Fig. 2 and 3). However, the resulting values for the branching fractions of the $P_{13}(1720)$ were significantly different from previous analyses reported in the literature and well outside the reported errors[1, 8, 9].

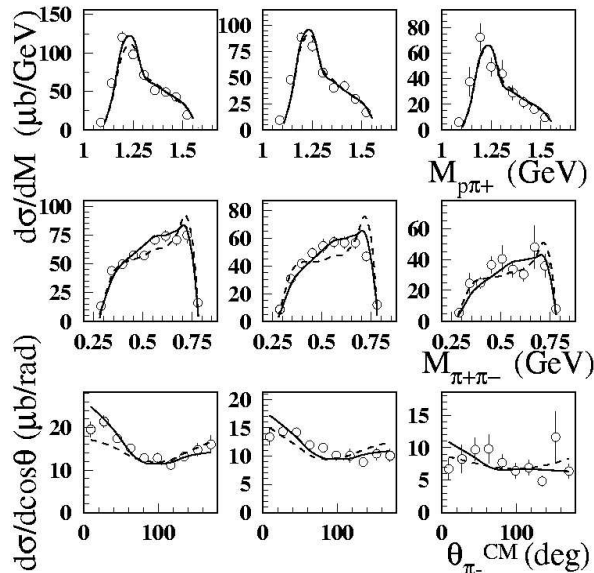


Figure 2: $\frac{d\sigma_v}{dM_{p\pi^+}}$, $\frac{d\sigma_v}{dM_{\pi^+\pi^-}}$, and $\frac{d\sigma_v}{d\cos\theta_{\pi^-}}$ from CLAS (from top to bottom) at $W=1.7-1.725$ GeV and for the three mentioned Q^2 intervals (left to right). The error bars include statistical errors only. Curves (see text) correspond to the fits (F2) (solid), and (F4) (dashed).

In a final multiresonance fit (fit F4), we varied only the electromagnetic excitation of all three candidate states, but no better solution was found (Fig. 2 and left panel of Fig. 3). A good fit was also obtained by introducing a new P_{13} state (isospin could not be determined) with mass of about 1720 MeV, a width of about 90 MeV, about 40 % decay to $\Delta\pi$ and 17 % to ρp . The visual quality of the fit was very similar to the (F2) curves in Fig. 2. The quality of the fit of the total cross sections was also comparable to (F2) (Fig. 3).

In conclusion, the new high quality data from CLAS have shown the clear presence of resonance structures, not visible in the previous, technically limited experiments. In analysing the new data from CLAS, we adopted a phenomenological approach, based on the database of measured electromagnetic and hadronic resonance properties. Our analysis of the data revealed that the prominent structure at 1.7 GeV seems difficult to explain when existing information combined with quark model assumptions is used for the electromagnetic transition matrix elements. Moreover, the expected N^* branching fractions to $\Delta\pi$ and ρp seem to be quite different from those inferred from the experimental mass distributions. A good fit to the data is indeed obtained by varying the properties of the ordinary $P_{13}(1720)$, but at the price of significantly changing the electromagnetic form factors with respect to the model expectations and at the additional price of attributing to this state branching fractions significantly different from the existing hadronic analyses. On the other hand,

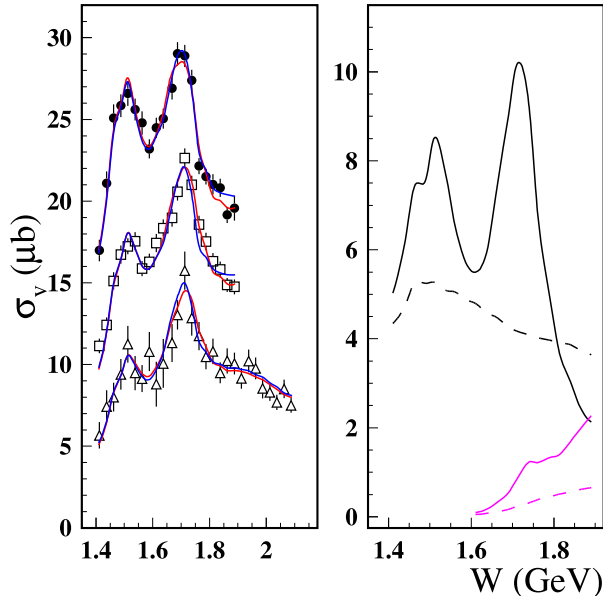


Figure 3: Left: Total cross section for $\gamma_v p \rightarrow p\pi^+\pi^-$ as a function of W from CLAS at the 3 mentioned Q^2 intervals (see fig.1). The error bars are statistical only. The curves (see text) correspond to the fits (F2) (red), and (F4) (blue). Right: subdivision of the fitted cross section (F2) for $Q^2=0.5-0.8$ (GeV/c) 2 into resonant $\Delta^{++}\pi^-$ (black solid), continuum $\Delta^{++}\pi^-$ (black dashed), resonant $\rho^0 p$ (magenta solid), and continuum $\rho^0 p$ (magenta dashed). Notice the different vertical scales.

our analysis indicates that the new CLAS cross sections are compatible with the presence of a new, previously unobserved state, although alternative scenarios involving multiquark transitions or even exotic components[10] cannot be ruled out.

References

- [1] K. Hagiwara et al., Phys. Rev. **D66**, 010001 (2002).
- [2] R. Koniuk and N. Isgur, Phys. Rev. Lett. **44**, 845 (1980); Phys. Rev. **D21**, 1868(1980).
- [3] M.M. Giannini, Rep. Prog. Phys., **54**, 453 (1990).
- [4] M. Ripani et al., hep-ex/0304034.
- [5] M. Ripani et al., Phys. Rev. Lett. **91**, 022002 (2003).

- [6] M. Ripani et al., Phys. of At. Nucl., **63**, 1943 (2000).
- [7] V. D. Burkert et al., Phys. Rev. **C67**, 035204 (2003).
- [8] D.M.Manley, E.M.Salesky, Phys. Rev. **D45**, 4002 (1992).
- [9] T.P. Vrana et al., Phys. Rept. **328**, 181 (2000).
- [10] H. Walliser, V.B. Kopeliovich., hep-ph/0304058.

2.10 E93-008

Inclusive η Photoproduction in Nuclei

M. F. Vineyard (Union College)
and the CLAS Collaboration

2.10.1 Introduction

Jefferson Lab Experiment 93-008 uses the CEBAF Large Acceptance Spectrometer (CLAS) and the photon tagging system in Hall B to measure inclusive η photoproduction in nuclei. The primary motivation of this experiment is to investigate nuclear medium modifications of nucleon resonances and the η -nucleus interaction. This experiment is part of both the g2 and g3 run groups of the CLAS Collaboration.

Through the study of the excitation, propagation, and decay of nucleon resonances in the nuclear environment one ultimately expects to understand how the strong interaction is affected by baryon structure. A wealth of information on the $\Delta(1232)$ and its dynamics within the nuclear medium has been obtained through pion studies. However, very little is known about medium properties of the higher-energy excited states of the nucleon. This is primarily due to the fact that the dominance of the Δ and the overlapping of higher resonances prevents the study of only a single specific state by π -production experiments. The η meson, on the other hand, couples only with isospin- $\frac{1}{2}$ N^* resonances since it is an isoscalar particle, and therefore provides a way to isolate these resonances. In this experiment, inclusive measurements of the photoproduction of η mesons in nuclei are performed to investigate medium modifications of the $S_{11}(1535)$ and possibly other isospin- $\frac{1}{2}$ resonances.

These measurements will also provide information on the η -nucleus interaction. Due to the lack of η beams, very little is known about the interaction of η mesons with nuclei. In this experiment, final-state interactions of the η meson propagating through the nucleus will be used to investigate the η -nucleus interaction. The study of η interactions with nucleons and nuclei can provide significant tests of our understanding of meson interactions which has been developed through pion studies.

Data were obtained several years ago at MAMI for the inclusive reaction on ^{12}C , ^{40}Ca , ^{93}Nb , and ^{nat}Pb nuclei for photon energies up to 790 MeV [Ro96]. However, though these data are of high quality, the energy range covered is from threshold to just below the peak of the $S_{11}(1535)$ resonance. From the analysis of these data, it was concluded that the total cross section scales as $A^{2/3}$ and a Glauber model analysis indicated an η -N cross section of about 30 mb. No evidence of a shift in mass or a depletion of strength of the $S_{11}(1535)$ was

observed from a comparison with an effective Lagrangian model [Ca93]. However, it should be stressed that this conclusion was drawn from a comparison of the slopes of the data and calculations on the low-energy side of the $S_{11}(1535)$ rather than over the entire line shape of the resonance.

Recently, the $^{12}\text{C}(\gamma,\eta)$ reaction was investigated at photon energies between 0.68 and 1.0 GeV at the 1.3-GeV electron synchrotron at KEK-Tanashi [Yo00]. The cross section as a function of incident photon energy was observed to increase with photon energy up to 0.9 GeV and then begin to decrease. This was interpreted as the first observation of the $S_{11}(1535)$ resonance in the carbon nucleus. It was shown that some of the differences between the shapes of the cross sections measured on carbon and hydrogen can be accounted for by medium effects such as Fermi motion, Pauli blocking, and η -N and N-N* collisions in quantum molecular dynamics calculations.

There have been a number of theoretical results on η photoproduction from nuclei in the last decade. In the effective Lagrangian approach of Carrasco *et al.* [Ca93], the η -N final state interactions are taken into account by a Monte Carlo code using calculated reaction probabilities. In the work of Lee *et al.* [Le96], the quasifree production is calculated in the distorted-wave impulse approximation and the final state interactions are treated with an η -A optical potential. Effenberger *et al.* [Ef97] use the production cross sections on the free nucleon as input and take into account the final state interactions with a coupled-channel Boltzmann-Uehling-Uhlenbeck model. Recently, Hedayati-Poor and Sherif [He98] introduced a relativistic model in which an effective Lagrangian approach is used to describe the elementary production process and the dynamics of the nucleon motion is based on a relativistic mean field theory. Several of these models provide reasonable descriptions of the MAMI total cross sections. However, detailed agreement with the differential cross sections is not obtained with any of the models.

The Jefferson Lab experiment discussed here will extend the MAMI and KEK-Tanashi measurements to higher energies and more targets. The extended energy range will completely cover the region of the $S_{11}(1535)$ resonance and allow for a more thorough investigation of possible nuclear medium modifications. It will also allow for the measurement of contributions to the cross section from other resonances and non-resonant production. The measurements are being made on a variety of targets enabling the study of the evolution of medium effects with target mass and the investigation of the η -nucleus interaction.

2.10.2 Experiment Status

Data are currently being analyzed for neutral meson photoproduction on ^1H (g1c run) and ^3He (g3 run) targets. Shown in Figure 1 are invariant mass spectra for $\gamma\gamma$ events from a hydrogen target for four bins in beam energy and meson angle. The spectra are fitted to extract yields for π^0 and η meson photoproduction. As a cross-check, neutral meson photoproduction from the proton is also being analyzed using the missing mass technique. Shown in Figure 2 are missing mass spectra for $\gamma p \rightarrow pX$ for four bins in beam energy and proton center-of-mass angle. Acceptance calculations are underway and the analysis will be extended to data obtained on ^2H (g2a run) and ^4He (g3 run) targets.

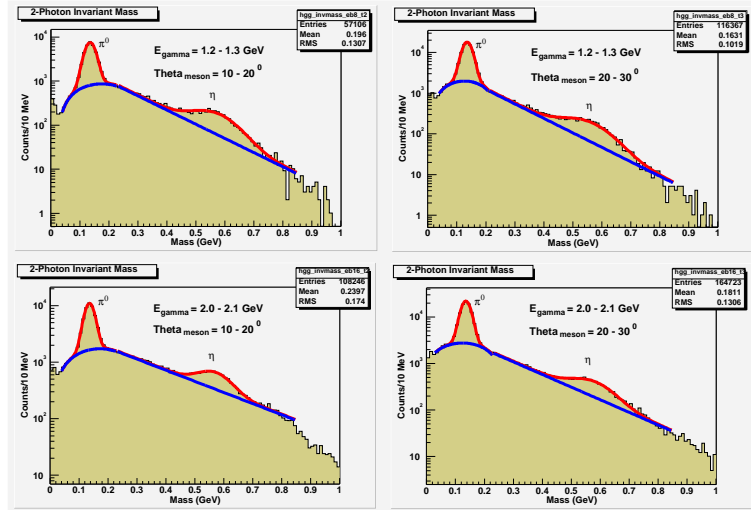


Figure 1: Invariant mass spectra for $\gamma\gamma$ events from a hydrogen target for four bins in beam energy and meson angle. The spectra are fitted with a background function and two gaussian functions to extract yields for π^0 and η photoproduction.

References

- [Ro96] M. Roebig-Landau, *et al.*, Phys. Lett. **B373**, 45 (1996).
- [Ca93] R.C. Carrasco, Phys. Rev. **C48**, 2333 (1993).
- [Yo00] T. Yorita *et al.*, Phys. Lett. **B476**, 226 (2000).
- [Le96] F.X. Lee, L.E. Wright, C. Bennhold, and L. Tiator, Nucl. Phys. **A603**, 345 (1996).

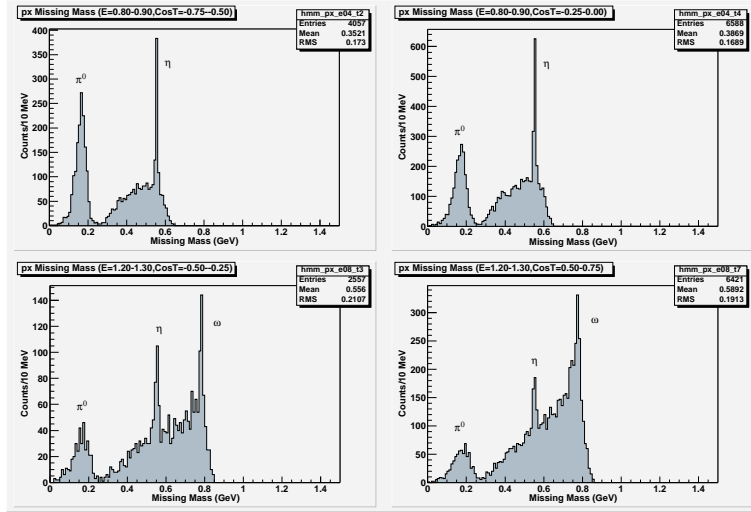


Figure 2: Missing mass spectra for $\gamma p \rightarrow pX$ for four bins in beam energy and proton center-of-mass angle.

- [Ef97] M. Effenberger *et al.*, Nucl. Phys. **A614**, 501 (1997).
- [He98] M. Hedayati-Poor and H.S. Sherif, Phys. Rev. **C58**, 326 (1998).

2.11 E94-003

Study of the $\Delta(1232)$ using double-polarization asymmetries

A. Biselli*, P. Stoler V. Burkert and R. Minehart (Spokespersons)
and the CLAS Collaboration

2.11.1 Introduction

Experiment 94-003 is part of the EG1 running period whose aim is to measure inclusive, semi-exclusive, and exclusive reactions with the CLAS detector using longitudinally polarized electrons scattering off longitudinally polarized protons and deuterons. The EG1 running period was split into two parts: the first part was completed in 1998 with a total of about 10^9 triggers at two beam energies, 2.5 and 4 GeV, leading to publications for both inclusive[1, 2] and exclusive channels [3, 4]. The second part of the run was completed in 2000-2001 with a total 2.3×10^{10} triggers at beam energies of 1.7, 2.4, 4.2 and 5.7 GeV. Analyses of these data are in progress.

Experiment 94-003 is focused on the exclusive channel $\vec{e}\vec{p} \rightarrow e'p\pi^0$ with particular attention to the region of the $\Delta(1232)$, which is the most accessible resonance since it does not overlap with other states and decays strongly via π emission. At the intermediate energies used in this analysis pQCD is not valid and effective field theories were developed. These models use previous unpolarized photo- and electroproduction data to fix the various free parameters that arise in the calculation. The polarized cross-sections can then be predicted, and by performing experiments with polarized beams and polarized targets it is possible to verify or constrain the models. For this experiment four models were tested against the data: the Mainz unitary isobar model MAID[5], the dynamical model DMT[6], the dynamical model by T. Sato and H. Lee[7], and the effective Lagrangian model by N. Mukhopadhyay and R. Davidson[8]. Results from the analysis of the first data showed that the models all predict a double spin asymmetry, which is dominated by the $|M_{1+}|^2$ term, in agreement with the data. They, however, differ in their predictions of the target asymmetry, which is sensitive to interference with background multipoles such as E_{0+} , S_{0+} , M_{1+} , and S_{1-} . The data showed a preference for the Sato and Lee model. Preliminary results from the second data set show asymmetries with much improved statistical accuracy. In addition, the different beam energies will allow us to explore a wider range in Q^2 .

2.11.2 Status of the analysis and results

For the first part of the EG1 run, only the data at the beam energy of 2.5 GeV were considered [3]. This analysis concentrated on the $\Delta(1232)$ resonance region and the target and double spin asymmetries as a function of the decay angles in the center of mass frame of the pion were extracted. The asymmetries were calculated by combining the counts of events for the four possible combinations of beam-target polarizations N_{ij} according to:

$$A_t = \frac{\frac{d\sigma_t}{d\Omega^*}}{\frac{d\sigma_0}{d\Omega^*}} = \frac{1}{P_t^b} \frac{(N_{\uparrow\uparrow} + N_{\downarrow\uparrow}) - (N_{\uparrow\downarrow} + N_{\downarrow\downarrow})}{(N_{\uparrow\uparrow} + N_{\downarrow\uparrow}) + \alpha(N_{\uparrow\downarrow} + N_{\downarrow\downarrow}) - 2(1 + \alpha)\frac{d\sigma_0}{d\Omega^*} N} A_{et} = \frac{\frac{\sigma_{et}}{d\Omega^*}}{\frac{d\sigma_0}{d\Omega^*}} = \frac{1}{P_e P_t^b} \frac{-(N_{\uparrow\uparrow} - N_{\downarrow\uparrow}) + (N_{\uparrow\downarrow} - N_{\downarrow\downarrow})}{(N_{\uparrow\uparrow} + N_{\downarrow\uparrow}) + \alpha(N_{\uparrow\downarrow} + N_{\downarrow\downarrow})} \quad (1)$$

where $\frac{d\sigma_0}{d\Omega^*} N$ is the contribution from the scattering off ^{15}N nuclei and the liquid helium coolant, P_e is the beam polarization, P_t^a and P_t^b , are the magnitudes of positive and negative target polarizations, respectively, and

$$\alpha = \frac{P_t^a}{P_t^b}. \quad (2)$$

The contribution of the ^{15}N background was removed by using data from separate runs with a ^{12}C target. The product $P_e P_t^{a,b}$ was experimentally extracted using the well known asymmetry in the elastic region. The π^0 was identified with a missing mass cut. Radiative corrections were studied using the Mo and Tsai [9] approach. The results of this work were compared to the four models previously mentioned. An example of the comparisons can be seen in Fig 1. For the second part of the run, so far only data at the beam energy of 1.6 GeV have been analyzed, but an analysis of the higher energy 5.6 GeV data is in progress. In comparison to the previous analysis, the preliminary results for the $\Delta(1232)$ region show a greatly improved statistical accuracy, which will allow a finer binning in all the variables. An example of the new results can be seen in Fig 2. A study of the asymmetries as a function of W and for higher W bins is on-going.

* Contact person

References

- [1] R. Fatemi *et al.* [CLAS Collaboration], Phys. Rev. Lett. **91**, 222002 (2003)
- [2] J. Yun *et al.* [CLAS Collaboration], Phys. Rev. C **67**, 055204 (2003)
- [3] A. Biselli *et al.* [CLAS Collaboration], Phys. Rev. C **68**, 035202 (2003)

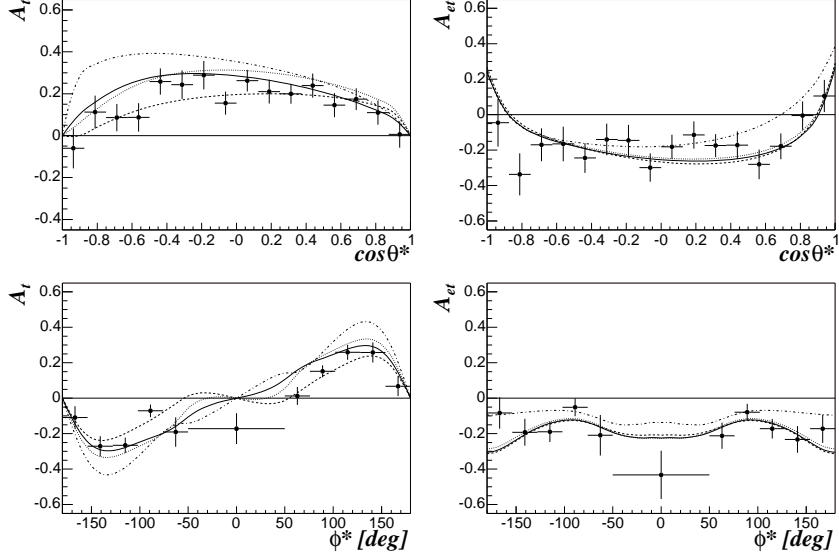


Figure 1: Asymmetries A_t and A_{et} as a function of the center-of-mass angle of the pion $\cos \theta^*$ integrated over $0 \text{ deg} < \phi^* < 180 \text{ deg}$ and $-180 \text{ deg} < \phi^* < 180 \text{ deg}$, respectively (top) and as a function of the center-of-mass angle of the pion ϕ^* integrated over $\cos \theta^*$ (bottom) for $0.5 \text{ GeV}^2/c^2 < Q^2 < 0.9 \text{ GeV}^2/c^2$. The curves represent the predictions from the MAID2000 model (solid), Davidson-Mukhopadhyay model (dash-dotted), Sato-Lee model (dashed), and DMT model (dotted). Figures are taken from [3]

- [4] R. De Vita *et al.* [CLAS Collaboration], Phys. Rev. Lett. **88**, 082001 (2002)
- [5] D. Drechsel, O. Hanstein, S.S. Kamalov and L. Tiator, Nucl. Phys. **A645**, 145 (1999)
- [6] S. S. Kamalov and G. Y. Chen and D. Drechsel and L. Tiator, Phys. Lett. **B27**, 522(2001)
- [7] T. Sato and T.S. Lee, Phys. Rev. **C54**, 2660 (1996)
- [8] R.M. Davidson, N.C. Mukhopadhyay and R.S. Wittman, Phys. Rev. **D43**, 71 (1991)
- [9] L.W. Mo and Y.S. Tsai, Rev. Mod. Phys., **45**, 205 (1969).

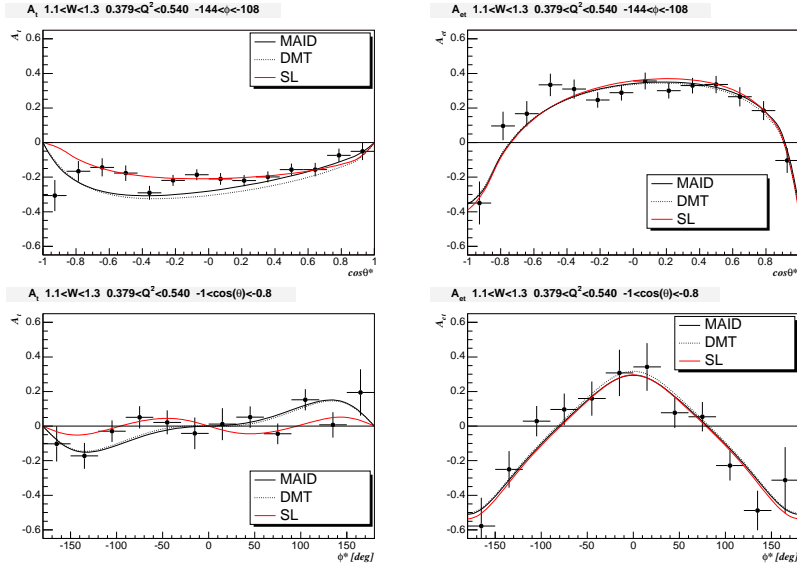


Figure 2: Asymmetries A_t and A_{et} as a function of the center-of-mass angle of the pion $\cos\theta^*$ integrated over $-144 \text{ deg} < \phi^* < -105 \text{ deg}$ (top) and as a function of the center-of-mass angle of the pion ϕ^* integrated over $-1 < \cos\theta^* < -0.8$ (bottom) for $0.379 \text{ GeV}^2/c^2 < Q^2 < 0.540 \text{ GeV}^2/c^2$. The curves represent the predictions from the MAID2000 model (solid), DMT (dotted), and Sato-Lee model (red).

2.12 E94-017

The Neutron Magnetic Form Factor from Precision Measurements of the Ratio of Quasielastic Electron-Neutron to Electron-Proton Scattering in Deuterium

W. K. Brooks (Jefferson Lab), M. F. Vineyard (Union College)

2.12.1 Introduction

The E5 run of the CLAS Collaboration in Hall B initially consisted of a single experiment, E94-017. The goal of this experiment is to determine the neutron magnetic form factor over a Q^2 range from 0.2 to 4.8 $(GeV/c)^2$ from precision measurements of the ratio of quasielastic electron-neutron to electron-proton scattering in deuterium.

Nucleon structure is one of the most fundamental issues in hadronic physics. Elastic electron scattering can be used to probe the electromagnetic structure of the nucleon. The differential cross section for elastic electron-nucleon scattering in the one-photon-exchange approximation is given by the Rosenbluth formula [Ro50] in which the nucleon structure information is contained in the Sachs electromagnetic form factors, G_E and G_M . These form factors provide information on the distributions of charge and magnetization current within the nucleon and are used for comparison between experiment and theoretical models of nucleon structure.

Until recently, the electromagnetic form factors for the proton have been determined experimentally from elastic ep scattering using the Rosenbluth separation technique [Ro50]. The magnetic form factor of the proton, G_M^p , appeared to be rather well determined over the range $0 < Q^2 < 30 (GeV/c)^2$, while the electric form factor, G_E^p , was determined with much less precision, particularly at high Q^2 where the cross section is dominated by G_M^p [Bo95]. These results indicated that the ratio $\mu_p G_E^p / G_M^p \simeq 1$, where $\mu_p = 2.79$ is the magnetic moment of the proton.

Recent measurements of $\mu_p G_E^p / G_M^p$ in Hall A at Jefferson Lab using a polarization transfer technique have shown that the form factor ratio decreases significantly from unity above $Q^2 = 1 (GeV/c)^2$ [Jo00, Ga01]. These results have led to intense theoretical activity [Bl00, De00, Ca00, Mi02] and a reanalysis of most of the world ep elastic cross section data using these new data as a constraint [Br02].

The neutron form factors have been determined with much less precision than those of the proton [Bo95]. Until the last decade most of the neutron form factor data came

from analyses of inclusive quasielastic electron scattering from deuterium that introduce a number of significant systematic errors. More recently progress has been made in measurements [Ma93, Br95, An94, An98] of the neutron magnetic form factor, G_M^n , at low Q^2 values by measuring the ratio of quasielastic electron-neutron to electron-proton scattering in deuterium, a method in which many of the systematic uncertainties cancel. However, there are discrepancies among these measurements. Recently, measurements [Xu00] of inclusive quasielastic scattering of polarized electrons off a polarized ^3He target were performed in Hall A at Jefferson Lab and used to extract G_M^n at $Q^2 = 0.1$ and 0.2 $(\text{GeV}/c)^2$ with an experimental uncertainty of less than 2%. Also, significant progress is being made on the extraction of G_E^n from measurements of the $\vec{d}(\vec{e}, e'n)p$ [Zh01] and $d(\vec{e}, e'\vec{n})p$ [Ma93] reactions in Hall C at Jefferson Lab.

In this experiment, precise measurements of the ratio of quasielastic electron-neutron to electron-proton scattering in deuterium have been made over a broad range in Q^2 with the CLAS. The neutron magnetic form factor will be extracted from this ratio with the use of the more accurately known proton form factors. Data were taken simultaneously on separated hydrogen and deuterium targets. The $e + p \rightarrow e' + n + \pi^+$ reaction on the hydrogen target is used to measure the neutron detection efficiency. The data from electron-proton and electron-neutron scattering in deuterium are treated in an identical way insofar as possible. The use of this ratio technique, with the simultaneous calibration of the neutron detection efficiency, significantly reduces or eliminates many of the systematic errors associated with inclusive quasielastic scattering from deuterium. The results of this experiment will provide a significant improvement in our knowledge of the neutron magnetic form factor over the Q^2 coverage of existing measurements, and will extend the range to 4.8 $(\text{GeV}/c)^2$. In addition to providing accurate information on the magnetic structure of the neutron, these data will be important for the extraction of the electric form factor of the neutron from measurements of polarization observables which determine a linear combination of the electric and magnetic form factors (see for example Refs. [Zh01, Ma93]) and will allow a more accurate extraction of the strange quark form factor [An99].

2.12 .2 Experiment Status

Data for E94-017 were collected during the E5 run in April and May of 2000 with the CLAS detector in Hall B at Jefferson Lab and are currently being analyzed. Approximately 2.3 billion triggers were acquired, about half at an electron beam energy of 2.6 GeV and half at 4.2 GeV. The low beam energy data were divided into two-thirds normal torus polarity and one-third reversed torus polarity. The reversed torus polarity data were taken to reach the lowest possible limit in Q^2 . There is considerable overlap in Q^2 between the data taken at the two beam energies that provide important systematic cross-checks.

Table 1: Active research projects associated with the CLAS E5 run period.

Experiment	Title	Spokespersons <i>PhD Student</i>
E-94-017	The Neutron Magnetic Form Factor from Precision Measurements of the Ratio of Quasielastic Electron-Neutron to Electron-Proton Scattering in Deuterium	W. K. Brooks, M. F. Vineyard <i>J. Lachniet</i>
E-94-019	Measuring Nuclear Transparency in Double Rescattering Processes	K. Egiyan, K. Griffioen, M. Strikman <i>C. Butuceanu</i>
CAA-03-02	Out-of-Plane Measurements of the Structure Functions of the Deuteron	G. Gilfoyle
E-02-012	Investigation of Coherent Production of Vector Mesons Off Deuteron	F. Klein, L. Kramer, S. Stepanyan <i>A. Gonec</i>
E-97-001	Electroproduction of the $pp\pi^-$ System off the Deuteron Beyond the Quasifree Region	N. Pivniouk, L. Vorobyev

2.12 .3 Additional Experiments

While the neutron magnetic form factor was the initial justification for obtaining the beam time for CLAS, there are other analyses which are now making use of the E5 data. Because of the non-restrictive trigger and large acceptance of CLAS, there is a wealth of physics that may be mined from the data. Because E5 had both deuterium and hydrogen targets in the beam simultaneously, a number of systematic cross-checks can be performed using well-studied interactions on hydrogen such as elastic scattering and single pion production. These cross-checks then benefit the deuterium studies by reducing systematic errors and increasing confidence in the analysis.

Table 1 shows the list of active projects that include data from the E5 run period in their analysis. The ordering approximately represents the current status of the analysis, with the projects nearing completion listed first.

Experiment E-94-019, “Measuring Nuclear Transparency in Double Rescattering Processes” has made significant progress in the past year. This analysis, which combines data from the E5 and E6 runs, has obtained preliminary results that are connected with color transparency, a fundamental prediction of QCD that has proved elusive at Jefferson Lab energies. This analysis exploits rescattering in the final state by analyzing the shape of the missing momentum as a function of Q^2 . Theoretical predictions indicate this to be a robust signal for color transparency, and experimentally the method is immune to many common systematic uncertainties that plague other searches for this phenomenon. The preliminary results show excellent consistency between the three beam energies investigated, and offer tantalizing hints of transparency in the few- GeV^2 region.

Experiment CAA-03-02¹, “Out-of-Plane Measurements of the Structure Functions of the Deuteron,” takes advantage of the large acceptance of CLAS to look for out-of-plane polarization asymmetries in order to derive the fifth structure function. Since this function is highly sensitive to final state interactions, it provides a unique opportunity to test this very important feature of deuteron models, as well as suggesting another possible avenue to access color transparency. A substantial amount of work was performed over the past year on this project, and the initial indications are that the overall sensitivity of the measurement will substantially surpass that of previous attempts to isolate this structure function. In addition to the fifth structure function, the possibility of performing an analysis of *all* structure functions is being evaluated. While the systematic errors come from different sources for the other structure functions, the breadth of kinematics accessible is impressive. This study makes use of both of the E5 beam energies.

Progress on experiment E-02-012, “Investigation of Coherent Production of Vector Mesons Off Deuterons,” has continued over the past year. This experiment will investigate the space-time picture of high energy two-body reactions and the onset of the perturbative QCD regime for exclusive processes through the coherent production. ρ , ϕ and ω mesons will be simultaneously detected over a broad kinematic range ($1 < Q^2 < 3.5 \text{ GeV}^2$, $0.1 < -t < 1 \text{ GeV}^2$). This kinematic range covers the soft limit (small Q^2), hard limit (large Q^2), and especially the transition region between the two limits, where data is scarce. By covering the range from where vector meson dominance describes the process to the edge of where pQCD becomes important, we are able to probe the transition region. Of special interest here is the investigation of color coherence where the quarks are brought close together and, hence, have reduced interactions. The studies will lead to a very sensitive investigation of color coherence. Over the past year efforts have been focused on identifying the reaction channel and systematic studies of the data set.

Experiment E-97-001, “Electroproduction of the $pp\pi^-$ System off the Deuteron Beyond

¹A CLAS Approved Analysis.

the Quasifree Region,” is a search for a narrow resonance with mass $M \approx 2.06 \text{ GeV}$ that may have been seen in pp scattering and which has been predicted in some quark model approaches. In addition to the final state listed in the title, recent work in the past year has focused on looking at the $nn\pi^+$ system in the E5 data.

2.12.4 Preliminary Results for G_M^n

The data from the E5 run will ultimately provide the magnetic form factor of the neutron over the Q^2 range from 0.2 to 4.8 $(\text{GeV}/c)^2$, with uncertainties of a few percent over most of the range, with many systematic cross-checks. These measurements should eclipse and extend the entire world’s data for this fundamental quantity. Preliminary results have been obtained for G_M^n for $Q^2 > 1 \text{ GeV}^2$, and it is expected that preliminary results for the full Q^2 range will be available in mid-2004. The early indications from the higher Q^2 data so far are that there is minimal deviation from the dipole form. This is quite significant in that previous data appeared to indicate a more rapid falloff of G_M^n than the dipole; for example, a modern parameterization of the historical data [Bo95] indicated a value that is 10-15% smaller at $Q^2 = 5 \text{ GeV}^2$ than the new preliminary Hall B data. Because the new data have smaller errors and give a continuous measurement in Q^2 , they provide a strong constraint on the functional form of G_M^n . While still a preliminary conclusion, a revision of this magnitude in a quantity as essential as a nucleon form factor will have a major impact on our understanding of neutron structure. In particular, now that the precision of the neutron data nearly matches that of the proton data at high Q^2 , the isospin structure of the nucleon can be extracted in kinematics where a quark-level description is required.

References

- [Ro50] M.N. Rosenbluth, Phys. Rev. **79**, 615 (1950).
- [Bo95] P.E. Bosted, Phys. Rev. **C51**, 409 (1995); and references therein.
- [Jo00] M.K. Jones *et al.*, Phys. Rev. Lett. **84**, 1398 (2000).
- [Ga01] O. Gayou *et al.*, Phys. Rev. **C64**, 038202 (2001).
- [Bl00] J.C.R. Bloch, C.D. Roberts, and S.M. Schmidt, Phys. Rev. **C61**, 065207 (2000).
- [De00] M. De Sanctis *et al.*, Phys. Rev. **C62**, 025208 (2000).
- [Ca00] F. Cardarelli and S. Simula, Phys. Rev. **C62**, 065201 (2000).

- [Mi02] G.A. Miller, private communication (2002).
- [Br02] E.J. Brash *et al.*, Phys. Rev. **C65**, 051001 (2002).
- [Ma93] P. Markowitz *et al.*, Phys. Rev. **C48**, R5 (1993).
- [Br95] E.E.W. Bruins *et al.*, Phys. Rev. Lett. **75**, 21 (1995).
- [An94] H. Anklin *et al.*, Phys. Lett. **B336**, 313 (1994).
- [An98] H. Anklin *et al.*, Phys. Lett. **B428**, 248 (1998).
- [Xu00] W. Xu *et al.*, Phys. Rev. Lett. **85**, 2900 (2000).
- [Zh01] H. Zhu *et al.*, Phys. Rev. Lett. **87**, 081801 (2001).
- [Ma93] R. Madey (spokesperson), CEBAF Experiment Proposal E-93-038 (1993).
- [An99] K.A. Aniol *et al.*, Phys. Rev. Lett. **82**, 1096 (1999).

2.13 E6

The E6 Run Group
K. Egiyan, K. Griffioen, S. Kuhn and M. Strikman (spokespersons)
and the CLAS collaboration

2.13 .1 Introduction

The E6 run group (6 GeV beams, unpolarized deuteron target) within CLAS obtained beam time from January to March 2002. During this period experiments E94-019 (*Measuring Nuclear Transparency in Double Rescattering Processes*) and E94-102 (*Electron Scattering from a High Momentum Nucleon in Deuterium*) obtained their proposed statistics, and E02012 (*Coherent Vector Meson Production off the Deuteron*) saw the first quarter of its data.

2.13 .2 Experiment Status

Both E94-019 and E94-102 detected recoil protons with momenta above 250 MeV/c. This required an innovative target, in which liquid deuterium was pumped through a conical 5 cm long target cell with upstream diameter of 1.2 cm and downstream diameter of 0.7 cm. This shape maximized the flow of liquid while minimizing the amount of material in the way of the slow protons. The taper allowed bubbles to migrate back to the return loop.

E6 ran at the highest stable beam energy available, 5.77 GeV, with a luminosity of 10^{34} $\text{cm}^{-2} \text{s}^{-1}$ and a current of 7 nA. With the torus magnet set at 2250 A, the data rate was 3000 events per second with a minimal trigger, for both in-bending and out-bending electrons. E6 collected 3.5 billion events and logged an integrated luminosity of 14.4 fb^{-1} .

Calibration and cooking of the data was finished by the end of 2002, and the physics analysis has progressed well in 2003. Two students, Cornel Butuceanu from William & Mary and Alexei Klimenko from Old Dominion University are analyzing these data for their PhD theses. Kim Egiyan and his group from Yerevan are analyzing the color transparency measurement.

2.13 .3 Preliminary Results

E6 relies on a good understanding of the CLAS acceptance. As a first step, Cornel Butuceanu has determined the absolute inclusive cross sections for $D(e, e')$ at $x_{Bj} > 1$ at various fixed

values of Q^2 from 1.6 GeV² to 4.0 GeV². This physics is interesting in its own right because very large x_{Bj} corresponds to high internal nucleon momentum.

Fig. 1 shows $d\sigma/dQ^2dx$ versus x for representative intervals in Q^2 . Monte Carlo acceptance corrections run for E6 bring the data into fair agreement with a full model of the physics by M. Sargsian that includes elastic and inelastic contributions, realistic deuteron wavefunctions, short-range correlations, etc. The E6 data set extends the world's data to higher x over a large range of Q^2 .

Details of the E94-019 and E94-102 analyses are given in the following sections.

2.14 E94-019

Measuring Nuclear Transparency in Double Rescattering Processes
K. Egiyan, K. Griffioen and M. Strikman (spokespersons)
and the CLAS collaboration

2.14.1 Introduction

Perturbative quantum chromodynamics indicates that quasi-elastic electron scattering from a nucleon at high momentum transfer will sample the components of the nucleon wavefunction with the quarks close together. Recent calculations indicate that the distance over which the resulting point-like nucleon wave-packet expands to normal size is little more than the internucleon spacing for $Q^2 < 6 \text{ GeV}^2$. Therefore, only interactions with nearest-neighbor nucleons would be suppressed at Jefferson Lab beam energies. This implies we should use the very lightest nuclei, such as the deuteron, ^3He and ^4He , as targets[Eg94, Fr95]. A precise measure of the final-state interactions in light nuclei as a function of Q^2 provides a complementary approach to quasi-elastic scattering from heavy nuclei. We rely on the ratio of measured cross sections $D(e, e'p_{\text{forward}})$ observed at the kinematics dominated by double scattering (where the proton scatters first from the electron and then from the spectator neutron) to those measured at the kinematics dominated by screening (where the Born and final-state interaction amplitudes destructively interfere). This ratio is maximally sensitive to the presence of final-state interactions which should disappear with increasing Q^2 . Exclusive quasi-elastic events were selected over a range from $1 < Q^2 < 6 \text{ GeV}^2$, and the evolution of the ratio observed.

2.14.2 Experiment Status

As part of the E6 run group, the experiment was completed in 2002 and the physics analysis has been done in earnest in 2003. The data analysis is nearly complete and publication of the results is expected by the end of 2004.

2.14.3 Preliminary Results

Preliminary results have been generated by Kim Egiyan using the $(e, e'p_{\text{forward}})$ reaction to reconstruct the momentum of the spectator neutron in quasi-elastic scattering ($x_{Bj} = 1.0 \pm 0.1$). From such an analysis, the ratio of events with neutron momentum around 0.2 GeV/c to those around 0.5 GeV/c is observed as a function of Q^2 . The data have been corrected for detector acceptance determined from Monte Carlo simulations. Since final-

state interactions will enhance the high momentum components, this ratio is smaller with final-state interactions than without. The signature for color transparency is a ratio that grows away from the standard nuclear physics predictions with Q^2 . Fig. 2 shows data for these ratios using the E6 deuteron data. The curves correspond to calculations of J-M. Laget; both data and theory have absolute normalizations. The data and the calculations have very different dependencies on Q^2 , as one might expect for a scattered proton that becomes color transparent. At present there is a discrepancy between theory and experiment at low Q^2 where no transparency is expected which needs to be understood and resolved.

The results from directly measuring the proton spectator, constitute Cornel Butuceanu's PhD thesis, along with the $D(e, e')$ inclusive measurements.

References

[Eg94] K.Egiyan *et al.*, Nucl. Phys. **A580**, 395 (1994).

[Fr95] L.L. Frankfurt *et al.*, Z.Phys. **A352**, 97 (1995).

2.15 E94-102

Electron Scattering from a High Momentum Nucleon in Deuterium
K. Griffioen and S. Kuhn (spokespersons) and the CLAS collaboration

2.15 .1 Introduction

When an electron scatters from a nucleon inside the deuterium nucleus, the initial state of this nucleon is unknown, and therefore the inclusive cross sections are averages over all possible initial nucleon momenta. In the spectator model, the struck nucleon is assumed to be off-shell, the spectator nucleon is on-shell, and the spectator recoils with its initial internal momentum without undergoing a final-state interaction. Thus, the measurement of a recoiling backward-going spectator proton in the reaction $d(e, e' p_{\text{back}})X$ tags the neutron on which the interaction took place. A test of this spectator model and its limitations is one of the main goals of E94-102. In the kinematic region where this model works, it can be used to study the properties of the bound neutron, and in particular the modifications to the neutron's internal structure when it is part of a tightly bound pair. In the kinematic regions where it does not work, it can be used to identify final-state interactions and other deviations from the impulse approximation.

2.15 .2 Experiment Status

As part of the E6 run group, the experiment was completed in 2002 and the physics analysis has been done in earnest in 2003. The data analysis is nearly complete and publication of the results is expected by the end of 2004.

2.15 .3 Preliminary Results

Figure 3 shows sample results of this analysis. The left panels display the number of observed events versus the cosine of the proton emission angle, for two different bins in proton momentum. The agreement with the spectator model using a light cone wave function (lower black curve) for the initial proton momentum distribution is quite good at the lower momentum and for angles larger than 107.5° . The calculation using a non-relativistic deuteron wave function (upper red curve) is in less good agreement, in particular at large backward angles. The data exceed both model calculations by a large factor at high momentum and emission angles around 90° . This enhancement can be attributed to a strong final state interaction between the struck neutron and the spectator proton. By excluding this region (requiring proton emission angles larger than 107.5°), we can select kinematics where the spectator

approximation is reasonable. The right panels show the distribution of events for kinematics where the spectator model works as a function of the invariant mass of the (unobserved) final state of the struck neutron, for recoil proton momenta between 320 and 360 MeV/c. The elastic peak and some indication of neutron resonances are visible. The lower left panel shows the momentum distribution of the backward protons when the final state mass of the struck neutron lies in the resonance region ($1 \text{ GeV} \leq W^* \leq 2 \text{ GeV}$). Once again, a relatively good agreement with the spectator model using the light-cone wave function can be observed.

This analysis constitutes the Ph.D. thesis of Alexei Klimenko (ODU, expected May 2004).

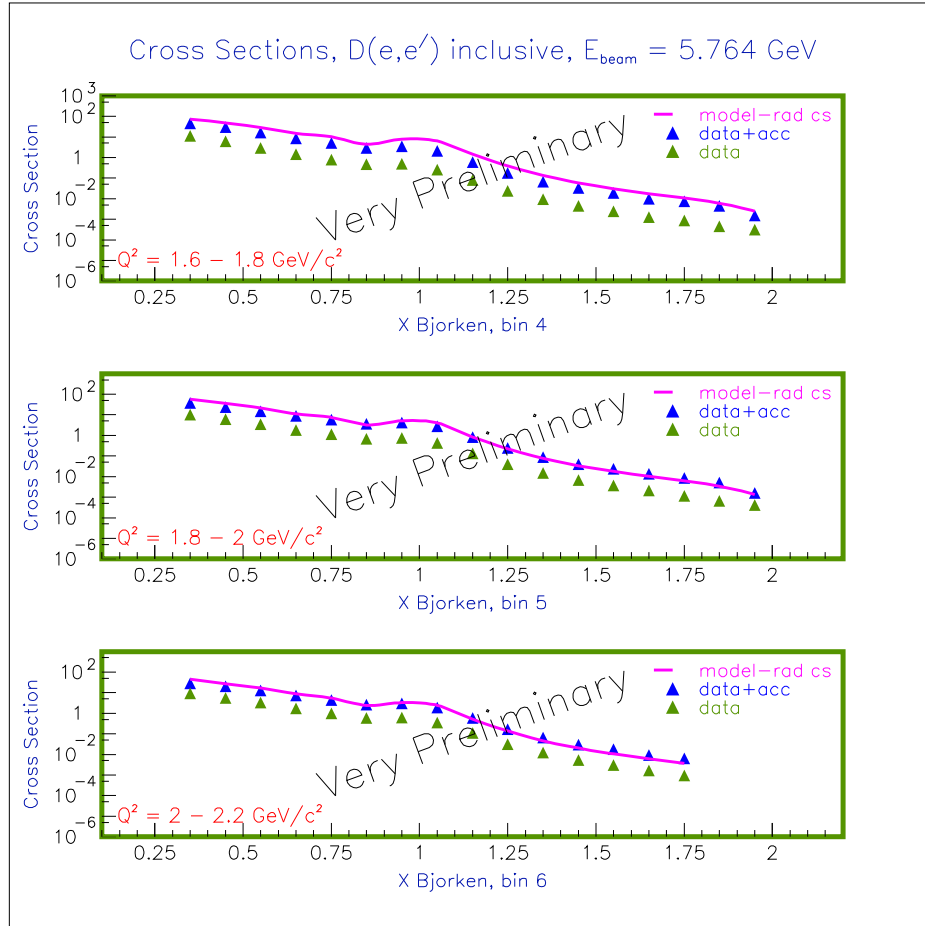


Figure 1: Preliminary $D(e, e')$ inclusive cross sections with (upper blue triangles) and without (lower green triangles) detector acceptance corrections. The data have not been radiatively corrected. The solid magenta line shows the radiated Sargsian model, which should be compared directly with the upper blue triangles. The panels correspond to three representative Q^2 intervals.

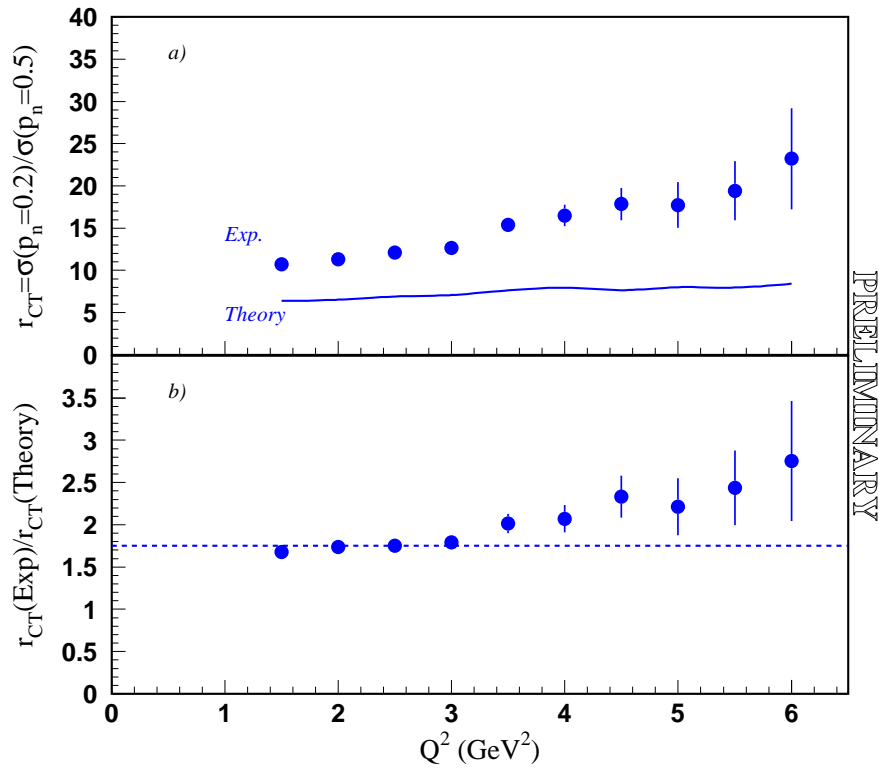


Figure 2: Experimental ratio of 200 MeV/c spectator neutrons to 500 MeV/c spectator neutrons for quasi-elastic scattering events. This ratio is maximally sensitive to final-state interactions. The upper panel shows the data together with the calculation of Laget without color transparency. The lower panel shows the ratio of experimental points to the theory. The horizontal line is simply to guide the eye.

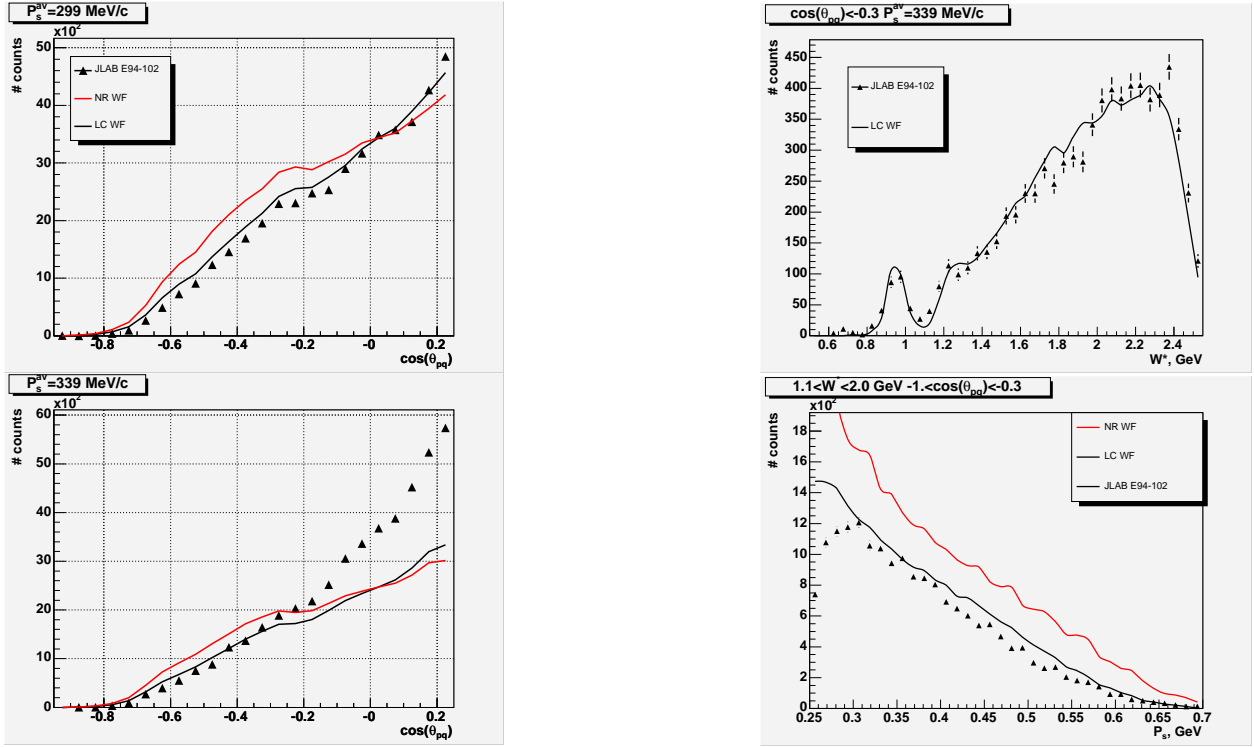


Figure 3: Left: cosine of the proton emission angle with respect to the direction of the momentum transfer for proton momenta of 300 (upper) and 340 (lower) MeV/c. The curves are simple model calculations based on the spectator picture for the reaction $d(e, e'p)X$ where the electron scatters off the (unobserved) neutron in deuterium and the proton retains its initial bound-state momentum. The red (upper) curves use the Paris potential wave function for the initial momentum distribution of the proton. The black (lower) curves use the light cone prescription for this momentum distribution. Right top: reconstructed invariant mass of the unobserved final state in the reaction $d(e, e'p)X$, for protons emitted with momenta between 320 and 360 MeV/c and at angles larger than 107.5° with respect to momentum transfer. Right bottom: momentum distribution for protons emitted at angles larger than 107.5° for the case where the invariant mass of the final neutron state is in the resonance region ($1 \text{ GeV} \leq W^* \leq 2 \text{ GeV}$). The curves have the same meaning as in the left-hand panels.

2.16 E99-006

Polarization Observables in the $p(\vec{e}, e'K^+)\Lambda$ Reaction

D.S. Carman (*Ohio University*),
B.A. Raue, R. Nasseripour (*Florida International University*)
M.D. Mestayer (*Jefferson Laboratory*)
for the CLAS Collaboration

2.16.1 Introduction

Jefferson Laboratory experiment E99-006 was designed to provide the first measurements in the nucleon resonance region for the exclusive $p(\vec{e}, e'K^+)\Lambda$ reaction of both the beam-recoil spin transfer and the so-called fifth structure function $\sigma_{LT'}$. Understanding nucleon resonance excitation continues to provide a major challenge to hadronic physics due to the non-perturbative nature of QCD at these energies. Studies of strange final states can potentially uncover baryonic resonances that do not couple or couple only weakly to the πN channel due to the different hadronic vertices. Symmetric quark models tend to predict many more states than have been found experimentally. Whether these “missing” states do in fact exist is a question central to our understanding of baryon structure. The first results from this experiment were recently published in the journal *Physical Review Letters* [1] and were featured in the *CERN Courier* [2].

In the absence of direct QCD predictions, the theoretical framework involving hadrodynamic models has been extensively applied to the study of kaon electroproduction [3, 4, 5, 6]. The predictive powers of these isobar models are severely limited by a sparsity of data. Model fits to the existing cross section data are generally obtained at the expense of many free parameters, and these unpolarized data alone are not sufficiently sensitive to fully understand the reaction mechanism as they probe only a small portion of the full response. Polarization data can provide significant new constraints on the basic parameters of these models, that is, the specific intermediate resonances involved in the reaction, increasing their discriminatory power and allowing for a quantitative measure of whether or not new missing resonances might be required to explain these and other hyperon production data. In addition, newly developed gauge invariant models based on Regge exchanges may provide a convenient formalism over these kinematics, as well as above the resonance region.

E99-006 was part of the e1 run group and was carried out using the CLAS spectrometer in Hall B. Data were acquired with a polarized electron beam ($\langle P_b \rangle \sim 70\%$) in several different running periods with beam energies from 2.6 GeV to 5.5 GeV. The event readout for e1 was triggered by a scattered electron candidate whose signal was a coincidence between

a forward calorimeter and a Cerenkov counter hit in the same CLAS sector. In this analysis, identification of the final state K^+ was required. The large acceptance of CLAS has enabled us to study the reaction of interest over a broad range of momentum transfer Q^2 from 0.5 to 4.5 $(\text{GeV}/c)^2$ and invariant energy W spanning the full nucleon resonance region, while providing full angular coverage in the kaon center-of-mass system.

Hyperon identification with CLAS relies on missing-mass reconstructions. Fig. 1 shows the $p(e, e'K^+)X$ missing mass from our 2.6 GeV data set at various stages. The hyperon resolution is better than 10 MeV (σ) with a very clean final spectrum.

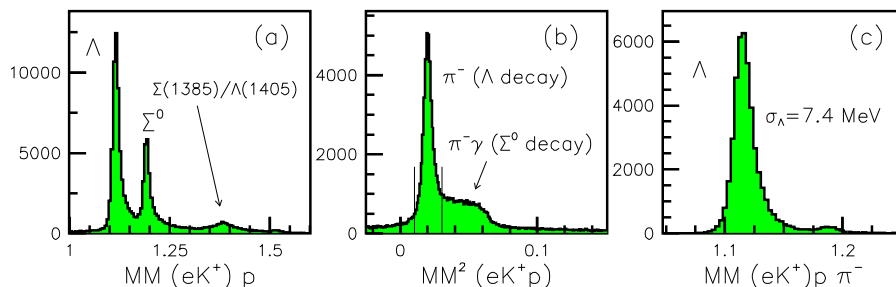


Figure 1: Missing-mass spectra (GeV) for the reactions (a) $p(e, e'K^+)X$ and (b) $p(e, e'K^+p)X$. (c) The hyperon distribution after cutting on the low-mass peak in (b). CLAS data from 2.567 GeV summing over all Q^2 and W .

2.16.2 Data Analysis and Results

The Λ hyperon decays mesonically via $\Lambda \rightarrow p\pi^-$ (B.R.=64%). This weak decay has an asymmetric angular distribution with respect to the Λ spin direction such that the decay-proton distribution in the Λ rest frame (RF) for each beam helicity state (+ or -) is of the form:

$$\frac{dN^\pm}{d \cos \theta_p^{RF}} = N[1 + \alpha(P^0 \pm P_b P') \cos \theta_p^{RF}], \quad (1)$$

where P_b is the average beam polarization, $\alpha=0.642 \pm 0.013$ is the weak decay asymmetry parameter, and θ_p^{RF} is the RF polar angle between the proton momentum and the chosen spin axis. The Λ polarization is the sum of P^0 , the induced polarization, and P' , the helicity-dependent transferred polarization, both defined with respect to a particular set of spin-quantization axes. In order to maximize the statistical precision in the measurement, this analysis was performed integrating over all angles Φ between the electron scattering plane and the $K^+\Lambda$ reaction plane. In this integration, the induced polarization vanishes. We can express the acceptance-corrected yield asymmetries in terms of the average transferred

polarization for each kinematic bin as:

$$A_\xi(\cos\theta_p^{RF}) = \frac{N_\xi^+ - N_\xi^-}{N_\xi^+ + N_\xi^-} = \alpha P_b \cos\theta_p^{RF} P'_\xi. \quad (2)$$

Here N_ξ^\pm are the decay-proton helicity-gated yields with respect to the different spin-quantization axes ξ . A direct extraction of P' in a given kinematic bin is performed with a linear fit of A_ξ to $\cos\theta_p^{RF}$. A sample of our results for P' are shown in Fig. 2 as a function of $\cos\theta_K^*$ for three different W bins spanning the nucleon resonance region. Here the z' axis is along the hyperon direction and x' lies in the hadronic reaction plane normal to z' . The component $P'_{y'}$ is consistent with zero as required by the Φ integration. The error bars in these figures include statistical but not systematic uncertainties for P' , which we estimate to be ≤ 0.084 on the polarization.

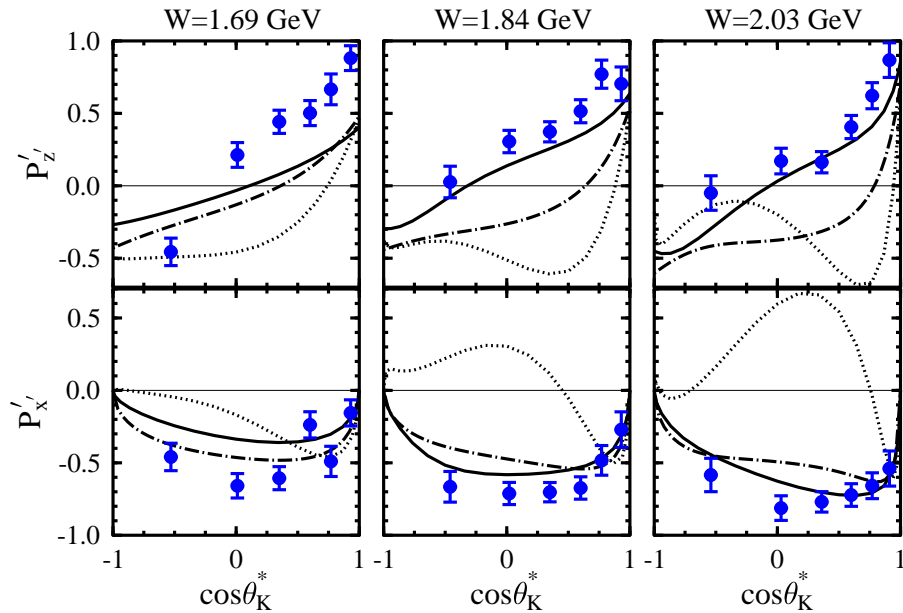


Figure 2: Transferred Λ polarization components $P'_{z'}$ and $P'_{x'}$ at 2.567 GeV vs. $\cos\theta_K^*$ summed over all Q^2 and Φ for three W bins centered at 1.69, 1.84, and 2.03 GeV. Curves correspond to the hydrodynamic models: WJC92 [3] (dotted), BM02 [6] (solid), and J02 [5] (dot-dash), averaged over the experimental bins.

The data are compared to several hydrodynamic model calculations. Each of these models differs in the mix of N^* resonances included. Recent calculations have been guided by coupled-channels analyses that recognize the importance of the $S_{11}(1650)$, $P_{11}(1710)$, and $P_{13}(1720)$ s -channel resonances, which are the only ones with a known significant branching into strange channels. However, other N^* states seem to be needed to explain the available

cross section data [7]. The models also include the $K^*(892)$ and $K_1(1270)$ to account for t -channel strength and Y^* resonances in the u channel.

In general the calculations do not reproduce the data, but while the comparison of the calculations to the data is illustrative to highlight the present deficiencies in the current models and their parameter values, the next step in the study of the reaction mechanism is to include our polarization data in the available database and to refit the set of coupling strengths.

The fifth structure function $\sigma_{LT'}$ is extracted from the polarized beam asymmetry:

$$A_{LT'} = \frac{1}{P_e} \frac{N^+ - N^-}{N^+ + N^-} = \frac{\sqrt{2\epsilon_L(1-\epsilon)}\sigma_{LT'}\sin\phi}{\sigma_0} \quad (3)$$

where N^+ and N^- are the acceptance-corrected helicity-gated yields of the $p(\vec{e}, e'K^+)\Lambda$ reaction and σ_0 is the unpolarized cross section. The structure function $\sigma_{LT'}$ is extracted from the asymmetry by multiplying by σ_0 [8]. Fig. 3 shows the preliminary result of our measurement for $\sigma_{LT'}$ versus W for $Q^2 = 0.7$ (GeV)² compared to several isobar models. In the regions where u and s -channel processes are expected to dominate ($\cos\theta_K^* < 0.5$), $\sigma_{LT'}$ is significantly non-zero indicating a large interference between the resonant and non-resonant background. At forward angles, ($\cos\theta_K^* > 0.5$), $\sigma_{LT'}$ is essentially zero indicating little interference between resonant terms and the dominant t -channel mechanism.

The extraction of the polarization transfer (including the induced hyperon polarization P^0) and the fifth structure function are nearing completion. These observables each provide unique information for the kaon electroproduction process. Our analysis group is working with several theorists and phenomenologists to employ these data to improve the very weak constraints on the reaction mechanism for the associated strangeness production process. This in turn will allow for a better understand of which N^* states couple to strangeness and what their properties are, which will allow for a better understanding of hadronic structure.

References

- [1] D.S. Carman *et al.* *CLAS Collaboration*, Phys. Rev. Lett. **90**, 131804 (2003).
- [2] CERN Courier feature article “JLab’s New Spin Puzzle”, CERN Courier Volume 43, Number 5, June 2003.
- [3] R.A. Williams *et al.*, Phys. Rev. C **46**, 1617 (1992).

- [4] H. Haberzettl *et al.*, Phys. Rev. C **58**, R40 (1998).
- [5] S. Janssen *et al.*, Phys. Rev. C **65**, 015201 (2002).
- [6] T. Mart and C. Bennhold, Phys. Rev. C **61**, 012201 (2000).
- [7] C. Bennhold, H. Haberzettl, and T. Mart, Pre-print nucl-th/9909022, (1999).
- [8] R. Feuerbach, CMU Analysis of Λ and Σ^0 electroproduction, (2001).
- [9] R.A. Adelseck and L.E. Wright, Phys. Rev. C **38**, 1965 (1988).

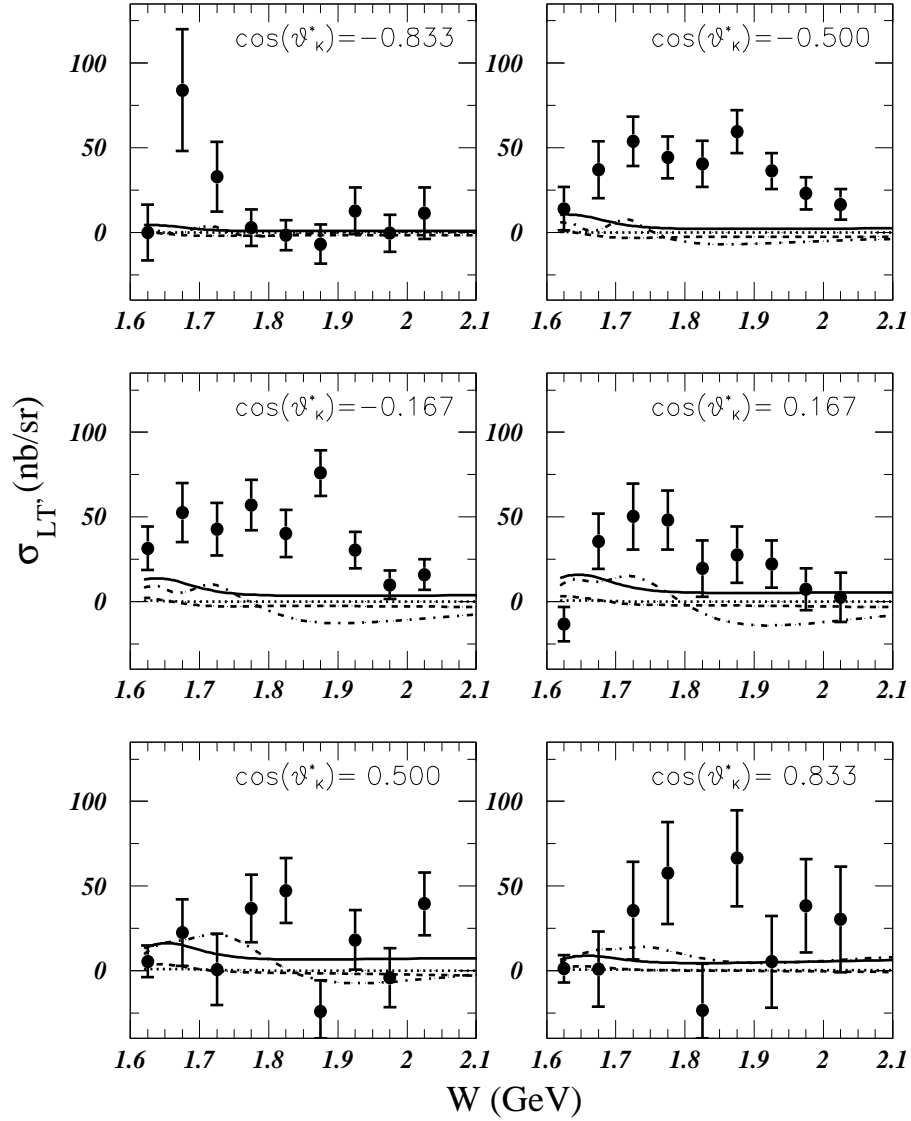


Figure 3: $\sigma_{LT'}$ (nb/sr) versus W (GeV) for six $\cos\theta_K^*$ bins. Data are shown for $Q^2 = 0.7$ (GeV/c) 2 . Curves correspond to the hydrodynamic models: AW [9] (solid), WJC [3] (dashed), BM98 [4] (dotted), BM02 [6] (dot-dash). The error bars represent the statistical uncertainties.

2.17 E00-112

Kaon Electroproduction at 6 GeV

D.S. Carman, A. Tkabladze (*Ohio University*),
B.A. Raue, P. Ambrozewicz (*Florida International University*),
M.D. Mestayer (*Jefferson Laboratory*)
for the CLAS Collaboration

2.17.1 Introduction

Jefferson Laboratory experiment E00-112 was designed to study kaon electroproduction associated with the ground state Λ and Σ^0 hyperons at 6 GeV electron beam energy using the CLAS spectrometer in Hall B. The measurement program was developed to encompass a number of aspects of existing Hall B experiments focusing on strangeness production. These include extending the kinematic range over which these final states are measured, the production mechanisms for s -channel N^* creation and decay and t -channel meson exchange are probed, and the hyperon polarization observables are measured. The data acquired will ultimately allow for detailed tests of hadrodynamical models, constituent quark models, and models based on Reggeon exchange. Each of these individual aspects is important for a better understanding of the reaction mechanism of open-strangeness production and ultimately of hadronic structure.

While these data are essential to improve existing low-energy theoretical descriptions of the elementary strangeness-production process, the extension of strangeness production studies to higher-beam energies will also help to elucidate the transition from hadronic to quark-gluon degrees of freedom. This will allow for tests of the validity of non-perturbative QCD in these kinematics. Additionally, the higher-energy data will allow for exploration of the wavefunction of the $s\bar{s}$ quark pair created through the color flux-tube breaking in the intermediate state and possible access to the underlying quark-distribution functions of the proton. This analysis represents a stepping-stone toward the 12-GeV strangeness physics program that is part of the Jefferson Laboratory energy upgrade [1].

E00-112 was part of the e1-6 run group and was carried out using the CLAS spectrometer in Hall B. Data were acquired at an electron beam energy of 5.75 GeV (the highest accelerator energy available) with longitudinally polarized electrons ($\langle P_b \rangle \sim 70\%$) in the period from October 2001 through January 2002. The event readout was triggered by a scattered electron candidate whose signal was a coincidence between a forward calorimeter and a Cerenkov counter hit in the same CLAS sector. The reaction kinematics at 6 GeV span momentum transfer Q^2 from 1.5 to 5 (GeV/c)², invariant energy W from 1.6 to 3.0 GeV,

and $|t|$ beyond 5 (GeV/c)^2 using CLAS at maximum magnetic field. This will allow for study of open-strangeness production at energies well above the resonance region while providing substantial overlap with the kinematic coverage at 4 GeV, which spans Q^2 from 1 to 2.5 (GeV/c)^2 , W from 1.6 to 2.4 GeV, and $|t|$ up to 3 (GeV/c)^2 .

Hyperon identification with CLAS relies on missing-mass reconstructions. Fig. 1 shows the $p(e, e'K^+)X$ missing mass from our 5.75 GeV data set at various stages in the analysis. The hyperon resolution is better than 12 MeV (σ) with a very clean final spectrum. The average CLAS acceptance for the detected three-body final state is roughly 5-10%.

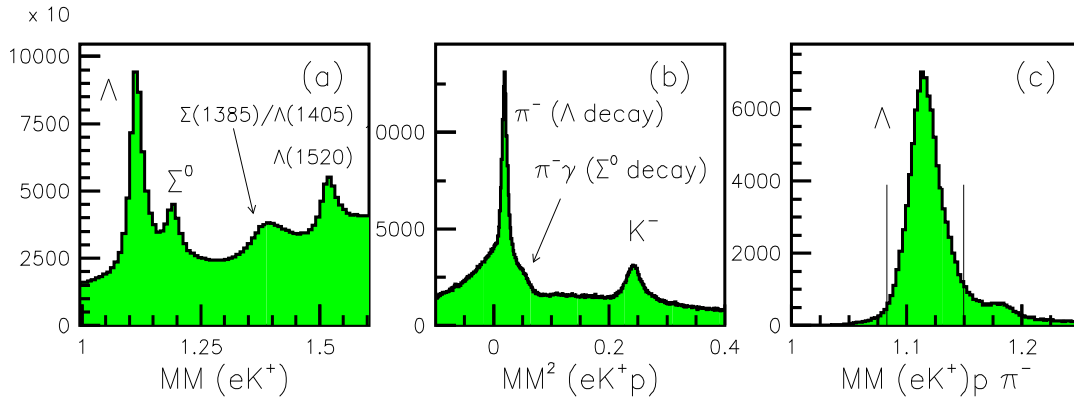


Figure 1: Missing-mass spectra (GeV) for the reactions (a) $p(e, e'K^+)X$ and (b) $p(e, e'K^+p)X$. (c) The hyperon distribution after cutting on the low-mass peak in (b). CLAS data from 5.754 GeV summing over all Q^2 and W .

2.17.2 Ongoing Analysis Work

The calibration and data processing for the entire **e1-6** data set was completed by the end of 2002. This was no small task given that the final data set includes over 600 runs and 4.5 billion triggers. The analysis efforts on this experiment are moving along several distinct tracks, with significant efforts and progress in both directions. These two tracks include (i). a global analysis of all CLAS $e - p$ data sets in the **e1** and **e1-6** run groups and (ii). extraction of hyperon single and double polarization observables. The data from this experiment represents a sizeable fraction of the world's data on kaon electroproduction.

Global $e - p$ Data Analysis

Up until now, our group's analysis of the CLAS data sets for $ep \rightarrow eK^+\Lambda, \Sigma^0$ has proceeded in a serial fashion from one $e - p$ data set to another. However by undertaking a global simultaneous analysis of all of the $e - p$ data sets, we are much less sensitive to

systematic uncertainties and can mine the available data statistically as much as possible, while extracting the data over the broadest possible kinematic region.

To better understand what will be measured in this work, it is necessary to understand the general form for the K^+Y cross section. The differential cross section for the exclusive kaon electroproduction reaction is given by the product of the virtual photon flux factor Γ_v and the $\gamma^*p \rightarrow K^+Y$ virtual photo-absorption differential cross section $d\sigma_v/d\Omega_K^*$. Averaging over the spins of all reaction participants, the unpolarized differential cross section can be expressed as:

$$\sigma_0 \equiv \frac{d\sigma_v}{d\Omega_K^*} = \sigma_T + \epsilon\sigma_L + \epsilon\sigma_{TT} \cos 2\Phi + \sqrt{\epsilon(\epsilon + 1)/2} \sigma_{LT} \cos \Phi. \quad (1)$$

The terms σ_i are the transverse, longitudinal, and interference structure functions that relate to the underlying hadronic current. Here ϵ is the virtual photon polarization parameter and Φ is the angle between the electron scattering plane and KY hadronic reaction plane. This expression is modified for a polarized beam experiment (summing over all recoil hyperon polarization states) by another term $h\sigma_0 A_{LT'}$, where h is the electron beam helicity. The extraction of the complete set of five structure functions, σ_T , σ_L , σ_{TT} , σ_{LT} , and $\sigma_{LT'}$ for both $K^+\Lambda$ and $K^+\Sigma^0$ over the full kinematic range of the available CLAS data is the primary goal of this portion of the data analysis. The full list of data sets included in the analysis is shown in Table 1.

Data Set	Experiment	Energy (GeV)	CLAS Field	Triggers (million)
1	e1c	2.567	40%	530
2	e1c	2.567	60%	370
3	e1c	4.056	60%	370
4	e1c	4.247	60%	470
5	e1c	4.247	90%	150
6	e1c	4.462	90%	420
7	e1d	4.817	90%	300
8	e1-6	5.574	90%	4500
9	e1f	5.479	60%	5000
10	e1g	3.178	40%	2500

Table 1: Listing of the data sets within the e1 and e1-6 run groups that are part of the five structure function global analysis of E00-112. The column ‘‘CLAS Field’’ represents the magnetic field setting of the CLAS torus relative to its maximum value.

The analysis approach is a simultaneous fit of all measured cross sections with a func-

tional form that depends on five variables, W , Q^2 , $\cos\theta_K^*$, Φ , and ϵ . At the present time our efforts have been focussed on developing the tools to perform background subtractions and fit the hyperon mass distributions for the Λ and Σ^0 yields, in addition to working to determine the appropriate radiative correction factors, bin centers, and photon flux factors to correct all of the data. At the same time we are also staging and running the sizeable amount of Monte Carlo simulation required for this effort in order to accurately determine the CLAS acceptance function for each of the different running conditions.

Hyperon Polarization Analysis

The polarization analysis that is part of this experimental effort includes a continuation of CLAS experiment E99-006 (spokesmen D.S. Carman and B.A. Raue). The observables that are being analyzed include the helicity-independent recoil hyperon polarization and the helicity-dependent transferred polarization for both Λ and Σ^0 hyperons. Further details on the data analysis procedure and the importance of these data as constraints for the theory can be found in the report for experiment E99-006 and will not be repeated here.

2.1 7.3 Experiment Status

The majority of the theoretical models for kaon electroproduction rely on fitting to the existing data base. Presently the amount and the type of KY data that are available is extremely limited. Ultimately all observables will be required to fully constrain the theory as each different quantity is expressed in terms of a different set of the underlying amplitudes that contribute to this process. When the full E00-112 analysis is completed, we will provide cross sections and structure functions, along with both single and double polarization observables, all spanning a broad kinematic domain. This data set will then represent by far the world's best and most complete kaon electroproduction data base for ground state Λ and Σ^0 production. These data are essential to provide for tight constraints on the properties of the intermediate states that couple to the strangeness.

References

- [1] See the web page for the JLab energy upgrade white paper:
http://www.jlab.org/div_dept/physics_division/pCDR_public/Hall%20B/

3.1 Hall C Overview

Since the fall of 1995, twenty one experiments have been fully completed and an additional three experiments half completed in Hall C. These experiments cover a broad spectrum of topics in nuclear physics. Fifty six graduate students have conducted their Ph.D. research using the Hall C facility. Presently, forty one of these students have obtained their Ph.D. degrees. The research program has produced thirty refereed experimental publications, not counting three instrumentation papers. Hall C has at the moment 324 active users, representing eighteen different countries.

The initial complement of equipment in Hall C includes two general purpose magnetic spectrometers: the High Momentum Spectrometer (HMS), which has a large solid angle, moderate resolution ($\delta p/p=10^{-3}$), and a maximum momentum of 7.3 GeV/c; and the Short Orbit Spectrometer (SOS), which has a large momentum acceptance and a very short (7.4 meter) optical path length to facilitate the detection of particles having short lifetimes, such as low momentum π s and Ks. This base set of equipment has now been used to conduct sixteen completed and two partially completed experiments. The experiments completed in 2003 were: F_2^N at low Q^2 (E00-002), Resonance Electroproduction at High Q^2 (E01-002), Measurement of Hydrogen and Deuterium Inclusive Resonance Cross Sections at Intermediate Q^2 for Parton-Hadron Duality Studies (E00-116), The Charged Pion Form Factor Extension (E01-004), and Duality in Meson Electroproduction (E00-108, half completed).

By now, the understanding of the base equipment of Hall C is essentially complete. The optics and acceptances of the magnetic spectrometers are in detail understood. The ARC energy measurement system agrees, within the total error of $\pm 0.06\%$, with the independent beam energy measurements of Hall A. Precision L/T separations have been proven with correlated systematic uncertainties between 1.1 and 1.5%.

New Hall C base equipment fully commissioned in 2003 consists of a “diffuse” aerogel Cerenkov counter for the HMS, and a novel, highly uniform, fast raster system to scan the JLab electron beam over the cryogenic targets. In addition, the Møller polarimeter was shown to work at beam currents up to 20 μ A, with concrete plans existing to increase this beam current limit to 100 μ A in 2004 (maintaining the sub-1% precision level of the apparatus). Lastly, work has progressed well on replacing the existing HMS magnet controls in 2004.

Hall C also supports the installation of specialized equipment designed to investigate specific problems. Up to now, five of these have been completed, and one half completed. The T_{20} experiment (E94-018) was the first major installation experiment in Hall C, and

separated the elastic form factors of the deuteron to high momentum transfer. The HNSS experiment (E89-009) was an investigation of the feasibility of performing hypernuclear physics experiments in which a proton in the nucleus is replaced by its strange counterpart, the Λ hyperon. After the successful completion of the HNSS experiment, the next phase of this program has been approved. It consists of the Enge split-pole spectrometer used in the original hypernuclear experiment plus a new High resolution Kaon Spectrometer system (HKS) constructed and funded by the Japanese collaborators. The system will have ~ 350 keV resolution and a 50 fold increase in data collection rate with respect to the first generation experiment. All parts of this new spectrometer were moved to JLab in 2003, and are being pre-assembled.

Two additional large installation experiments were complementary measurements of the electric form factor of the neutron; one using a neutron detector in conjunction with a polarized target and low-current polarized beam (E93-026), and the other employing a neutron polarimeter together with an unpolarized deuterium target and high current polarized beam (E93-038). Lastly, an experiment utilizing the polarized target was run adjacent to E93-026 to study the spin structure in the nucleon resonance region (E01-006).

Early 2003 included the end of the first engineering run of the G0 experiment (E00-006). This experiment constituted the largest installation to date in Hall C, requiring a dedicated superconducting magnet system with associated detectors, a new cryogenic target system, a dedicated beam line, and a separate electronics room. The aim of this experiment is precision measurements of parity violation in the scattering of polarized electrons from protons to investigate their weak neutral current structure and possible contributions from strange quarks. At the end of 2003 the G0 apparatus was installed again, and the second engineering run started. A $40 \mu\text{A}$ beam with G0 time structure (31 MHz) and all parity-quality requirements were established in December, 2003.

Beyond the mentioned G0 and HKS experiments, three major installation efforts in preparation are an experiment measuring the ratio of the proton charge to magnetic form factor to the highest momentum transfer achievable at a 6-GeV JLab, an experiment to measure the spin structure of the proton at the highest momentum transfer achievable (same), and an experiment to conduct a search for physics beyond the standard electroweak model via a precision measurement of the weak charge of the proton (Q_{weak}). Tremendous progress has been made for these experiments in 2003. The large calorimeter required for the first two experiments mentioned is nearly complete. The Q_{weak} collaboration has produced a detailed project management document and has nearly completed the design of the resistive magnet at the heart of this experiment.

3.2 E01-004

The Charged Pion Form Factor

H.P. Blok, G.M. Huber, and D.J. Mack for the F_π Collaboration

3.2.1 Introduction

Of the experimentally accessible electromagnetic form factors of elementary hadrons, F_π stands out because the asymptotic normalization of the charged pion wave function is known from pion beta decay. Furthermore, because the charged pion contains only two valence quarks, this “pQCD limit” should be approached at relatively low Q^2 since only a single hard gluon must be exchanged. This means that NLO or NNLO calculations may eventually be directly comparable to data from an upgraded (12 GeV) JLab.

The lack of a practical pion target has historically been circumvented by two very different techniques. Elastic scattering of very high energy pion beams from atomic electrons measures F_π at the low Q^2 needed for the determination of the pion radius.[1] Higher momentum transfers can be accessed by pion electroproduction in the virtual pion field of the proton, because the longitudinal response at small $-t$ is dominated by pion exchange and hence proportional to F_π^2 . Of course, a detailed model of pion electroproduction is needed. In the gauge-invariant Regge formalism of [2], most hadronic parameters were fitted to pion *photoproduction* data, leaving $F_\pi(Q^2)$ as the only significant free parameter in the description of forward longitudinal *electroproduction*. Using this Regge model and L-T separations obtained with JLab Hall C facilities, our collaboration has revolutionized the F_π database at intermediate Q^2 .

Experiment 93-021 was the first phase in our program in which $F_\pi(Q^2)$ was measured for $Q^2 = 0.6-1.6$.¹ The data were found to be well described by several models whose predictions happen to resemble an extrapolation of a phenomenological monopole fit to $\pi + e$ elastic data.[3] Non-perturbative contributions are clearly very important since the data are twice the magnitude of a pQCD prediction including k_{perp} corrections.[4] Recently, Lattice QCD calculations have become available above $Q^2 = 1$ for the first time.[5] Their predictions are not inconsistent with our data, but have such large statistical and systematic errors that they remain uncompetitive with models.

The availability of higher beam energies at JLab has allowed us to extend these measurements to $Q^2 = 2.45$ in our new experiment, 01-004. We also took advantage of the higher beam energy to remeasure our previous $Q^2 = 1.6$ point at higher W . This is an important

¹Momentum transfer squared will be understood to have units of $(GeV/c)^2$.

test of the model dependence of our extraction of F_π because the new kinematics are at smaller $-t$ (*i.e.*, closer to the pion pole) and further from the resonance region.

3.2 .2 Experiment Status and Anticipated Uncertainties

The experiment ran successfully in July-August 2003. Because we are performing an L-T separation, control of systematic errors was very important to us. Fortunately, this was much easier in 2003 than in late 1997 due to a mature understanding of the absolute beam energy, spectrometer optics and kinematic offsets, improvements in the Fast Raster system, and the upgrade of all Beam Position Monitors (BPMs) to Switched Electrode Electronics (SEE). The SEE BPM closest to the experimental target showed some current dependence and had to be excluded from the data analysis. This was unfortunate since the determination of stable spectrometer momentum offsets requires tracking vertical target spot changes at the level of $\pm 50 \mu\text{m}$. Other SEE BPMs located further from the target were used.

The data are under calibration/analysis by the Ph.D. thesis student (Tanja Horn, U. Maryland), together with a team from the U. of Regina, JLab, and the Vrije Universiteit. Analysis of the $e + p$ elastic data, both for kinematic offsets and cross sections, was completed within 4 months of the end of the experiment. Detector calibrations required for the full $p(e, e'\pi^+)n$ analysis are presently 2/3 complete. The anticipated magnitude of the uncertainties for F_π remains consistent with the proposal. (See Figure 1).

References

- [1] S.R. Amendolia *et al.*, Nucl. Phys. **B277** (1986) 168-196.
- [2] M. Vanderhaeghen, M. Guidal, and J.-M. Laget, Phys. Rev. C **57** (1997) 1454; Nucl. Phys. **A627** (1997) 645.
- [3] J. Volmer *et al.*, Phys. Rev. Lett. **86** 1713 (2001), and Jochen Volmer, Ph.D. thesis, Vrije Universiteit, Amsterdam (2000), unpublished.
- [4] N.G. Stefanis *et al.*, Phys. Lett. **B449** (1999) 299-305.
- [5] J. van der Heide *et al.* Phys. Lett. **B566** (2003) 131-136.
- [6] P. Maris, P.C. Tandy, Phys. Rev. C **62** (2000) 055204.

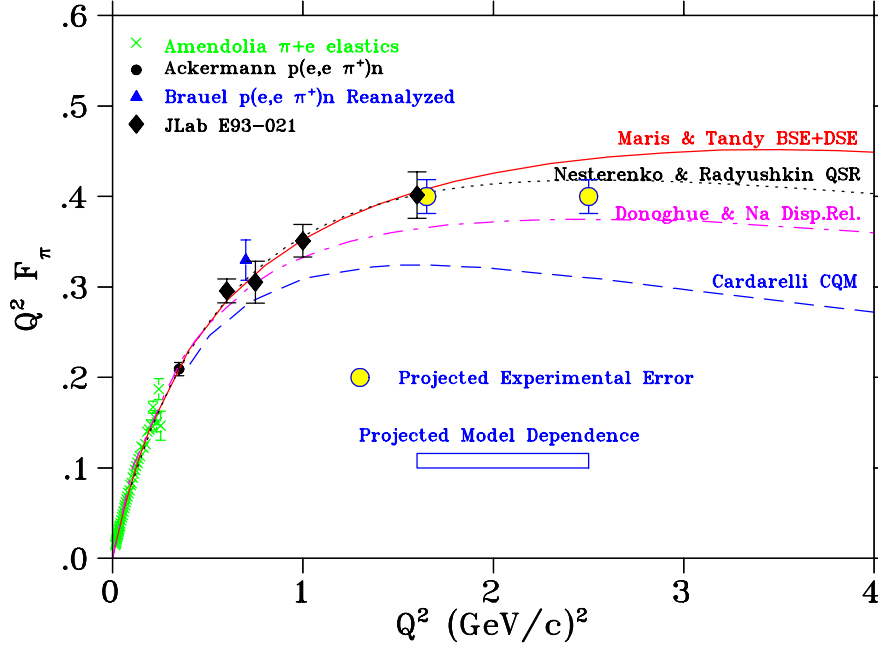


Figure 1: The world F_π database with the projected uncertainties for our recent measurement. The model calculations are from Refs. [6, 7, 8, 9].

- [7] V. A. Nesterenko and A. V. Radyushkin, Phys. Lett. **B115** (1982) 410; A. V. Radyushkin, Nucl. Phys. **A532**, (1991) 141.
- [8] J.F. Donoghue, E.S. Na, Phys. Rev. D **56** (1997) 7073.
- [9] F. Cardarelli *et al.*, Phys. Lett. **B332** (1994) 1.

3.3 E93-026

A Measurement of the Electric Form Factor of the Neutron through $\vec{D}(\vec{e}, e'n)p$
D.B. Day, G. Warren, M. Zeier, Spokespersons

3.3.1 Introduction

The source of the nucleon anomalous magnetic moments is the strong interaction which gives rise to complex electromagnetic currents of quarks and antiquarks in the nucleon. The non-zero value of the neutron's magnetic moment implies that the neutron must have a charge distribution. Precise knowledge of this charge distribution will give important information about the strong force that binds quarks together in neutrons and protons and other composite particles. The distribution of the charge is contained in an experimentally determined quantity, G_E^n , the electric form factor, a function of momentum transfer.

In E93-026¹ it was proposed to extract G_E^n by measuring the spin-dependent part of the elastic electron-neutron cross section. A measurement of the asymmetry in the quasielastic scattering of longitudinally polarized electrons from polarized deuterium nuclei in deuterated ammonia (ND₃) can determine the product $G_E^n \cdot G_M^n$.

In one-photon-exchange the differential coincidence cross section for inelastic polarized electron-polarized deuteron scattering is written as [2]

$$\sigma \approx \sigma_0(1 + hP_1^d A_{ed}^V)$$

where σ_0 is the unpolarized cross section and A_{ed}^V is the electron-deuteron vector asymmetry, respectively. Here P_1^d is the target vector polarization and h is the beam helicity times the electron polarization degree (P_b). A_{ed}^V has been shown to be of special interest [2] when measured in kinematics that emphasize quasi-free neutron knockout where it is especially sensitive to G_E^n and relatively insensitive to the nucleon-nucleon (NN) potential describing the ground state of the deuteron, to meson exchange currents (MEC) and to final state interactions (FSI).

3.3.2 Experiment Status

E93-026 took beneficial occupancy of Hall C in April, 2001 and after a several month installation period started its data taking in July which continued until late December.

¹Data at $Q^2 = 0.5$ (GeV/c)² was taken in 1998[1] and in 2001 measurements were made at both $Q^2 = 0.5$ and 1.0 (GeV/c)².

Polarized electrons from the accelerator were delivered to Hall C at a current of $\approx 100\text{nA}$. The beam polarization was measured at regular intervals in a Möller polarimeter just upstream of the target. The beam was rastered over the face of the target cylinder in order to prevent localized heating of the target material and to insure uniform irradiation of the target material. The beam was scattered from a polarized target of $^{15}\text{ND}_3$. The material was polarized by driving forbidden transitions in the free electron - deuteron system with 140 GHz microwaves. The polarization was measured continuously via NMR.

Electrons were detected in Hall C's High Momentum Spectrometer (HMS) and the neutrons in a specially constructed detector of multiple vertical planes of segmented plastic scintillators. Two planes of thin scintillators served to distinguish charged particles. Behind these were six planes of thick scintillators to detect the neutrons. The detector was shielded from direct gamma rays from the target by a 2.5 cm lead curtain, and the entire assembly was housed in a thick-walled concrete hut, which was open to the target.

The trigger was set up so that the neutron detector was read out for every electron trigger in the HMS. Coincidences between the electrons and the knock-out nucleon were determined offline.

The experimental asymmetry was diluted by scattering from materials other than polarized deuterium nuclei. This includes the nitrogen in $^{15}\text{ND}_3$, the liquid helium in which the target was immersed, the NMR coils, and target entrance and exit windows. A Monte Carlo was developed to aid in the determination of the dilution factor and to perform the detector averaging of the theoretical asymmetries. The good agreement of the distributions indicates that quasielastic scattering is the dominant process for events meeting our selection criteria; see Fig. 1.

3.3.3 Results

In order to extract G_E^n the corrected experimental asymmetry was compared to the Monte Carlo simulation that folds theoretical calculations of the asymmetry with the event distribution across the acceptances of the electron spectrometer and the neutron detector. The theoretical A_{ed}^V values were calculated using the approach of [2]. The grid of asymmetries was calculated for different values of G_E^n given by the Galster parameterization and the dipole parametrization for G_M^n .

The value of G_E^n was determined by comparing the acceptance averaged A_{ed}^V of the data to that of the MC. The theoretical asymmetries were determined for a range of scaling factors of the Galster parameterization to determine the corresponding G_E^n : $G_E^n/\text{Galster} =$

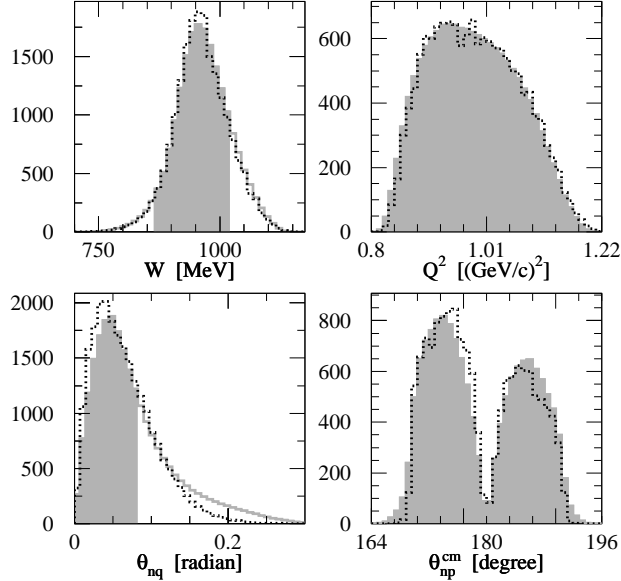


Figure 1: Comparison of $Q^2 = 1.0$ MC and data electron-neutron event distributions from all materials in the target for four kinematic variables: invariant mass W , Q^2 , angle between the neutron and \vec{q} in lab frame θ_{nq} , and angle between neutron-proton system and the momentum transfer in the center-of-momentum frame θ_{np}^{cm} . The solid grey histograms correspond to the data, and the dotted black histograms correspond to the simulation.

1.003 ± 0.064 and 1.172 ± 0.140 for $Q^2 = 0.5$ and 1.0 , respectively. The values for G_E^n are:

$$\begin{aligned}
 G_E^n(Q^2 = 0.5) &= 0.0526 \pm 0.0033 \pm 0.0026, \\
 G_E^n(Q^2 = 1.0) &= 0.0454 \pm 0.0054 \pm 0.0037,
 \end{aligned}$$

where the first uncertainty is statistical and the second is systematic. The $Q^2 = 0.5$ result agrees well with the previous result reported in Ref. [1].

Many recent models [3]–[7] have attempted to predict or fit the nucleon electromagnetic form factors. Fig. 2 compares the data with two recent calculations that use covariant formulations of the constituent quark model with quark-quark interactions fitted to spectroscopic data. The point-form spectator approximation (PFSA) of [3] (dot-dash) uses a Goldstone boson exchange interaction with pointlike constituent quarks while the light-front (LF) calculation of [4] (short dash) uses a one-gluon exchange interaction with constituent

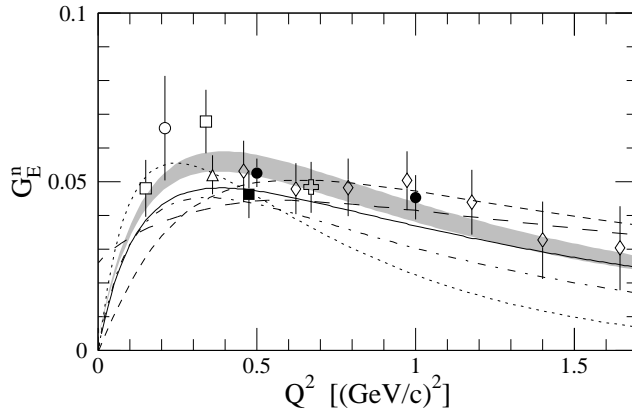


Figure 2: Comparison of this experiment with data from recent measurements. See [8] for the corresponding references and the text for a description of the curves.

quark form factors fitted to data for $Q^2 < 1$. The use of constituent form factors improves the fit to the nucleon magnetic form factors at larger Q^2 , but the PFSA seems to describe G_E^n better at low Q^2 with fewer parameters.

Also shown in Fig. 2 are the results from a hybrid model that interpolates between vector-meson dominance at low Q^2 and perturbative QCD at high Q^2 [5] (solid line), from a light front model where the nucleon is considered a system of three bound quarks surrounded by a cloud of pions [6] (long dash) and from a soliton model [11] (dotted) whose basic features include an extended object, partial coupling to the vector mesons and relativistic recoil corrections. While all these models agree qualitatively with the data, none agree with the data for the entire range of Q^2 .

E93-026 has made a significant contribution to the body of data on G_E^n and provides the highest Q^2 measurement to date using a polarized target and the most precise measurement near the maximum of G_E^n . A paper describing E93-026 and presenting its results has been accepted for publication [8].

References

- [1] H. Zhu *et al.*, Phys. Rev. Lett. **87**, 081801 (2001).
- [2] H. Arenhövel, W. Leidemann and E. L. Tomusiak, Phys. Rev. **C46**, 455 (1992),
H. Arenhövel, W. Leidemann and E. L. Tomusiak, Z. Phys. **A331**, 123 (1988).

- [3] S. Boffi, L. Ya. Glozman, W. Klink, W. Plessas, M. Radici, and R.F. Wagenbrunn, Eur. Phys. J. A **14**, 17 (2002).
- [4] F. Cardarelli and S. Simula, Phys. Rev. C **62**, 065201 (2000). Phys. Lett. B **467**, 1 (1999).
- [5] E.L. Lomon, Phys. Rev. C **66**, 045501 (2002).
- [6] G.A. Miller, Phys. Rev. C **66**, 032201(R) (2002).
- [7] G. Holzwarth hep-ph/020138; Z. Phys. A **356**, 339 (1996) [Fit B2 is shown in Fig. 2].
- [8] G. Warren *et al.* [Jefferson Lab E93-026 Collaboration], arXiv:nucl-ex/0308021, to be published in Phys. Rev. Lett, 2004.

3.4 E00-006

Measurement of the Neutral Weak Form Factors of the Nucleon
D. Beck, Spokesperson, P. Roos, Deputy Spokesperson
with collaborators from
Caltech, Carnegie Mellon, Hampton, Illinois,
IPN Orsay, LPSC Grenoble, Jefferson Lab (Hall C), Kentucky,
Louisiana Tech, Manitoba, Maryland, New Mexico State, Northern B.C.,
TRIUMF, William & Mary, Virginia Tech, Yerevan

3.4.1 Introduction

The G0 experiment will determine the neutral weak form factors of the nucleon by measuring parity-violating electron scattering from hydrogen and deuterium targets. By combining these form factors with those from ordinary electromagnetic scattering, the contributions of strange quarks to nucleon currents can be extracted. [1, 2] It is important for our overall picture of the nucleon to understand the role of the gluon fields and associated sea quarks; measurements of the strange quark contributions to the ground state charge and magnetization distributions provide the only low energy observables of the sea that can be directly related to QCD. [3]

The experiment is run in two stages. In order to separate the charge and magnetic form factors, measurements at forward and backward angles are required. By detecting recoil protons, the forward angle electron scattering asymmetry can be measured over the complete momentum transfer range of the experiment, $0.1 \leq Q^2 \leq 1 \text{ GeV}^2$. In the backward direction, individual measurements are required at each momentum transfer (each requiring different beam energies) and electrons are detected. Because there is a significant contribution to the asymmetries from the unknown axial-vector form factor, particularly at backward angles, quasi-elastic measurements using a deuterium target are also planned. In the case of deuterium, the predominantly isovector axial current changes relative to the isoscalar strange quark currents because of the additional scattering from the neutron. We will also be able to measure inelastic electron asymmetries in the backward measurements to study the neutral weak transition form factor of the Δ resonance.

3.4.2 Physics

The electroweak scattering of electrons by nucleons may be thought of in terms of the point-like interaction of photons and Z^0 s with the point-like (current) quarks in the nucleon.

Although we cannot yet calculate the structure of the nucleon at this level, we can take advantage of the different relative coupling of the photon and Z^0 to separate the contributions of different flavors. For example, the ordinary charge form factor of the proton can be written as

$$G_E^{\gamma,p} = \frac{2}{3}G_E^{u,p} - \frac{1}{3}(G_E^{d,p} + G_E^{s,p}) \quad (1)$$

and the corresponding neutral weak analog is

$$G_E^{Z,p} = \left(1 - \frac{8}{3}\sin^2\theta_W\right)G_E^{u,p} - \left(1 - \frac{4}{3}\sin^2\theta_W\right)(G_E^{d,p} + G_E^{s,p}) \quad (2)$$

where the form factors $G_E^{j,p}$ are the contributions of quark flavor j (actually the sum of contributions of quarks and anti-quarks) to the charge form factor of the proton. The key is that these same form factor contributions appear in both the electromagnetic and neutral weak form factors, but in different linear combinations. Assuming charge symmetry, the corresponding neutron form factor may also be written in terms of these contributions

$$G_E^{\gamma,n} = \frac{2}{3}G_E^{d,p} - \frac{1}{3}(G_E^{u,p} + G_E^{s,p}) \quad (3)$$

thereby allowing us to separate the strange quark contributions explicitly.

A number of nucleon models have attempted to include strange quark degrees of freedom, relying on hadronic expansions of baryon and meson resonances (loop calculations), vector dominance models of the photon-nucleon interaction (pole calculations), combinations of these (dispersion calculations), heavy baryon chiral perturbation calculations, $SU(3)_f$ Skyrme calculations, and lattice calculations. Most of the attention has been focused on the strange quark contribution to the magnetic moment, generally calculated to be negative and of order -0.2 n.m. A more comprehensive set of data over a range of momentum transfers from this and other experiments (SAMPLE, HAPPEX and other Hall A measurements, PVA4) will allow us to better understand the role of the strange quark mass and the interactions of sea quarks with the medium of the nucleon.

The axial current form factor measured in parity-violating electron scattering is similar to that measured in neutrino scattering (effectively the tree-level graph), with one important difference. Because the electron is charged, there is also an effective axial interaction of the photon which involves a weak interaction in the target, an effect known in general terms as the anapole interaction. It is therefore interesting because it is sensitive to the weak interaction between quarks in the nucleon and turns out to have sensitivity to quark orbital angular momentum.[4] This effect has been measured[5] and computed[6] in the SAMPLE measurement at MIT-Bates and is found to reduce the magnitude of the tree-level axial

form factor by about 25%. In the G0 experiment, the momentum transfer dependence of this effective axial form factor, $G_A^e(Q^2)$, will be determined.

The asymmetries for backward angle inelastic electron scattering are expected to be dominated at the moderate momentum transfers of these measurements by the isovector axial $N - \Delta$ transition form factor, $G_{N\Delta}^A(Q^2)$. This form factor has previously been determined indirectly from pion electroproduction of the Δ resonance (e.g. JLab experiment 94-005), as well as from semi-leptonic charged current excitation. In the G0 experiment, the form factor is determined using the neutral current interaction. The results will help constrain the first order momentum transfer dependence of the form factor.

3.4.3 Apparatus

These measurements are being performed with dedicated apparatus in Hall C. It consists of specialized beam monitoring hardware, a cryogenic liquid hydrogen target and a toroidal superconducting spectrometer fitted with a symmetric array of detectors and associated data acquisition electronics. The spectrometer is designed to accept a 20 cm liquid target with a solid angle of about 0.9 sr. The detector system is replicated for each of the eight octants of the spectrometer.

In the forward measurement, the recoil protons are focused into one of 15 focal plane detectors (FPDs) per octant according to the Q^2 of the scattering; inelastic protons and pions are separated using time-of-flight (TOF). The TOF measurements are made possible by a special beam structure with pulses every 32 ns rather than the usual 2 ns. Because of the high rates in the experiment (~ 1 MHz per detector), counts are scaled according to TOF by custom time encoding electronics.

In the backward scattering measurement, all detectors are used for the single Q^2 of the measurement. In this case, however, two additional detector elements are necessary. In order to separate elastic and inelastic electrons, a set of cryostat exit detectors (CEDs) are placed between the spectrometer and the FPDs. In addition, an aerogel Cherenkov detector is used to reject negative pions arising primarily from elementary production on neutrons (in the deuterium target and in the aluminum target windows). The forward angle electronics are supplemented with logic arrays to allow simultaneous measurement of elastic and inelastic electrons.

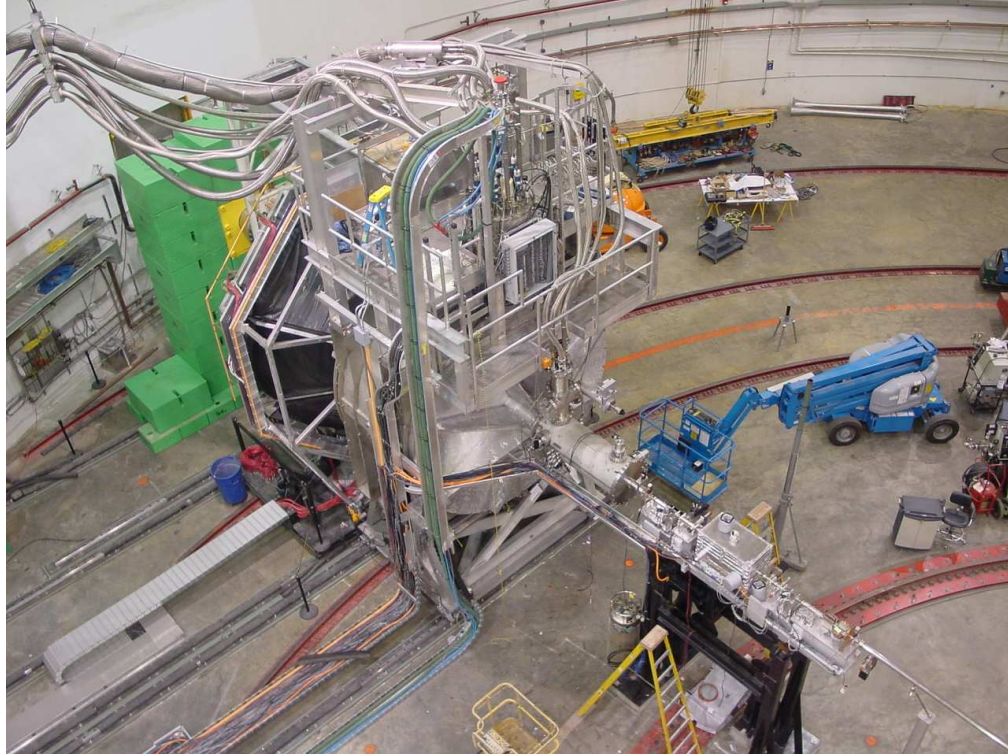


Figure 1: G0 experiment installed in Hall C. Installation was completed in October 2002.

3.4.4 Status

In 2002/3 the G0 experiment was installed and completed its forward angle engineering runs. A photograph of the completed setup on the beamline in Hall C is shown in Figure 1.

During the first part of the engineering run for the experiment (winter 02-03), the basic function of all parts of the experimental apparatus was established. Operation of the magnet at full current (5000 A) was established early in the run. Target density fluctuations were measured by reducing the beam raster size and shown to be negligible as shown in Figure 2. The initial checkout of the detectors showed a low energy background originating from the beampipe downstream of the experiment. Lead shielding (at least 4 in.) around the beampipe reduced this background to manageable levels. Subsequently, good TOF spectra, basically in accord with expectations, were obtained for all detectors as shown in Figure 3.

In the last part of the engineering run (winter 03-04), the parity-quality beam properties were established and several improvements were made to the setup. False asymmetries due to helicity-correlated changes in beam properties are controlled both by reducing the

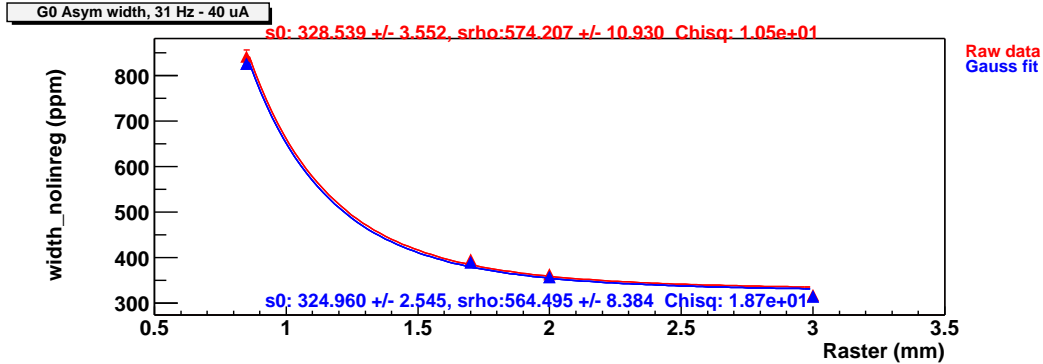


Figure 2: The effect of density fluctuations in the target are determined by measuring the change in width of the detector yield (asymmetry) as a function of beam power density at the target (changed by varying the beam raster size).

beam property changes and the sensitivity of the apparatus to them (typically by making the detector as symmetric as possible). In the end, the natural helicity-correlated changes in beam charge and position must be controlled using feedback. We have successfully demonstrated this control as shown in Figure 4. The main improvement in the setup was made in the target. From the first engineering run, we were able to determine that a substantial amount of the background under the elastic proton peak was due to inelastic protons from the aluminum target exit window. Between the runs, the central region of the window (~ 1 cm dia.) was thinned from 0.011 in. to 0.003 in. This contribution is now comparable to that from the corresponding entrance windows (each about 3%). Separate runs on gaseous H_2 and Al targets, together with the asymmetries measured for the inelastic protons near the elastic peak are used to remove the background contribution from the elastic asymmetry.

The engineering runs have been completed, with the experimental apparatus performing as designed. Production running for the forward angle measurement is expected to take place in spring 2004, with the backward angle turnaround and running to follow.

References

- [1] R. D. McKeown, Phys. Lett. **B219**, 140 (1989).
- [2] D. H. Beck, Phys. Rev. D **39**, 3248 (1990).

- [3] For recent reviews, see D. H. Beck and R. D. McKeown, *Ann. Rev. Nucl. Part. Sci.* **51**, 189 (2001); D. H. Beck and B. H. Holstein, *Int. J. Mod. Phys.* **E10**, 1 (2001); and K. Kumar and P. Souder, *Prog. Nucl. Part. Phys.* **45**, S333 (2000).
- [4] C. Bouchiat and C. Piketty, *Z. Phys.* **C49**, 91 (1991).
- [5] SAMPLE collaboration, T. M. Ito *et al.*, *subm. Phys. Rev. Lett.* , (nucl-ex/0310001).
- [6] S.-L. Zhu, *et al.*, *Phys. Rev. D* **62**, 033008 (2000).

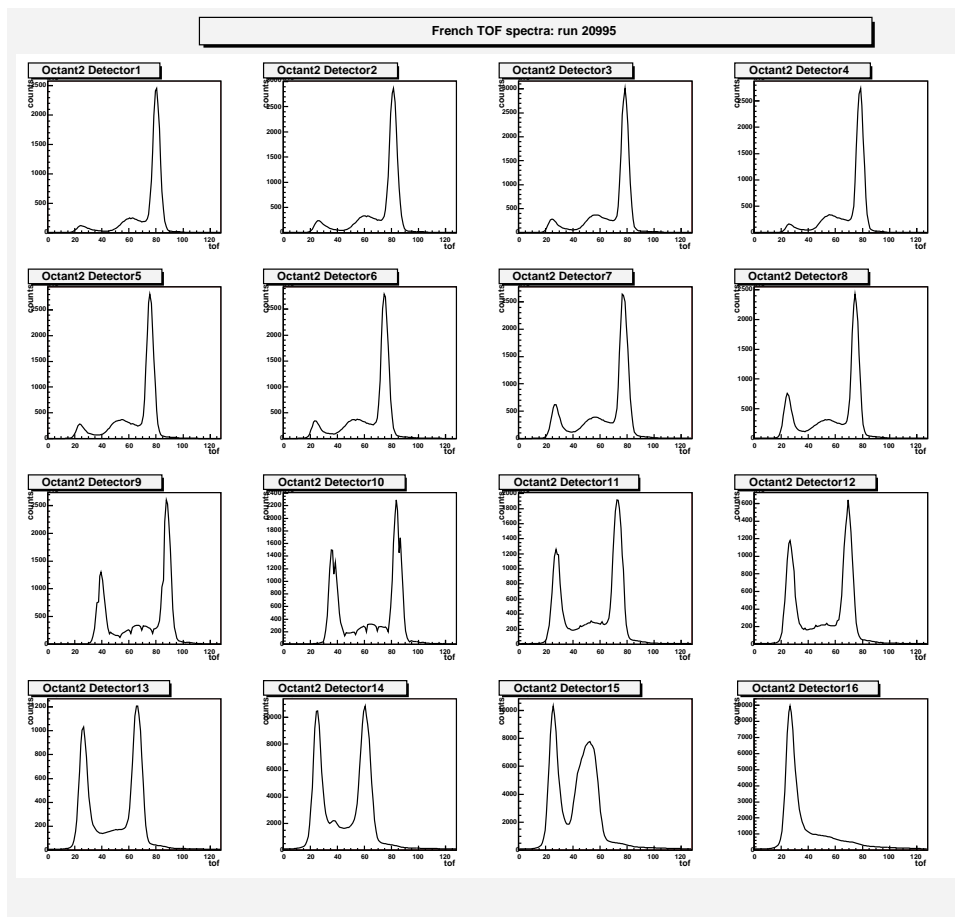


Figure 3: TOF spectra (1/4 ns/channel) for the 16 detectors (1-4 in the first row, etc.) of a single octant. The peak to the right is due to elastic protons, that to the left to pions. Inelastic protons appear in the intermediate region. Elastic protons appear in a limited range on the focal surface with the lowest Q^2 events in detector 1 - detector 16 is purposely placed just beyond the edge of this acceptance as a monitor. Protons corresponding to the highest momentum transfers wrap around in detector 15 (hence the width of the peak) and appear twice in detector 14.

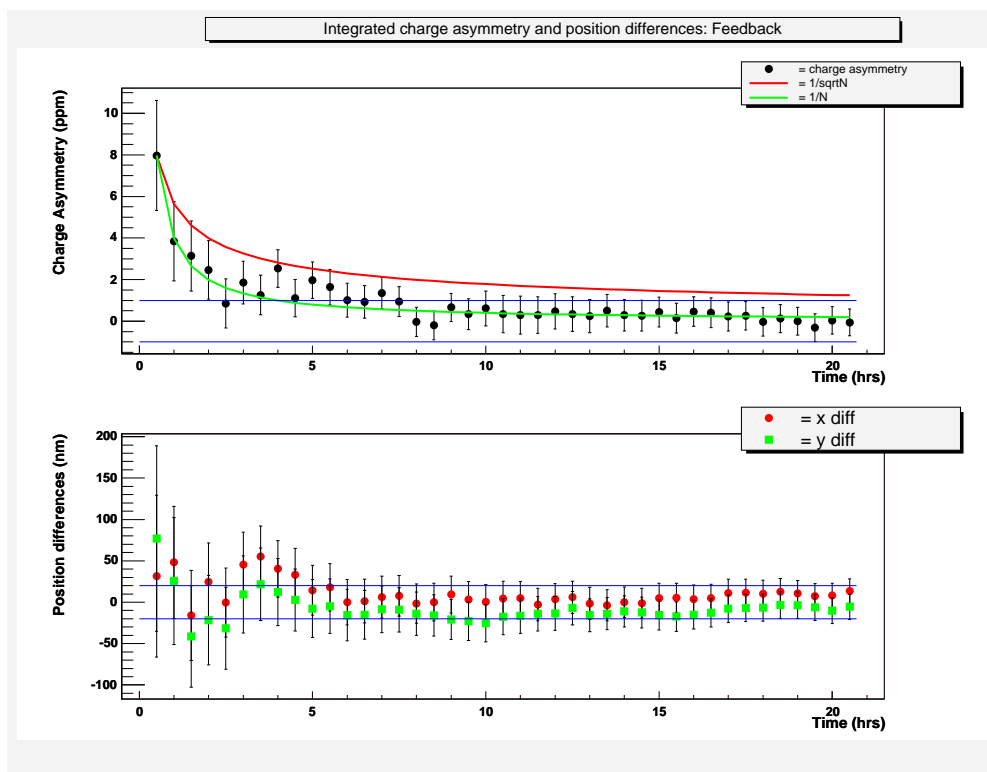


Figure 4: Convergence of feedback systems for helicity-correlated beam current (charge) asymmetry (top) and position differences (bottom). After a few hours, the charge asymmetry is controlled at the 1 ppm level and the position differences to 20 nm - the specs for the experiment. The points with the error bars are the cumulative asymmetries/differences in each case; the dots represent various convergence criteria.

3.5 E01-006

Resonances' Spin Structure - *RSS* The *RSS* Collaboration¹

3.5.1 Introduction

This experiment was designed to make high precision and high resolution measurements of the spin structure of the proton and the deuteron in the region of the nucleon resonances (final state invariant mass $W \lesssim 2$ GeV), at the four-momentum transfer $Q^2 \sim 1.3$ [GeV/c]². The physics goals were to explore fundamental properties of the nucleon and QCD and to test local duality for the polarized structure functions. The neutron spin asymmetries will be extracted from the measured proton and deuteron asymmetries.

The spin asymmetries $A_1(\nu, Q^2)$ and $A_2(\nu, Q^2)$ extend the Deep Inelastic Scattering (DIS) description of the nucleon spin structure functions (SSF's) to the region of the resonances ($\nu = E - E'$ is the lepton energy loss, E and E' are the beam and scattered electron energies). In the scaling limit of DIS, the SSF's $g_1(x)$ and $g_2(x)$ depend (up to logarithmic corrections) only on the scaling variable $x = Q^2/(2M\nu)$. In the resonance region the spin structure can be described in terms of either the non-scaling form $G_1(\nu, Q^2)$ and $G_2(\nu, Q^2)$ or of the spin asymmetries, which are related to virtual photon absorption cross sections $\sigma_{1/2}^T$, $\sigma_{3/2}^T$, and $\sigma_{1/2}^{TL}$ for photon helicities +1, -1, 0, respectively:

$$A_1 = \frac{\sigma_{1/2}^T - \sigma_{3/2}^T}{\sigma_{1/2}^T + \sigma_{3/2}^T} = \frac{M\nu G_1(\nu, Q^2) - Q^2 G_2(\nu, Q^2)}{W_1(\nu, Q^2)}$$

$$A_2 = \frac{\sigma^{TL}}{2\sigma^T} = \frac{\sqrt{Q^2}(MG_1(\nu, Q^2) + \nu G_2(\nu, Q^2))}{W_1(\nu, Q^2)}, \quad (1)$$

where $2\sigma^T = \sigma_{3/2}^T + \sigma_{1/2}^T$, M is the nucleon mass and $W_1(\nu, Q^2)$ is transverse unpolarized structure function.

In unpolarized lepton-nucleon scattering, DIS and the resonances are connected by Bloom-Gilman (B-G) or local duality [Bl70]. B-G duality can be summarized as the averaging out of the magnitude of the unpolarized structure function (SF), νW_2 , in the resonance region compared to the extrapolation of its DIS counterpart, F_2 . Quantitatively, local duality is expressed as the equality of the integrals of νW_2 and F_2 taken at constant Q^2 over the same

¹U. Basel, Florida International U., Hampton U., U. Massachusetts, U. Maryland, Mississippi S. U., North Carolina A&T U., U. of N. C. at Wilmington, Norfolk State U., Old Dominion U., S. U. New Orleans, U. of Tel-Aviv, TJNAF, U. of Virginia, Virginia P. I. & S. U., Yerevan Physics I.; Oscar A. Rondon-Aramayo, UVA and Mark K. Jones, JLab, Spokesmen

limited W range. Unpolarized local duality has been confirmed at JLab [Ni00] for the F_2 structure functions of the proton and the deuteron.

The earliest mention of local duality for the SSFs can be found in the original proposal of this experiment [Ro95]. If local duality is a reflection of some fundamental nucleon properties and not just the result of some fortuitous coincidences, it should also be present for the neutron and for the polarized structure functions [Cl01]. If local duality obtains for all SSFs, it can be a powerful tool to extend our understanding of the nucleon, by allowing indirect but quantitative access to experimentally inaccessible kinematic regions. Existing spin structure data [Ab98, Mepc, Kupc, Ai03] hint at duality in the SSFs. One of *RSS* goals is to contribute with model independent data on SSFs for a quantitative confirmation of local spin duality.

The precise measurement of A_1 and A_2 in *RSS* will also improve our understanding of the quarks' contribution to the nucleon spin and explore the effects of quark-gluon interactions which can be represented by twist-3 matrix elements calculable in Lattice QCD.

3.5.2 Experiment Status

The experiment took data in Hall C from January to early March, 2003. Polarized electrons of 5.755 GeV beam energy were incident on the University of Virginia (UVA) polarized target. The scattered electrons were detected in the High Momentum Spectrometer – HMS, parked at 13.15deg, at two central momentum settings of 4.7 and 4.09 GeV/c, which allowed coverage of W to ~ 2 GeV.

The Hall C Møller polarimeter was used to measure the beam polarization. The average effective beam polarizations for the two configurations of asymmetry measurements (beam and target spins perpendicular (A_{\perp}) and parallel (A_{\parallel}) to each other) are summarized in Table 1. The deflection of the beam by the target field upstream of the target was corrected by the Hall C's two-magnet chicane. Downstream of the target a special beam pipe and helium bag were used. The Hall C beam raster system, as modified for E93-026 (*GEN01*) [Da93], was used to distribute the beam uniformly over the target cell face. The relative positions of the beam and the target cells were monitored with an optics cell with Tungsten wire cross-hairs.

Data were taken on 3 cm long solid ammonia and deuterated ammonia targets ($^{15}\text{NH}_3$ and $^{15}\text{N}^2\text{H}_3 - \text{ND}_3$ for short). The ammonia was polarized by Dynamic Nuclear Polarization in a 5 T magnetic field cooled to ~ 1 K by a ^4He evaporation refrigerator. The polarization was measured by NMR. Table 1 lists the average polarizations for each species during the corresponding measurement periods. The Jefferson Lab and UVA target groups provided

Configuration	Beam polarization	Target	Beam I [nA]	Target polarization
A_{\perp}	65.6%	NH ₃	100	68.9%
		ND ₃	115	19.8%
A_{\parallel}	71.0%	NH ₃	91	66.4%
		ND ₃	112	15.1%

Table 1: Average beam polarization, beam current and target polarization.

full support for the target operation.

3.5.3 Preliminary Measured Asymmetries

In addition to the asymmetry data, data on a C disk target and on a cell alternately empty or filled only with LHe were taken for optics studies of the HMS and to correct for the dilution introduced by the unpolarized materials in the target. The packing fraction of ammonia in the cells is calculated by comparing the measured C and He rates to model rates. The same model is used to calculate the dilution factor. Model vs data agreement at the 10% level has been achieved (better for the parallel configuration than for the perpendicular one). Work to improve the agreement is ongoing.

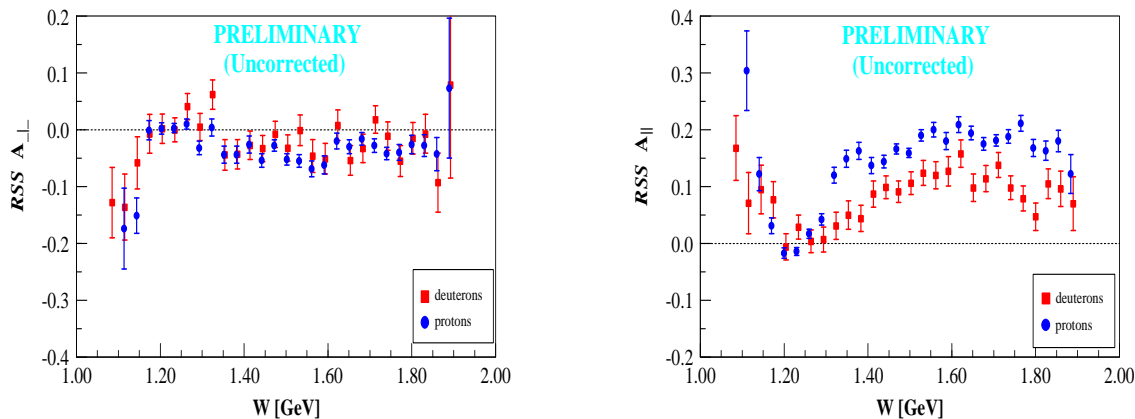


Figure 1: Preliminary measured asymmetry for the perpendicular configuration (left panel) and parallel configuration (right panel) for protons (blue circles) and deuterons (red squares), without corrections (see text for details).

The measured asymmetries are extracted from the counts asymmetries $\epsilon = (L - R)/(L + R)$, where L , R are charge normalized numbers of counts for opposite

beam helicities, corrected for dead time and pion contamination. A_{\parallel} and A_{\perp} are related to ϵ by

$$A_{\parallel,\perp} = \frac{1}{C_N f_{RC}} \left(\frac{\epsilon}{f P_b P_t} - C_D \right) + A_{RC}. \quad (2)$$

where C_N, C_D are corrections for the small contribution of the polarized proton in ^{15}N , f is the dilution factor, f_{RC} and A_{RC} are multiplicative and additive radiation corrections, and P_b and P_t are the beam and target polarizations, respectively.

Preliminary uncorrected asymmetries $A_{\perp,\parallel}$, based on preliminary dilution factors, are shown in Figure 1. The asymmetries are shown only for the restricted kinematic region $1.1 \text{ GeV} \leq W \leq 1.9 \text{ GeV}$. Data below and above these limits are still being analyzed. Corrections for the actual packing fractions, electromagnetic radiative effects and nitrogen polarization are not included. The A_{\perp} results are the first and only ones of their kind in the world. A clear difference between the proton and deuteron asymmetries can be seen, in particular for A_{\parallel} . A clean extraction of the neutron asymmetry is expected on this basis.

A_1 and A_2 are related to the measured asymmetries A_{\parallel} and A_{\perp} by the simplified expressions (neglecting the out-of-plane angle)

$$A_1 = \frac{C}{D} (A_{\parallel} - dA_{\perp}), \quad A_2 = \frac{C}{D} (c'A_{\parallel} + d'A_{\perp}),$$

where C, c', d, d' and D are functions of kinematic variables only (D has an additional mild dependence on the unpolarized structure function $R(\nu, Q^2)$). Exact expressions are available at the *RSS* Web site

<http://www.jlab.org/~jones/rss/technotes>.

Work to obtain the SSFs from the measured asymmetries is ongoing.

References

- [Bl70] E.D. Bloom and F.J. Gilman, *Phys. Rev. Lett.* **25**, 1140 (1970); *Phys. Rev. D* **4**, 2901 (1971).
- [Ro95] O. Rondon-Aramayo, *Precision Measurement of the Nucleon Spin Structure Functions in the Region of the Nucleon Resonances*, CEBAF proposal PR95-005, and CEBAF PAC 10 report.
- [Ni00] I. Niculescu *et al.*, *Phys. Rev. Lett.* **85**, 1186 (2000).

- [Cl01] F. E. Close and N. Isgur, Phys. Lett. **B509**, 18 (2001).
- [Ab98] E143 collaboration (K. Abe *et al.*), Phys. Rev. D **58**, 112003 (1998).
- [Mepc] TJNAF E94-010, Z-E. Meziani, private communication.
- [Kupc] TJNAF eg1, S. Kuhn, private communication.
- [Ai03] HERMES Collaboration (A. Airapetian *et al.*), Phys. Rev. Lett. **90**, 092002-1 (2003), and A. Fantoni, private communication
- [Da93] D. Day, *The Charge Form Factor of the Neutron*, CEBAF E93-026.

Theory Overview Missing.